Spots, Traps, and Patches: Asymptotic Analysis of Localized Solutions to some Linear and Nonlinear Diffusive Systems

M. J. WARD

Michael J. Ward; Department of Mathematics, University of British Columbia, Vancouver, British Columbia, V6T 1Z2, Canada,

Dedicated to the memory of Joseph B. Keller (1923–2016)

Localized spatial patterns commonly occur for various classes of linear and nonlinear diffusive processes. In particular, localized spot patterns, where the solution concentrates at discrete points in the domain, occur in the nonlinear reaction-diffusion (RD) modeling of diverse phenomena such as chemical patterns, biological morphogenesis, and the spatial distribution of urban crime. In a 2-D spatial domain we survey some recent and new results for the existence, linear stability, and slow dynamics of localized spot patterns by using the Brusselator RD model as the prototypical example. In the context of linear diffusive systems with localized solution behavior, we will discuss some previous results for the determination of the mean first capture time for a Brownian particle in a 2-D domain with localized traps, and the determination of the persistence threshold of a species in a 2-D landscape with patchy food resources. Common features in the analysis of all of these spatially localized patterns are emphasized, including the key role of certain matrices involving various Green's functions, and the derivation and study of new classes of interacting particle systems and discrete variational problems arising from various asymptotic reductions. The mathematical tools include matched asymptotic analysis based on strong localized perturbation theory, spectral analysis, the analysis of nonlocal eigenvalue problems, and bifurcation theory. Some specific open problems are highlighted and, more broadly, we will discuss a few new research frontiers for the analysis of localized patterns in multi-dimensional domains.

Key Words: strong localized perturbations, spot patterns, Brusselator model, nonlocal eigenvalue problem, Green's matrix, Bravais lattice, logarithmic capacitance, persistence threshold.

1 Introduction

The method of matched asymptotic expansions is a well-known and powerful systematic analytical method for asymptotically calculating solutions to singularly perturbed PDEs. It has been successfully used in a wide variety of applications (cf. [40]). In this article we consider some singularly perturbed linear and nonlinear diffusive processes that have spatially localized "defects" in 2-D domains. This type of perturbation, which has a large magnitude but small spatial extent, is called a strong localized perturbation (cf. [100], [99]). It may be contrasted with a weak perturbation, which is of small magnitude but may have large extent. Strong localized perturbations are singular perturbations in the sense that they produce large, but localized, changes in the solutions of the problems in which they occur. As such, the perturbed solutions can be constructed by a matched asymptotic analysis, which matches an inner solution defined near the strong perturbation to an outer solution defined in the region away from the defect. This matching procedure is facilitated using Dirac masses, and as a result certain Green's functions feature prominently in the analysis.

For strong localized perturbation PDE problems in a 2-D domain, a direct and naive asymptotic expansion of the solution often leads to infinite logarithmic series in powers of $\nu = -1/\log \epsilon$, where ϵ is a small positive parameter. However, since $\nu \to 0$ very slowly as ϵ decreases, unless many coefficients in the infinite logarithmic series can be obtained analytically, the resulting low order truncation of this series will typically not be very accurate unless ϵ is very small. As such, it is desirable to devise a hybrid asymptotic-numerical method for these problems that has the effect of "summing" any infinite logarithmic series. Such a method was introduced in [99] for calculating eigenvalues for the Laplacian in a planar 2-D domain containing small holes. As discussed in detail below, the goal of this article is to survey how a similar theoretical framework can be used in a nonlinear context of analyzing localized spot patterns for certain reaction-diffusion (RD) systems in the singular limit of a large diffusivity ratio.

Localized spatio-temporal patterns are well-known to occur in a wide variety of experimental settings ([**53**], [**23**], [**2**], [**96**], [**47**]). A detailed survey of localized pattern formation, with applications to chemical physics, is given in [**96**]. For a recent comprehensive survey of localized patterns leading to snaking-type bifurcation diagrams in various applications see [**47**]. Localized patterns are "far-from-equilibrium" structures [**67**], and are not typically amenable to study through a conventional Turing-type stability analysis [**95**].

In the context of two-component RD systems, the 2-D numerical PDE computations of [**71**] using the simple Gray-Scott kinetics revealed a surprisingly large variety of very complex spatio-temporal localized patterns including, self-replicating spot patterns, stripe patterns, and labyrinthian space-filling curves (see also [**64**], [**65**]). This pioneering numerical study of [**71**] provided one key impetus for the development of a theoretical understanding of some of the dynamical behaviors and instabilities of localized patterns in two-component RD systems in the "far-from-equilibrium" regime. Although the specific 2-D patterns observed in [**71**] are still largely intractable to a detailed mathematical analysis, over the past 20 years there have been many theoretical studies for the existence, linear stability, and dynamics of localized patterns in the so-called "semi-strong" regime, which is based on assuming a large diffusivity ratio between the solution components. In this semi-strong regime, there is now a rather extensive literature for the analysis of 1-D patterns for various specific RD systems arising in different contexts (see [**27**], [**26**], [**97**], [**28**], [**85**], [**102**], [**41**], [**46**], and [**66**], and the references therein).

In contrast to the rather well-studied 1-D problem, there have been far fewer studies of the existence, linear stability, and dynamics of localized spot patterns for two-component RD systems in the semi-strong regime in several space dimensions. One key challenge for the development of this theory in 2-D domains is that the relevant asymptotic parameter is $\nu = -1/\log\epsilon$, where $\epsilon^{-2} \gg 1$ is the diffusivity ratio. In order to accurately resolve interactions between localized spots that are only logarithmically weak, a hybrid asymptotic-numerical approach, based on ideas originating in the strong localized perturbation theory of [**99**] and [**100**], was first developed in [**44**] to analyze the existence, linear stability, and slow dynamics of localized spot patterns for the Schnakenberg RD system. This hybrid approach has subsequently been extended to analyze localized spot patterns for RD systems arising in concrete applications, including the Gray-Scott RD model of chemical physics [**18**], a RD model for hot-spots of urban crime [**46**], and a RD model for the initiation of plant root hair cells mediated by the plant hormone auxin [**3**]. We remark that a different type of hybrid asymptotic-numerical approach has recently been developed in [**60**] and [**61**] for analyzing localized patterns with thin interfaces for the Gierer-Meinhardt model with activator saturation.

In this article we survey and present some new results for the analysis of spatially localized spot patterns for RD systems in 2-D domains in the large diffusivity limit. Certain key aspects of this methodology use ideas from strong localized perturbation theory in order to develop a hybrid asymptotic-numerical framework. To more readily illustrate this theory, we will focus almost exclusively on the well-known Brusselator RD model, as formulated in [**74**]. This prototypical RD system has been a well-studied model for analyzing various aspects of weakly nonlinear patterns in RD systems (cf. [**11**]). In a 2-D bounded domain Ω, the Brusselator has the form

$$V_\sigma = \epsilon_0^2 \Delta V + E_{\rm f} - (B+1)V + UV^2 , \qquad U_\sigma = \mathcal{D}\Delta U + BV - UV^2 ; \qquad \sigma > 0 , \quad \mathbf{x} \in \Omega , \qquad (1.1)$$

where $\partial_n U = \partial_n V = 0$ on $\partial\Omega$. In (1.1) we allow the feed-rate $E_{\rm f}$ to be spatially-dependent. In contrast to performing a conventional weakly nonlinear analysis of pattern formation from a spatially homogeneous background state as a parameter in the reaction-kinetics crosses through a bifurcation value (cf. [**95**], [**11**]), we will instead survey and present some new results for localized spot patterns of (1.1) that occur in the large diffusivity ratio limit $\epsilon_0 \to 0$. As shown in [**81**] and [**89**], localized spot patterns for (1.1) occur when $E_{\rm f} = \mathcal{O}(\epsilon_0)$, so that we introduce a constant E_0 by $E_{\rm f} = \epsilon_0 E_0 E(\mathbf{x})$. We then define the new variables $V = E_0 v/\epsilon_0$, $U = \epsilon_0 Bu/E_0$, and $\sigma = t/(B+1)$, so that (1.1) becomes

$$v_t = \epsilon^2 \Delta v + \epsilon^2 E - v + fuv^2 , \qquad \tau u_t = D\Delta u + \frac{1}{\epsilon^2}\left(v - uv^2\right) ; \qquad t > 0 , \qquad \mathbf{x} \in \Omega , \qquad (1.2)$$

where $E = E(\mathbf{x}) = \mathcal{O}(1)$, and $\partial_n u = \partial_n v = 0$ on $\partial\Omega$. In (1.2) the positive parameters are

$$f \equiv \frac{B}{B+1} < 1 , \qquad \tau \equiv \frac{(B+1)^2}{E_0^2} , \qquad D \equiv \frac{\mathcal{D}(B+1)}{E_0^2} , \qquad \epsilon \equiv \frac{\epsilon_0}{\sqrt{B+1}} . \qquad (1.3)$$

When $\epsilon \ll 1$, (1.2) is a large-aspect ratio system, and so the dispersion relation obtained from linearizing around the spatially uniform state for (1.2) has a wide band of unstable modes (cf. [**81**]). Starting from an initial random perturbation of this spatially homogeneous steady state, the full numerical PDE computation of (1.2) on the unit sphere, performed originally in [**81**] and reproduced in Fig. 1, shows the transient formation of a localized spot pattern.

Mathematically, a spot pattern for (1.2) in the 2-D domain Ω is a spatial pattern where v is concentrated as $\epsilon \to 0$ near certain discrete points in Ω, which can evolve dynamically in time. Qualitatively, in this semi-strong regime where $\epsilon \ll 1$

(a) $m(v) = 0.113$, $M(v) = 0.114$ (b) $m(v) = 0.114$, $M(v) = 0.115$ (c) $m(v) = 0.114$, $M(v) = 0.115$

(d) $m(v) = 0.112$, $M(v) = 0.113$ (e) $m(v) = 0.0804$, $M(v) = 0.176$ (f) $m(v) = 0.0301$, $M(v) = 0.407$
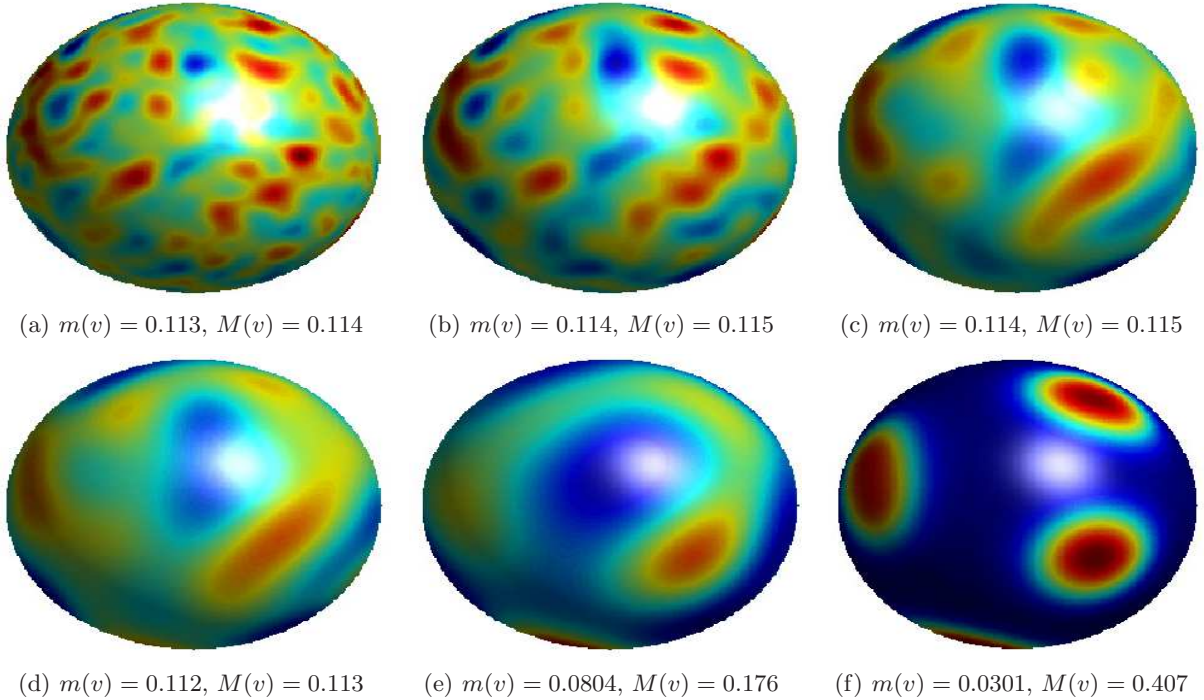
FIGURE 1. Numerical PDE simulations of (1.2) on the unit sphere for $f = 0.8$, $\epsilon = 0.075$, $D = 0.2$, $\tau = 1/f^2$, and $E = 4$. The initial condition was a 2% random perturbation from the spatially uniform state. A Turing stability analysis around the spatially uniform state predicts a wide band of unstable modes. The numerical results shows an intricate transient process leading to the formation of 8 localized spots when $t \approx 70.3$ (last frame). The indicated times are: $T = 0.281$ (top left); $T = 0.703$ (top middle); $T = 2.81$ (top right); $T = 7.03$ (bottom left); $T = 28.1$ (bottom middle); $T = 70.3$ (bottom right). Here $m(v)$ and $M(v)$ indicate the minimum and maximum value of v, respectively, for the computed solution. Figure reproduced from [**81**].

and $D = \mathcal{O}(1)$, localized spots interact with each other through the coupling induced by a global diffusion field, which depends on the domain shape. This "particle + field" interaction is distinctly different from the study of spot dynamics in the weak-interaction regime $D = \mathcal{O}(\epsilon^2)$, where spots interact with each other via their far-field, or "tail", behavior. The study of such weakly interacting spots for a few specific systems is given in [**30**]. A comprehensive and rigorous theory characterizing the dynamics of weakly interacting spots in any space dimension is given in [**111**]. Our study herein will focus on the semi-strong regime.

In different parameter regimes, spot patterns for (1.2) can exhibit three distinct types of fast $\mathcal{O}(1)$ time-scale linear instabilities: temporal oscillations of the spot amplitudes, instabilities of the spot amplitudes due to competition effects, and shape-deforming instabilities of the spot profile. In the absence of any of these instabilities, spot patterns for (1.2) will evolve slowly as t increases to some equilibrium configuration over the asymptotically long time scale $t = \mathcal{O}(\epsilon^{-2})$. In §2 we survey some linear stability and slow dynamics results for localized spot patterns for (1.2) that have been obtained in [**81**], [**89**], and [**93**] from a hybrid asymptotic-numerical theory that accounts for all powers of the logarithmic gauge ν. In §3, we announce some new linear stability results of [**17**] for localized spot patterns that are based on analyzing various nonlocal eigenvalue problems (NLEPs) that arise for the distinguished limiting regime where $D = \mathcal{O}(\nu^{-1})$. These new results, given in Proposition 3 of §3.1, in §3.2 and in §3.3, are derived in detail in [**17**]. Although conventional NLEP stability theory, developed in [**103**], [**104**], [**105**], [**106**], [**107**], [**109**] for other RD models, only determines leading-order-in-ν stability thresholds, this theory does provide rigorous stability results. One such result is given in Proposition 2 of §3.1. However, our primary focus in §3 is to extend this conventional NLEP framework, so as to determine a more accurate two-term asymptotic approximation for certain stability thresholds, and to overcome the limitation of conventional NLEP theory for analyzing Hopf bifurcations of the spot amplitudes. This latter issue will be discussed in §3.2.

We remark that our NLEP analysis only characterizes instabilities on an $\mathcal{O}(1)$ time-scale. There are possibly other stability thresholds associated with the small eigenvalues of order $\mathcal{O}(\epsilon^2)$ in the spectrum of the linearization, which we do not consider. Unstable eigenvalues of this type correspond to instabilities in the steady-state spot locations, but they are weak instabilities in that they are only realized on long $\mathcal{O}(\epsilon^{-2})$ time-scales. For certain RD systems, such as the

three-component Fitzhugh Nagumo model studied in [**98**], and the Schnakenberg-type system studied in [**110**], a drift bifurcation, resulting from a Hopf bifurcation of the small eigenvalues, has been shown to lead to spot dynamics that exhibit highly intricate oscillatory-type motion in planar domains. For the Brusselator (1.2), instabilities in the amplitudes of the spots, as governed by the NLEP, or shape-deforming instabilities of the spot profile, are the dominant instabilities on the range $\tau \ll \mathcal{O}(\epsilon^{-2})$ where we focus our analysis. No Hopf bifurcations of the translation mode can occur for our 2-D Brusselator model (1.2) for this range of τ.

In a 1-D setting, there have been many studies of NLEPs characterizing the linear stability on an $\mathcal{O}(1)$ time-scale of spike patterns for two-component RD systems in the semi-strong regime (cf. [**27**], [**26**], [**102**], [**90**], [**46**], [**97**] see also the references therein). One of the key differences between NLEPs in this 1-D setting for spike stability and our 2-D setting for spot stability, is that for the 2-D problem the multiplier of the nonlocal term in the conventional NLEP theory is typically either a bilinear or biquadratic function of the eigenvalue parameter, owing to the fact that stability thresholds occur in 2-D in the $D = \mathcal{O}(\nu^{-1})$ regime, where the Green's function can be approximated. For multiple-spike patterns on a finite 1-D domain, this NLEP multiplier typically has a rather intricate dependence on λ. However, in our 2-D setting, discrete eigenvalues of the NLEP cannot be reduced to the study of the roots of certain hypergeometric functions (cf. [**97**]) as in the 1-D case, owing to the fact that the 2-D spot profile is not known analytically. As such, NLEP studies in 1-D and in 2-D are largely rather different, with the 2-D case relying more heavily on a functional-analytic framework since solutions in terms of special functions are not available. We further remark that 1-D NLEP analysis has been used to study the transverse stability of a 1-D homoclinic stripe (cf. [**28**], [**41**], [**60**]). The breakup of the stripe, as characterized by unstable eigenvalues of the NLEP for a particular transverse wavenumber, is a key mechanism through which localized spots in 2-D are created. Finally, we mention that, in 1-D, instabilities resulting from the small eigenvalues in the linearization have been studied by extending the SLEP method, as developed in [**68**] and [**69**] for analyzing the linear stability of transition-layer solutions, to spike-type patterns (see [**43**] and the references in [**97**] and [**102**].)

In §4, we survey some previous results for two distinct linear singularly perturbed eigenvalue problems. The first problem, studied in §4.1, is related to the mean first capture time for a Brownian particle in a 2-D domain with small traps [**45**]. The second problem, with links to ecology and re-visited in §4.2 (cf. [**55**]), involves determining and then optimizing the persistence threshold for a species in a 2-D landscape with spatially localized food resources. These two specific problems are only two representative linear PDE problems with localized patterns. Other applications, not discussed herein, include mean first passage time problems in biophysics [**79**] and ecology [**51**], and narrow escape problems, where a Brownian particle can escape a bounded domain through small windows on the boundary (cf. [**36**], [**82**], [**73**], [**20**]).

Although the specific results in §4 have appeared previously, they are re-interpreted here so as to clearly exhibit the common elements between the analysis of spot patterns for (1.2) and the study of eigenvalue problems in singularly perturbed domains. All of the problems considered herein involve logarithmic interactions between localized structures. One particularly notable common feature in these problems is the role of certain matrices involving various Green's functions, and the derivation and study of new classes of interacting particle systems and discrete variational problems arising from the strong localized perturbation analysis. Some specific open problems in these areas will be highlighted. Finally, with a broader perspective, in §5 we briefly discuss a few new research frontiers for the analysis of localized patterns in multi-dimensional domains.

2 Localized Spot Patterns in 2-D: Existence, Linear Stability, and Slow Dynamics

In this section we survey some results for the existence, linear stability, and slow dynamics of localized spot patterns for (1.2). The hybrid analysis in this section provides an asymptotic theory that is accurate to all orders in ν.

Spatial patterns for which v concentrates as $\epsilon \to 0$ at a discrete set of points $\mathbf{x}_1, \ldots, \mathbf{x}_N$ in Ω are called spot patterns. To characterize such spot patterns in the limit $\epsilon \to 0$, strong localized perturbation theory is used to first construct a quasi-equilibrium N-spot pattern, resulting from neglecting the time-dependence in (1.2) and seeking an approximation of the solution to the steady-state problem for a given prescribed spatial configuration $\mathbf{x}_1, \ldots, \mathbf{x}_N$ of the spot centers, with $|\mathbf{x}_i - \mathbf{x}_j| = \mathcal{O}(1)$ for $i \neq j$. In this article, unless otherwise noted, our $\mathcal{O}(1)$ symbol means "strict" $\mathcal{O}(1)$, so that $|\mathbf{x}_i - \mathbf{x}_j|$ is bounded away from zero. Through a linear stability analysis, in certain parameter regimes such quasi-equilibrium patterns are known to be linearly stable on $\mathcal{O}(1)$ time-intervals (cf. [**81**], [**89**], [**93**]). In such parameter regimes, spot patterns exhibit slow dynamics, evolving over asymptotically long time scales of order $t = \mathcal{O}(\epsilon^{-2})$. This slow motion is characterized by a differential algebraic system (DAE) of ODEs for the evolution of the spot centers, as derived through a higher-order asymptotic construction.

The asymptotic analysis for the existence, linear stability, and slow dynamics of such localized 2-D spot patterns in 2-D was initially performed for the Schnakenberg model in [**44**], and subsequently for the Gray-Scott [**18**] and the Brusselator

models (cf. [**81**], [**89**], [**93**]). Our goal here is to only highlight the methodology and some of the main results, focusing on the Brusselator model, and to outline some interesting open problems for the analysis of these 2-D spot patterns.

For simplicity, we will outline the use of strong localized perturbation theory to construct an N-spot quasi-equilibrium pattern for (1.2) for the special case of a constant feed-rate where $E(\mathbf{x}) \equiv 1$ in (1.2). For $\epsilon \to 0$, we have $v = \mathcal{O}(1)$ in the core of the spot, where $|\mathbf{x} - \mathbf{x}_j| = \mathcal{O}(\epsilon)$, and $v \sim \epsilon^2$ away from the spot centers where $|\mathbf{x} - \mathbf{x}_j| = \mathcal{O}(1)$. In the core of each spot, and to leading-order in ϵ, u and v are determined by a locally radially symmetric BVP defined in terms of $\rho \equiv \epsilon^{-1}|\mathbf{x} - \mathbf{x}_j|$, where the local inhibitor field has an imposed logarithmic behavior as $\rho \to \infty$. In the limit $\epsilon \to 0$, the effect of the localized spots on the global inhibitor field u in (1.2) is to introduce a sum of Dirac-delta "forces" where the strength of the "force" induced by the spot at $\mathbf{x}_j$ is proportional to its source strength S_j, which is a parameter to be determined. In this way, the global inhibitor field u is represented as a superposition of Neumann Green's functions on Ω. Then, by asymptotically matching the local and global solutions for the inhibitor field, a nonlinear algebraic system for the source strengths $S_1, \ldots, S_N$ is derived for a given spatial configuration $\mathbf{x}_1, \ldots, \mathbf{x}_N$ of the spot centers.

For the Brusselator (1.2), in the inner region near the j-th spot we look for a locally radially symmetric solution in the form $v \sim D^{1/2}v_j(\rho)$ and $u \sim D^{-1/2}u_j(\rho)$. To leading-order, we readily obtain the following radially symmetric core problem near the j-th spot (cf. [**81**]):

$$\Delta_\rho v_j - v_j + f u_j v_j^2 = 0, \qquad \Delta_\rho u_j + v_j - u_j v_j^2 = 0, \qquad \rho > 0,$$
$$u_j'(0) = v_j'(0) = 0; \qquad v_j \to 0, \qquad u_j \sim S_j \log \rho + \chi(S_j) \quad \text{as} \quad \rho \to \infty, \qquad j = 1, \ldots, N, \tag{2.1}$$

where $\Delta_\rho \equiv \partial_{\rho\rho} + \rho^{-1}\partial_\rho$ with $\mathbf{y} = \epsilon^{-1}(\mathbf{x} - \mathbf{x}_j)$ and $\rho \equiv |\mathbf{y}|$. The central feature of this core problem is that we impose $u_j \sim S_j \log \rho$ as $\rho \to \infty$, so that each localized spot provides a Dirac source-term of strength proportional to the unknown S_j for the outer solution for u, which is defined in the region away from $\mathcal{O}(\epsilon)$ neighborhoods near the spots. As such, we refer to S_j as the *source strength* of the j-th spot, and it satisfies the integral identity $S_j = \int_0^\infty \left(v_j^2 u_j - v_j\right) \rho \, d\rho$. Since the core problem (2.1) cannot be solved analytically, the key constant $\chi(S_j)$, which also depends on f, must be determined from a numerical solution to (2.1) by calculating the limiting behavior $\lim_{\rho \to \infty}(u_j - S_j \log \rho) = \chi(S_j)$.

In the outer region, (1.2) yields that $v \sim \epsilon^2$. To determine the effect of the localized spots on the outer solution for u, we must estimate the term $\epsilon^{-2}(v - uv^2)$ in (1.2) in the sense of distributions as $\epsilon \to 0$. Upon using $v \sim \epsilon^2 + D^{1/2}v_j$ and $u \sim D^{-1/2}u_j$ near the j-th spot, we estimate for $\epsilon \to 0$ that

$$\epsilon^{-2}(v - uv^2) \to 1 + \sqrt{D} \sum_{j=1}^N \left(\int_{\mathbb{R}^2} (v_j - u_j v_j^2) \, d\mathbf{y} \right) \delta(\mathbf{x} - \mathbf{x}_j) = 1 - 2\pi\sqrt{D} \sum_{j=1}^N S_j \delta(\mathbf{x} - \mathbf{x}_j), \tag{2.2}$$

where we have used the identity $S_j = \int_0^\infty \left(v_j^2 u_j - v_j\right) \rho \, d\rho$. In this way, the outer, or global, inhibitor field satisfies

$$D\Delta u = -1 + 2\pi\sqrt{D} \sum_{j=1}^N S_j \delta(\mathbf{x} - \mathbf{x}_j), \quad \mathbf{x} \in \Omega; \qquad \partial_n u = 0, \quad \mathbf{x} \in \partial\Omega, \tag{2.3a}$$

subject to the following asymptotic matching conditions, where we have defined $\nu \equiv -1/\log \epsilon \ll 1$ and $\chi(S_j) \equiv \chi_j$:

$$u \sim D^{-1/2}\left(S_j \log |\mathbf{x} - \mathbf{x}_j| + S_j/\nu + \chi_j\right) \quad \text{as} \quad \mathbf{x} \to \mathbf{x}_j, \quad j = 1, \ldots, N. \tag{2.3b}$$

The central feature in (2.3b) is that the asymptotic matching provides a singularity structure of the form $u \sim A_j \log |\mathbf{x} - \mathbf{x}_j| + B_j$, where both the singular part, A_j, and the regular part, B_j, of each singularity condition is prescribed. The specification of the precise form of the regular part, which involves the key constant χ_j from the core problem, provides a constraint to determine S_j. By solving (2.3) exactly for any small fixed ν, we obtain a result that is accurate to all orders in the small parameter ν. In this way, this construction of a quasi-equilibrium N-spot solution effectively "sums" all the logarithmic correction terms defined by powers of ν.

To complete the construction, we observe from applying the divergence theorem to (2.3) that $2\pi\sqrt{D} \sum_{j=1}^N S_j = |\Omega|$, where $|\Omega|$ is the area of Ω. When this constraint holds, the solution to (2.3) can be written as

$$u = -2\pi D^{-1/2} \sum_{i=1}^N S_i G_0(\mathbf{x}; \mathbf{x}_i) + \bar{u}, \tag{2.4}$$

where $\bar{u}$ is an unknown constant, and where $G_0(\mathbf{x}; \mathbf{x}_0)$ is the Neumann Green's function satisfying

$$\Delta G_0 = \frac{1}{|\Omega|} - \delta(\mathbf{x} - \mathbf{x}_0), \quad \mathbf{x} \in \Omega; \qquad \partial_n G_0 = 0, \quad \mathbf{x} \in \partial\Omega;$$

$$\int_\Omega G_0 \, d\mathbf{x} = 0, \qquad G_0 \sim -\frac{1}{2\pi} \log|\mathbf{x} - \mathbf{x}_0| + R_0(\mathbf{x}_0) + \nabla_{\mathbf{x}} R_0(\mathbf{x})|_{\mathbf{x}=\mathbf{x}_0} \cdot (\mathbf{x} - \mathbf{x}_0) + \dots \text{ as } \mathbf{x} \to \mathbf{x}_0. \tag{2.5}$$

Here $R_0(\mathbf{x}_0)$ is called the *regular part* of G_0 at $\mathbf{x} = \mathbf{x}_0$, and it is depends on the shape of Ω. By expanding (2.4) as $\mathbf{x} \to \mathbf{x}_j$ and comparing with the required singularity behavior in (2.3 b), we readily derive that $S_1, \dots, S_N$ and $\bar{u}$ must satisfy the $N + 1$ nonlinear algebraic equations

$$S_j + 2\pi\nu \left(S_j R_{0j} + \sum_{j \neq i}^N S_i G_{0ji} \right) + \nu\chi(S_j) = \nu D^{1/2}\bar{u}, \qquad j = 1, \dots, N; \qquad \sum_{j=1}^N S_j = \frac{|\Omega|}{2\pi\sqrt{D}}, \tag{2.6}$$

where $R_{0j} \equiv R_0(\mathbf{x}_j)$ and $G_{0ji} \equiv G_0(\mathbf{x}_j; \mathbf{x}_i)$. By eliminating $\bar{u}$, we obtain, equivalently, in matrix form that

$$\mathbf{S} + 2\pi\nu \left(\mathcal{I} - \mathcal{E} \right) \mathcal{G}_0 \mathbf{S} + \nu \left(\mathcal{I} - \mathcal{E} \right) \boldsymbol{\chi} = \frac{|\Omega|}{2\pi N\sqrt{D}} \mathbf{e}, \qquad \bar{u} = \frac{1}{\nu N\sqrt{D}} \left(\frac{|\Omega|}{2\pi\sqrt{D}} + 2\pi\nu\mathbf{e}^T \mathcal{G}_0 \mathbf{S} + \nu\mathbf{e}^T\boldsymbol{\chi} \right). \tag{2.7 a}$$

Here $(\cdot)^T$ denotes the transpose, $\mathcal{I}$ is the $N \times N$ identity matrix, and we have defined

$$\mathbf{S} \equiv \begin{pmatrix} S_1 \\ \vdots \\ S_N \end{pmatrix}, \quad \boldsymbol{\chi} \equiv \begin{pmatrix} \chi_1 \\ \vdots \\ \chi_N \end{pmatrix}, \quad \mathbf{e} \equiv \begin{pmatrix} 1 \\ \vdots \\ 1 \end{pmatrix}, \quad \mathcal{E} \equiv \frac{1}{N}\mathbf{e}\mathbf{e}^T, \quad (\mathcal{G})_{0ij} \equiv \begin{cases} R_{0j} & i = j \\ G_0(\mathbf{x}_i; \mathbf{x}_j) & i \neq j \end{cases}, \quad i, j = 1, \dots, N. \tag{2.7 b}$$

Provided that the quasi-equilibrium spot pattern is linearly stable on $\mathcal{O}(1)$ time-scales (see §2.1 below), a higher-order asymptotic analysis, which accounts for $\mathcal{O}(\epsilon)$ correction terms to the core problem, can be used to derive the slow dynamics of the spot pattern on the long time scale $\sigma = \epsilon^2 t$ (cf. [89] and [93]). The collective coordinates characterizing this slow dynamics are the spot locations $\mathbf{x}_1, \dots, \mathbf{x}_N$ and their corresponding spot source strengths $S_1, \dots, S_N$, that both evolve slowly on the long time-scale $\sigma = \epsilon^2 t$. The resulting system for slow spot dynamics is a DAE system of ODEs as given in equation (3.8) of [93]. We summarize the result here as follows:

Proposition 1 *For $\epsilon \to 0$, and when there are no $\mathcal{O}(1)$ time-scale instabilities of the quasi-equilibrium spot pattern, then for any $\tau \ll \mathcal{O}(\epsilon^{-2})$ the time-dependent spot locations $\mathbf{x}_j$, for $j = 1, \dots, N$, on the slow time-scale $\sigma = \epsilon^2 t$ for the Brusselator (1.2) with $E \equiv 1$ satisfy a DAE system, consisting of the ODE dynamics*

$$\frac{d\mathbf{x}_j}{dt} = -2\epsilon^2\pi\gamma(S_j) \left(S_j \nabla_{\mathbf{x}} R_{0j} + \sum_{i \neq j}^N S_i \nabla_{\mathbf{x}} G_{0ji} \right), \quad j = 1, \dots, N, \tag{2.8 a}$$

for some $\gamma(S_j) > 0$, which is coupled to the constraints for $S_1, \dots, S_N$ in terms of $\mathbf{x}_1, \dots, \mathbf{x}_N$ given by the roots of the nonlinear algebraic system

$$\mathcal{N}(\mathbf{S}) \equiv \mathbf{S} + 2\pi\nu \left(\mathcal{I} - \mathcal{E} \right) \mathcal{G}_0 \mathbf{S} + \nu \left(\mathcal{I} - \mathcal{E} \right) \boldsymbol{\chi} - \frac{|\Omega|}{2\pi N\sqrt{D}} \mathbf{e} = \mathbf{0}. \tag{2.8 b}$$

Here $\nu \equiv -1/\log\epsilon$, $\nabla_{\mathbf{x}} R_{0j} \equiv \nabla_{\mathbf{x}} R_0(\mathbf{x})|_{\mathbf{x}=\mathbf{x}_j}$, and $\nabla_{\mathbf{x}} G_{0ji} \equiv \nabla_{\mathbf{x}} G_0(\mathbf{x}; \mathbf{x}_i)|_{\mathbf{x}=\mathbf{x}_j}$.

The DAE dynamics (2.8) characterizes slow spot dynamics for the Brusselator (1.2) in a bounded 2-D planar domain in the absence of any fast $\mathcal{O}(1)$ time-scale instabilities of the spot amplitudes. We remark that in the nonlinear algebraic system (2.7 a), the interaction between the spots is mediated by the Neumann Green's matrix $\mathcal{G}_0$, while the nonlinearities inherent in the core problem determine both $\chi(S_j)$ and $\gamma(S_j) > 0$ (see equation (3.8c) of [93]), which depend only on S_j and the Brusselator parameter f. These quantities are determined numerically in terms of the solution to the core problem (2.1), and are plotted in Fig. 2.

We remark that (2.8) provides a hybrid asymptotic-numerical description for slow spot dynamics, which is easily implemented using a DAE solver provided that the Neumann Green's function and its regular part from (2.5) are known. When Ω is a disk or rectangle, there are explicit analytical expressions for this Green's function (cf. [18]).
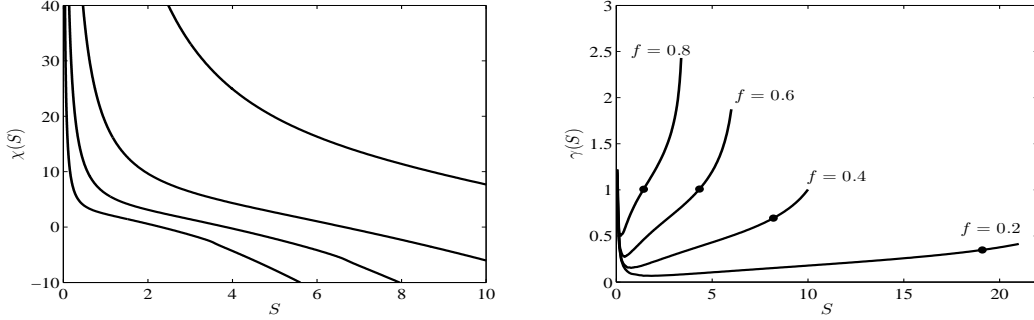
FIGURE 2. Left panel: the function $\chi(S)$ in (2.1) for $f = 0.2$, 0.4, 0.6 and 0.8. The higher (lower) curves correspond to smaller (larger) values of f. Right panel: $\gamma(S)$ versus S for a few values of f. The peanut-splitting instability threshold value of S, labeled by $\Sigma_2(f)$ and analyzed in §2.1, is indicated by the bullet points. For $S_j < \Sigma_2(f)$, the spot pattern is linearly stable to peanut-splitting.
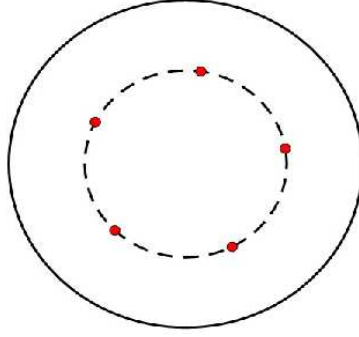

FIGURE 3. Schematic plot of a 5 spot ring pattern inside a disk.

An analytically tractable case of spot dynamics is for a ring pattern of spots where N-spots are equidistantly placed on a ring of radius r_0, with $0 < r_0 < 1$, inside the unit disk (see the schematic diagram in Fig. 3). For this spot configuration, the symmetric Neumann Green's matrix is also cyclic, and so $\mathbf{e}$ is an eigenvector of $\mathcal{G}_0$. Since $(\mathcal{I} - \mathcal{E})\mathbf{e} = \mathbf{0}$, (2.8 b) admits a solution of the form $\mathbf{S} = S_c \mathbf{e}$, where the common spot strength S_c is

$$S_c = \frac{|\Omega|}{2\pi\sqrt{D}N} \,. \tag{2.9}$$

Moreover, for a ring pattern we have that

$$\nabla_{\mathbf{x}} R_{0j} + \sum_{k \neq j}^{N} \nabla_{\mathbf{x}} G_{0jk} = \frac{p'(r_0)}{2N}(\cos\theta_j, \sin\theta_j)^T \,, \qquad \theta_j = \frac{2\pi j}{N} \,, \quad j = 1, \ldots, N \,, \tag{2.10}$$

where $\mathbf{x}_j = r_0(\cos\theta_j, \sin\theta_j)^T$. Here $p(r_0)$ is given explicitly by (see equation (4.11) of [45])

$$\mathcal{G}\mathbf{e} = \frac{p(r_0)}{N}\mathbf{e} \,, \qquad \text{where} \qquad p(r_0) = \frac{1}{2\pi}\left[-N\log(Nr_0^{N-1}) - N\log(1 - r_0^{2N}) + r_0^2 N^2 - \frac{3N^2}{4}\right] \,. \tag{2.11}$$

Upon substituting (2.10) and (2.11) into (2.8 a), we obtain the following simple scalar ODE for the ring radius r_0:

$$\frac{dr_0}{dt} = \epsilon^2 \gamma(S_c) S_c \left(\frac{(N-1)}{2r_0} - \frac{Nr_0^{2N-1}}{1 - r_0^{2N}} - r_0 N\right) \,, \qquad S_c = \frac{|\Omega|}{2\pi\sqrt{D}N} \,. \tag{2.12}$$

It is readily observed that the dynamics (2.12) has a unique stable steady-state solution r_{0e} in $0 < r_{0e} < 1$ for any $N > 1$. However, this stability conclusion for any N does not pertain to perturbations in the spot locations that deviate from a common ring radius. In fact, the study of this latter linear stability problem is an open problem (see below) and shares some common features with the well-known Thomson's Heptagon problem [9] for vortex dynamics.

Results similar to Proposition 1 have been derived in 2-D planar domains for the Schnakenberg [44] and the Gray-Scott

models [**18**]. Leading-order results for large D were derived in [**42**] for the 2-D Gierer-Meinhardt model. More recently, in [**89**] slow spot dynamics has been analyzed for the Brusselator (1.2) when posed on the boundary of the unit sphere. Although the leading-order core problem (2.1) is still valid, as it is defined locally on the tangent plane to the sphere at $\mathbf{x} = \mathbf{x}_j$, the higher-order asymptotic analysis for deriving the spot dynamics requires careful analysis of correction terms due to the non-zero curvature of the sphere. As for the 2-D planar problem, spot interactions are mediated through the Neumann Green's function, which for the sphere has the simple explicit form

$$G_0(\mathbf{x}; \mathbf{x}_0) \equiv -\frac{1}{2\pi} \log |\mathbf{x} - \mathbf{x}_0| + R_0 \,, \qquad R_0 = \frac{1}{4\pi} \left(\log 4 - 1 \right) . \tag{2.13}$$

As shown in [**89**], for $\epsilon \to 0$ and when there are no $\mathcal{O}(1)$ time-scale instabilities of the quasi-equilibrium spot pattern, the time-dependent spot locations $\mathbf{x}_j$, for $j = 1, \ldots, N$, for the Brusselator (1.2) on the surface of the unit sphere consists of the slow ODE dynamics

$$\frac{d\mathbf{x}_j}{dt} = -\epsilon^2 \gamma(S_j) \left(\mathcal{I} - \mathcal{Q}_j \right) \sum_{\substack{i=1 \\ i \neq j}}^{N} \frac{S_i \mathbf{x}_i}{|\mathbf{x}_i - \mathbf{x}_j|^2} \,, \qquad \mathcal{Q}_j \equiv \mathbf{x}_j \mathbf{x}_j^T \,, \qquad j = 1, \ldots, N \,, \tag{2.14 a}$$

coupled to the following nonlinear constraints, which replace (2.8 b):

$$\mathcal{N}(\mathbf{S}) \equiv \left[\mathcal{I} - \nu \left(\mathcal{I} - \mathcal{E} \right) \mathcal{G}_{0s} \right] \mathbf{S} + \nu \left(\mathcal{I} - \mathcal{E} \right) \boldsymbol{\chi} - \frac{2}{\sqrt{DN}} \mathbf{e} = \mathbf{0} \,. \tag{2.14 b}$$

Here $\nu \equiv -1/\log \epsilon$, $\mathcal{E} \equiv N^{-1} \mathbf{e}\mathbf{e}^T$ and $\mathcal{G}_{0s}$ is the $N \times N$ matrix with entries $(\mathcal{G}_{0s})_{ij} = \log |\mathbf{x}_i - \mathbf{x}_j|$ for $i \neq j$ and $(\mathcal{G}_{0s})_{ii} = 0$. In (2.14 a), $\mathcal{Q}_j$ is a projection matrix that ensures that spots remain on the sphere $|\mathbf{x}_j| = 1$.

One key property of the spot dynamics (2.14 a) is that, due to the positivity of $\gamma(S)$, any two spots that become too close will be repelled. To see this, suppose that $|\mathbf{x}_1 - \mathbf{x}_2| = \min_{i \neq j} |\mathbf{x}_i - \mathbf{x}_j|$, and that $\mathcal{O}(\epsilon) \ll |\mathbf{x}_1 - \mathbf{x}_2| \ll 1$. Then, considering only the dynamics of $\mathbf{x}_1$ and $\mathbf{x}_2$, (2.14 a) yields

$$\frac{d\mathbf{x}_1}{dt} \sim -\epsilon^2 \gamma(S_1) \left(\mathcal{I} - \mathcal{Q}_1 \right) \frac{S_2 \mathbf{x}_2}{|\mathbf{x}_1 - \mathbf{x}_2|^2} \,, \qquad \frac{d\mathbf{x}_2}{dt} \sim -\epsilon^2 \gamma(S_2) \left(\mathcal{I} - \mathcal{Q}_2 \right) \frac{S_1 \mathbf{x}_1}{|\mathbf{x}_1 - \mathbf{x}_2|^2} \,,$$

where $\mathcal{Q}_1 \equiv \mathbf{x}_1 \mathbf{x}_1^T$ and $\mathcal{Q}_2 \equiv \mathbf{x}_2 \mathbf{x}_2^T$. Since $|\mathbf{x}_1| = |\mathbf{x}_2| = 1$ for all t, we calculate that

$$\frac{d|\mathbf{x}_1 - \mathbf{x}_2|^2}{dt} = -2 \left(\mathbf{x}_2^T \mathbf{x}_1' + \mathbf{x}_1^T \mathbf{x}_2' \right) \sim \frac{2\epsilon^2}{|\mathbf{x}_1 - \mathbf{x}_2|^2} \left[S_2 \gamma(S_1) \mathbf{x}_2^T \left(\mathcal{I} - \mathcal{Q}_1 \right) \mathbf{x}_2 + S_1 \gamma(S_2) \mathbf{x}_1^T \left(\mathcal{I} - \mathcal{Q}_2 \right) \mathbf{x}_1 \right] \,, \tag{2.15 a}$$

$$= \frac{2\epsilon^2}{|\mathbf{x}_1 - \mathbf{x}_2|^2} \left[S_2 \gamma(S_1) \left(1 - |\mathbf{x}_1^T \mathbf{x}_2|^2 \right) + S_1 \gamma(S_2) \left(1 - |\mathbf{x}_1^T \mathbf{x}_2|^2 \right) \right] \,, \tag{2.15 b}$$

where we have used $\mathbf{x}_1^T \mathbf{x}_1 = 1$, $\mathbf{x}_2^T \mathbf{x}_2 = 1$, and $\mathbf{x}_2^T \mathcal{Q}_1 \mathbf{x}_2 = \mathbf{x}_1^T \mathcal{Q}_2 \mathbf{x}_1 = |\mathbf{x}_1^T \mathbf{x}_2|^2$. Since $\gamma(S) > 0$ and $|\mathbf{x}_1^T \mathbf{x}_2| < 1$, the last line in (2.15) yields that $\frac{d|\mathbf{x}_1 - \mathbf{x}_2|^2}{dt} \sim b/|\mathbf{x}_1 - \mathbf{x}_2|^2 > 0$ for some $b > 0$. Thus, two spots that become too close will be repelled.
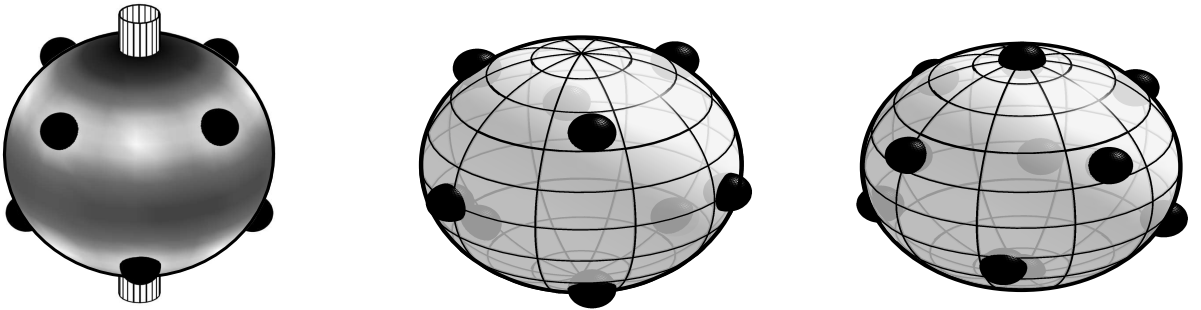

FIGURE 4. Schematic plot of steady-state spot configurations of the DAE dynamics (2.14) for the twisted cuboidal $N = 8$ configuration (left panel), for $N = 9$ (middle panel), and for $N = 10$ (right panel). In the left panel the polar axis is drawn as a reference. (Figure from [**38**] and [**89**]).

For spot patterns on the sphere, an interesting open question is to determine stable equilibrium spot configurations of the DAE dynamics (2.14) that have large basins of attractions for initial conditions. Since two-spot interactions are

repulsive, we expect that any such steady-state configuration will have spots that are, roughly, equally distributed on the sphere. For $N = 2, \ldots, 8$ and for $N = 9, 10$ such equilibria have been classified in [**89**] and [**38**] as follows: $N = 2$: two antipodal spots; $N = 3$: three equally-spaced spots on an equator of the sphere; $N = 4$: four spots centered at the vertices of a regular tetrahedron; $N = 5, 6, 7$: an $(N - 2) + 2$ pattern consisting of a pair of antipodal spots, with the remaining $N - 2$ spots equally-spaced on the equatorial mid-plane between the two polar spots; $N = 8$: a "twisted cuboidal" shape, consisting of two parallel rings of four equally-spaced spots, symmetrically placed above and below an equator. The spots are phase shifted by $45°$ between each ring. The perpendicular distance between the two planes is ≈ 1.12924 as compared to a minimum distance of ≈ 1.1672 between neighboring spots on the same ring, so that the pattern does not form a true cube; $N = 9$: pattern with 3 parallel planes of 3 spots each. The spots on the equatorial plane and the other two planes are $60°$ phase-shifted; $N = 10$: two polar spots together with two parallel planes with four equally-spaced spots on each plane, with a $45°$ relative phase-shift of the spots on the two planes. A schematic plot of the steady-state spot configurations for $N = 8$, $N = 9$, and $N = 10$, is shown in Fig. 4. For $N = 2 \ldots, 10$, stable spot configurations of the DAE dynamics (2.14) are found to coincide with elliptic Fekete point distributions (cf. [**89**], [**38**]), which correspond to minimizing the discrete logarithmic energy $H_2 \equiv -\sum \sum_{i \neq j} \log |\mathbf{x}_i - \mathbf{x}_j|$ on the sphere (cf. [**50**], [**75**]).

We now list several specific **open problems** related to the DAE dynamics for the Brusselator in a planar domain (2.8) and on the sphere (2.14). For the sphere, a few of these were also listed in [**38**].

- Extend the rigorous numerics methodology of [**4**] to prove the existence of solutions to the core problem (2.1) and the behavior of $\chi(S_j)$. Similar core problems, but with different nonlinearities, occur for other RD systems, such as the Gray-Scott model (cf. [**18**]).
- For a fixed N, numerically determine bifurcation properties of branches of equilibria to the DAE dynamics (2.8) in simple domains where the Green's function is analytically available and for (2.14) on the sphere (see Fig. 3–5 of [**89**] for the case $N = 3, 4$ on the sphere).
- For $N > 10$, and in particular for large values of N, determine whether there is a relationship between the spatial locations of spot equilibria on the sphere for (2.14) and elliptic Fekete point distributions.
- Analyze the linear stability properties of equilibria of the DAE dynamics. In particular, for a ring pattern of spots, there should be a maximum number of spots that can be equidistantly placed on a ring before stability is lost (see Fig. 15 of [**44**] for a numerical study of this issue for the related Schnakenberg model). Such a threshold, analogous to Thomson's Heptagon problem, has been established for the related problem of the stability of Eulerian point vortices on the sphere (cf. [**9**]). The analysis of the linear stability of equilibria of the DAE dynamics should provide an alternative method to analyzing the asymptotically small eigenvalues in the spectrum of the linearization of the Brusselator (1.2) around a steady-state spot pattern. Such an approach was used to [**91**] to analyze the small eigenvalues associated with spike patterns for the 1-D Brusselator model.
- Perform a numerical bifurcation study to examine how solution branches of spot equilibria on the sphere are related to the weakly nonlinear patterns analyzed in [**11**] (see also [**59**]) near a Turing bifurcation of the spatially homogeneous steady-state of the Brusselator. A possible homotopy parameter for this study is ϵ.
- Characterize DAE spot dynamics in the presence of various types of spatial heterogeneities. In particular, consider the effect of either spatially inhomogeneous terms in the RD system (1.2), a Robin boundary condition on $\partial \Omega$, or small obstacles in the domain such as holes, which act as barriers to diffusion or allow material to leave the domain. Some results in this direction are given in [**93**].
- Derive and analyze DAE dynamics when (1.2) is posed on a closed Riemannian manifold to determine how the local geometry of the manifold, such as the Gaussian curvature, influences the dynamics. The Neumann Green's function for the Laplace-Beltrami operator will be central to this extension, and in general must be computed numerically. However, recently, explicit formulae for it have been obtained for the torus [**33**] and for certain cylinders of revolution [**29**].

2.1 Linear Stability of Quasi-Equilibrium Spot Patterns

Next, we analyze the linear stability on an $\mathcal{O}(1)$ time-scale of the N-spot quasi-equilibria for the Brusselator (1.2) when $E(\mathbf{x}) \equiv 1$. We will show that there are three distinct types of instabilities that can occur in different parameter regimes. The first type is a peanut-splitting instability, which occurs when the source strength of a particular spot exceeds a threshold, depending on f, denoted by $\Sigma_2(f)$. This linear instability, which results from a zero-eigenvalue crossing for a locally non-radially symmetric eigenfunction near the spot, has been shown from full numerical PDE simulations (cf. [**81**], [**93**]) to trigger a nonlinear spot self-replication event where the spot splits into two. The two other types of linear instability mechanisms are instabilities of the spot amplitudes that are associated with locally radially symmetric perturbations near

the spots. In contrast to peanut-splitting instabilities, the resulting spectral problem governing spot amplitude instabilities is a globally coupled eigenvalue problem (GCEP) that combines both local behavior near the spots and global information arising from an eigenvalue parameter-dependent Green's matrix. A competition instability of the spot amplitudes, due to a zero-eigenvalue crossing, is a sign-changing linear instability that preserves the average spot amplitude, but which from full numerical PDE simulations (cf. [81], [93]) is found to ultimately trigger a nonlinear process leading to the annihilation of one or more spots. The second type of instability is an oscillatory instability of the spot amplitudes, which occurs through a Hopf bifurcation when a complex conjugate pair of eigenvalues crosses the imaginary axis in the spectral plane.

We now outline the linear stability analysis of N-spot quasi-equilibria, denoted by v_e and u_e, when $E \equiv 1$ in (1.2). We first introduce the perturbation

$$v = v_e + e^{\lambda t}\phi, \qquad u = u_e + e^{\lambda t}\eta, \tag{2.16}$$

into (1.2), where $|\phi| \ll 1$ and $\eta \ll 1$, to obtain the singularly perturbed eigenvalue problem

$$\epsilon^2 \Delta \phi - \phi + 2fu_e v_e \phi + fv_e^2 \eta = \lambda \phi, \quad \mathbf{x} \in \Omega, \qquad \partial_n \phi = 0, \quad \mathbf{x} \in \partial\Omega, \tag{2.17 a}$$

$$D\Delta\eta + \frac{1}{\epsilon^2}\left(\phi - 2u_e v_e \phi - v_e^2 \eta\right) = \tau\lambda\eta, \quad \mathbf{x} \in \Omega, \qquad \partial_n \eta = 0, \quad \mathbf{x} \in \partial\Omega. \tag{2.17 b}$$

Near the j-th spot centered at $\mathbf{x}_j$, we have $v_e \sim D^{1/2}v_j(\rho)$ and $u_e(\rho) \sim D^{-1/2}u_j(\rho)$, with $\mathbf{y} = \epsilon^{-1}(\mathbf{x} - \mathbf{x}_j)$ and $\rho = |\mathbf{y}|$, where v_j and u_j satisfy the radially symmetric core problem (2.1). Then, we let $\phi(\mathbf{x}) \sim \Phi_j(\mathbf{y})$ and $\eta(\mathbf{x}) \sim D^{-1}N_j(\mathbf{y})$ to obtain the leading-order local problem

$$\Delta_{\mathbf{y}}\Phi_j - \Phi_j + 2fu_j v_j \Phi_j + fv_j^2 N_j = \lambda\Phi_j, \qquad \Phi_j \to 0 \quad \text{as} \quad |\mathbf{y}| \to \infty, \tag{2.18 a}$$

$$\Delta_{\mathbf{y}}N_j + \Phi_j - 2u_j v_j \Phi_j - v_j^2 N_j = 0, \tag{2.18 b}$$

provided that the following consistency condition holds:

$$\tau|\lambda|\epsilon^2/D \ll 1. \tag{2.19}$$

Since $\epsilon \ll 1$, (2.19) will hold for $|\lambda| = \mathcal{O}(1)$ whenever $\tau \ll D/\epsilon^2$. For $D = \mathcal{O}(1)$, this implies that $\tau \ll \mathcal{O}(\epsilon^{-2})$. A further key point, as discussed in detail below, is that the far-field behavior of N_j in (2.18 b) will depend on the type of perturbation that is introduced.

To analyze the possibility of a shape-deforming instability near the j-th spot, we let $m = 0, 1, 2, \ldots$ and introduce

$$\Phi_j = \hat{\Phi}_j(\rho)e^{im\theta}, \quad N_j = \hat{N}_j(\rho)e^{im\theta}, \qquad \mathbf{y} = \rho(\cos(\theta), \sin(\theta))^T, \quad \rho = |\mathbf{y}|. \tag{2.20}$$

so that (2.18) becomes

$$\mathcal{L}_m\hat{\Phi}_j - \hat{\Phi}_j + 2fu_j v_j \hat{\Phi}_j + fv_j^2 \hat{N}_j = \lambda\hat{\Phi}_j, \qquad \hat{\Phi}_j \to 0 \quad \text{as} \quad |\mathbf{y}| \to 0, \tag{2.21 a}$$

$$\mathcal{L}_m\hat{N}_j + \hat{\Phi}_j - 2u_j v_j \hat{\Phi}_j - v_j^2 \hat{N}_j = 0, \tag{2.21 b}$$

where the linear operator $\mathcal{L}_m$ is defined by $\mathcal{L}_m v \equiv v_{\rho\rho} + \rho^{-1}v_\rho - m^2\rho^{-2}v$.

We first observe that the $m = 1$ mode corresponds trivially to translation invariance with $(\hat{\Phi}_j, \hat{N}_j) = (u_j', v_j')$ being an eigenpair associated with $\lambda = 0$ for any $S > 0$. Numerical computations (not shown) indicate that there is never a zero-eigenvalue crossing, corresponding to a drift instability, for this mode for any $S > 0$. We remark that if we were to consider the range $\tau = \mathcal{O}(\epsilon^{-2})$, for which (2.19) no longer holds, then the inner problem (2.21 b) would be modified by adding the term $\tau_c\lambda\hat{N}_j/D$ to the right-hand side of (2.21 b) where $\tau_c \equiv \tau\epsilon^2 = \mathcal{O}(1)$. With this modification of the local eigenvalue problem, a drift instability does occur at some critical value of τ_c. We do not pursue this here, since when $\tau = \mathcal{O}(\epsilon^{-2})$ the amplitudes of the spots will always be unstable on an $\mathcal{O}(1)$ time-scale. For the specific Schnakenberg-type system studied in [110], drift bifurcations were shown to have a lower stability threshold than spot amplitude instabilities, and this atypical feature was found in [110] to lead to intricate oscillatory dynamics in the trajectory of a spot.

As such, in our study, we will only consider the modes $m = 0, 2, 3, \ldots$. For locally non-radially symmetric perturbations, where $m \geq 2$, the $m^2\hat{N}_j/\rho^2$ term in (2.21 b) ensures that we can impose the far-field decay condition

$$\hat{N}_j \to 0 \quad \text{as} \quad \rho \to \infty. \tag{2.22}$$

Alternatively, for locally radially symmetric perturbations, where $m = 0$, we must allow $\hat{N}_j$ to grow logarithmically as $\rho \to \infty$. For this case, the local problems near each spot are coupled together through a global outer problem. As we show below this $m = 0$ mode analysis leads to a GCEP governing spot amplitude instabilities.
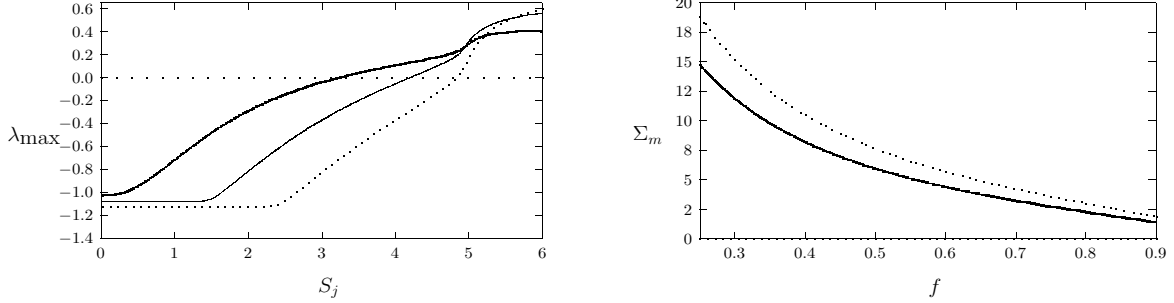
FIGURE 5. Left panel: plot of the principal eigenvalue $\lambda_{\max}$ of (2.21) versus S_j when $f = 0.7$: $m = 2$ (heavy solid curve), $m = 3$ (solid curve), and $m = 4$ (dotted curve). Right panel: plot of the threshold $S_j \equiv \Sigma_m$ versus f corresponding to the threshold condition $\lambda = 0$ for $m = 2$ (heavy solid curve) and $m = 3$ (dotted curve). Notice that the peanut-splitting threshold occurs first as S_j is increased. Computations yield that $\Sigma_2(0.3) \approx 11.89$, $\Sigma_2(0.4) \approx 8.21$, $\Sigma_2(0.5) \approx 5.96$, $\Sigma_2(0.6) \approx 4.41$, and $\Sigma_2(0.7) \approx 3.23$.

For $m = 2, 3, \ldots$, we let $\lambda_{\max}$ denote the largest eigenvalue of (2.21) subject to (2.22), as S_j is varied. In [**81**], $\lambda_{\max}$ was computed numerically from (2.21) and the result is shown in Fig. 5. For each $m = 2, 3, \ldots$, $\lambda_{\max}$ becomes positive as S_j crosses above the threshold $\Sigma_m(f)$. The numerical results of [**81**] showed that there is an ordering principle with $\Sigma_2(f) < \Sigma_3(f) < \Sigma_4(f) < \ldots$. In this way, the $m = 2$ peanut-splitting mode is the first to lose stability as S_j is increased. Numerical values of $\Sigma_2(f)$ for a few values of f are shown in the caption of Fig. 5. From the full numerical PDE computations performed in [**81**] it is conjectured that such a peanut-splitting instability is subcritical, and triggers a large-scale deformation process leading to spot self-replication.

As an application of the theory, consider a ring-pattern of spots, whereby N-spots are equidistantly-spaced on a ring concentric within the unit disk. For such a ring pattern, there is a common source-strength solution with $S_j = S_c$ for $j = 1, \ldots, N$, where $S_c = |\Omega|/(2\pi\sqrt{D}N)$ with $|\Omega| = \pi$ from (2.9). By setting $S_c = \Sigma_2(f)$, and solving the resulting expression for D, we predict that the N-spots will undergo simultaneous spot-splitting events whenever D is decreased below the spot-splitting threshold D_{split}, defined by

$$D_{\mathrm{split}} \equiv \frac{|\Omega|^2}{4\pi^2 N^2 \Sigma_2^2(f)}. \tag{2.23}$$

For the $m = 0$ mode we now outline the derivation of the GCEP. Since (2.18) is linear and homogeneous, we write

$$\Phi_j = c_j \tilde{\Phi}_j(\rho), \qquad N_j = c_j \tilde{N}_j(\rho), \tag{2.24}$$

where c_j is a constant to be determined. Then, (2.18) becomes

$$\Delta_\rho \tilde{\Phi}_j - \tilde{\Phi}_j + 2f u_j v_j \tilde{\Phi}_j + f v_j^2 \tilde{N}_j = \lambda \tilde{\Phi}_j, \qquad \tilde{\Phi}_j \to 0 \quad \text{as} \quad \rho \to \infty, \tag{2.25\,a}$$

$$\Delta_\rho \tilde{N}_j + \tilde{\Phi}_j - 2u_j v_j \tilde{\Phi}_j - v_j^2 \tilde{N}_j = 0, \qquad \tilde{N}_j \sim \log \rho + \tilde{B}_j \quad \text{as} \quad \rho \to \infty. \tag{2.25\,b}$$

We remark that the far-field logarithmic behavior in (2.25 b) is a normalization condition and uniquely fixes $\tilde{B}_j = \tilde{B}_j(S_j, \lambda)$.

To derive the GCEP we must construct an outer problem for η, and then asymptotically match the behavior η as $\mathbf{x} \to \mathbf{x}_j$ to the far-field behavior of $\tilde{N}_j$ as $\rho \to \infty$. In this way, we obtain that the outer problem is

$$\Delta\eta - \frac{\tau\lambda}{D}\eta = \frac{2\pi}{D} \sum_{i=1}^{N} c_i \delta(\mathbf{x} - \mathbf{x}_i), \quad \mathbf{x} \in \Omega, \qquad \partial_n \eta = 0, \quad \mathbf{x} \in \partial\Omega, \tag{2.26\,a}$$

$$\eta \sim \frac{c_j}{D}\left[\log|\mathbf{x} - \mathbf{x}_j| + \frac{1}{\nu} + \tilde{B}_j\right] \quad \text{as} \quad \mathbf{x} \to \mathbf{x}_j, \quad j = 1, \ldots, N, \tag{2.26\,b}$$

where $\nu \equiv -1/\log\epsilon$. We observe that in (2.26 b) both the singular and regular parts of the singularity structure are specified. This introduces a constraint, and will lead to the GCEP. The solution to (2.26) is

$$\eta = -\frac{2\pi}{D} \sum_{i=1}^{N} c_i G_\lambda(\mathbf{x}; \mathbf{x}_i), \tag{2.27}$$

where the eigenvalue-dependent Green's function $G_\lambda(\mathbf{x}; \mathbf{x}_i)$ satisfies

$$\Delta G_\lambda - \frac{\tau\lambda}{D} G_\lambda = -\delta(\mathbf{x} - \mathbf{x}_i), \quad \mathbf{x} \in \Omega; \qquad \partial_n G_\lambda = 0, \quad \mathbf{x} \in \partial\Omega;$$

$$G_\lambda \sim -\frac{1}{2\pi} \log|\mathbf{x} - \mathbf{x}_i| + R_\lambda(\mathbf{x}_i) + o(1) \quad \text{as} \quad \mathbf{x} \to \mathbf{x}_i. \tag{2.28}$$

By letting $\mathbf{x} \to \mathbf{x}_j$ in (2.27) and enforcing the matching condition in (2.26 b), we obtain the homogeneous linear system

$$-2\pi\nu \left(c_j R_{\lambda j} + \sum_{i \neq j}^{N} c_i G_{\lambda ji} \right) = c_j \left(1 + \nu \tilde{B}_j \right), \qquad j = 1, \ldots, N. \tag{2.29}$$

By writing (2.29) in matrix form, it follows that the discrete eigenvalues λ of (2.17) associated with locally radially symmetric perturbations near the spots satisfy the GCEP (cf. [**81**], [**93**])

$$\det \mathcal{M}(\lambda) = 0, \qquad \mathcal{M}\mathbf{c} = \mathbf{0}; \qquad \mathcal{M}(\lambda) \equiv \mathcal{I} + 2\pi\nu\mathcal{G}_\lambda + \nu\tilde{\mathcal{B}}, \tag{2.30 a}$$

where the symmetric Green's matrix $\mathcal{G}_\lambda$ and the diagonal matrix $\tilde{\mathcal{B}}$ have the matrix entries

$$(\mathcal{G}_\lambda)_{ij} \equiv \begin{cases} R_{\lambda j} & i = j \\ G_\lambda(\mathbf{x}_i; \mathbf{x}_j) & i \neq j \end{cases}, \qquad (\tilde{\mathcal{B}})_{ij} \equiv \begin{cases} \tilde{B}_j & i = j \\ 0 & i \neq j \end{cases}, \qquad i, j = 1, \ldots, N. \tag{2.30 b}$$

The eigenvalues λ of the GCEP (2.30) in $\text{Re}(\lambda) > 0$ correspond to instabilities in the amplitudes of the spots, owing to the fact that the perturbation in v has the form

$$v = v_e + \sum_{j=1}^{N} c_j \tilde{\Phi}_j \left[\epsilon^{-1} |\mathbf{x} - \mathbf{x}_j| \right] e^{\lambda t}. \tag{2.31}$$

2.2 The GCEP (2.30) For A Symmetric Configuration of Spots

We now examine the GCEP (2.30) in detail for a special spatial configuration of spots for which $\mathbf{e} = (1, \ldots, 1)^T$ is an eigenvector of the Neumann Green's matrix $\mathcal{G}_0$, i.e. that

$$\mathcal{G}_0 \mathbf{e} = \kappa_{01} \mathbf{e}, \tag{2.32}$$

for some κ_{01}. We refer to such spot configurations as "symmetric", as they are the conceptual analogue of equally-spaced spike patterns in the 1-D case. For symmetric spot patterns, the nonlinear algebraic system (2.7) characterizing spot quasi-equilibria admits a common source strength solution with $S_j = S_c = |\Omega|/(2\pi\sqrt{D}N)$ for $j = 1, \ldots, N$. A ring-pattern of spots, where the ring is concentric within the unit disk, is a simple example of a symmetric spot pattern.

For a symmetric spot pattern, where the core problem (2.1) is the same for each spot, the GCEP (2.30) can be simplified in that from (2.25), $\tilde{B}_j \equiv \tilde{B}(S_c, \lambda)$ for $j = 1, \ldots, N$. Moreover, when $\lambda = 0$ in (2.25), we identify that $\tilde{B}(S_c, 0) = \chi'(S_c)$, which is readily verified by differentiating the core problem (2.1) with respect to S_c and comparing with (2.25).

2.2.1 *Symmetric Spot Patterns: The Competition Instability Threshold*

For symmetric spot patterns, we will first study competition instabilities resulting from zero-eigenvalue crossings. Since the problem (2.28) for G_λ is not valid when $\lambda = 0$, to analyze any instability associated with a zero-eigenvalue crossing we must reformulate the GCEP (2.30) by first expanding $G_\lambda(\mathbf{x}; \mathbf{x}_0)$ for small λ as

$$G_\lambda \sim \frac{D}{|\Omega|\tau\lambda} + G_0(\mathbf{x}; \mathbf{x}_0) + \mathcal{O}\left(\frac{\tau\lambda}{D}\right), \tag{2.33}$$

where G_0 is the Neumann Green's function of (2.5). Upon using (2.33), the Green's matrix $\mathcal{G}_\lambda$ in (2.30 b) becomes

$$\mathcal{G}_\lambda \sim \frac{DN}{|\Omega|\tau\lambda} \mathcal{E} + \mathcal{G}_0 + \mathcal{O}\left(\frac{\tau\lambda}{D}\right), \qquad 0 < |\tau\lambda/D| \ll 1, \tag{2.34}$$

where $\mathcal{E} \equiv \mathbf{e}\mathbf{e}^T/N$ and the Neumann Green's matrix $\mathcal{G}_0$ are as in (2.7 b). Upon substituting (2.34) into (2.30 a), we get

$$\left(\mathcal{E} + \frac{2\pi\nu\tau\lambda}{\mu} \mathcal{G}_0 \right) \mathbf{c} = -\frac{\tau\lambda}{\mu} \left(1 + \nu\tilde{B} \right) \mathbf{c}, \qquad \text{where} \qquad \mu \equiv \frac{2\pi\nu DN}{|\Omega|}, \tag{2.35}$$

and where $\tilde{B} = \tilde{B}(S_c, \lambda)$ is defined by (2.25).

For a symmetric spot pattern, the Neumann Green's matrix $\mathcal{G}_0$ and $\mathcal{E}$ have a common eigenspace. Since $\mathcal{G}_0$ is symmetric, then for $N \geq 2$, we have

$$\mathcal{G}_0 \mathbf{e} = \kappa_{01} \mathbf{e}, \quad \kappa_{01} \equiv R_0(\mathbf{x}_1) + \sum_{j \neq 1}^{N} G_0(\mathbf{x}_1; \mathbf{x}_j); \qquad \mathcal{G}_0 \mathbf{q}_j = \kappa_{0j} \mathbf{q}_j, \quad \text{where} \quad \mathbf{q}_j^T \mathbf{e} = 0, \quad j = 2, \ldots, N, \tag{2.36}$$

where the $\mathbf{q}_j$ for $j = 2, \ldots, N$ are mutually orthogonal. This shows that there are two possible classes of perturbations corresponding to zero-eigenvalue crossings. The first type is the synchronous mode, obtained by setting $\mathbf{c} = \mathbf{e}$ in (2.35), which leads to the following expression for λ with $\tau |\lambda| / D \ll 1$:

$$1 + \frac{2\pi\nu\tau\lambda}{\mu} \kappa_{01} = -\frac{\tau\lambda}{\mu} \left[1 + \nu\tilde{B}(S_c, \lambda) \right]. \tag{2.37}$$

Since $\tilde{B}(S_c, \lambda) = \chi'(S_c) + \mathcal{O}(\lambda)$ as $\lambda \to 0$, (2.37) shows that there is no zero-eigenvalue crossing for the synchronous mode $\mathbf{c} = \mathbf{e}$. Alternatively, let $N \geq 2$ and consider the asynchronous modes $\mathbf{c} = \mathbf{q}_j$, for $j = 2, \ldots, N$. Then, for $\tau |\lambda| / D \ll 1$, (2.35) yields that

$$\mathbf{q}_j \left[1 + 2\pi\nu\kappa_{0j} + \nu\chi'(S_c) \right] + \mathcal{O}(\lambda) = 0, \qquad j = 2, \ldots, N. \tag{2.38}$$

By letting $\lambda \to 0$, we conclude that there exists a zero-eigenvalue crossing for these modes whenever S_c satisfies

$$\chi'(S_c) = -\frac{1}{\nu} - 2\pi\kappa_{0j}, \qquad j = 2, \ldots, N, \tag{2.39}$$

where κ_{0j} and $\chi(S_c)$ are defined by (2.36) and (2.1), respectively. Since there is a common spot source strength $S_c = |\Omega|/(2\pi\sqrt{D}N)$, (2.39) can be viewed as a nonlinear algebraic equation for the threshold value $D_{j\epsilon}$ of the inhibitor diffusivity D at which a zero-eigenvalue crossing occurs. This linear instability is referred to as a "competition" instability since, owing to the fact that the perturbation mode $\mathbf{c} = \mathbf{q}_j$ satisfies $\mathbf{q}_j^T \mathbf{e} = 0$, the sum of the amplitudes of the spots is preserved (see (2.31)). For $\nu \ll 1$, we can derive a two-term asymptotic expansion in powers of ν for the threshold $D_{j\epsilon}$. To do so, we first must determine the small S behavior for $\chi(S)$ associated with the core problem (2.1). The result is given in Lemma 4 of Appendix A.

From this Lemma, we use (A.1 a) for $\chi(S)$ in (2.39), together with $S_c = |\Omega|/(2\pi\sqrt{D}N)$, to obtain the following two-term expansion for the critical values $D_{j\epsilon}$, for $j = 2, \ldots, N$, of the inhibitor diffusivity at which a competition instability occurs:

$$D_{j\epsilon} = \frac{f^2 |\Omega|^2}{4b(1 - f)N^2\pi^2\nu} \left[1 + \nu \left(\tilde{\chi}_1 + 2\pi\kappa_{0j} \right) \right] + \mathcal{O}(\nu). \tag{2.40}$$

Numerical computations on (2.35) show that the unstable real eigenvalues cross through the origin into the unstable right-half plane $\text{Re}(\lambda) > 0$ as D increases above $D_{j\epsilon}$. Although this result predicts the zero-eigenvalue crossing accurately, it does not provide any information about the spectrum of the linearization near the origin near criticality. Such a detailed result is given below in Proposition 3 of §3.1.

Combining the result in (2.40) with the spot self-replication threshold (2.23), for $N \geq 2$ we conclude that whenever (2.32) holds and τ is sufficiently small, the symmetric spot pattern is linearly stable on an $\mathcal{O}(1)$ time-scale when D satisfies

$$D_{\text{split}} < D < D_{\text{comp}}; \qquad D_{\text{comp}} \equiv \min_{2 \leq j \leq N} D_{j\epsilon}. \tag{2.41}$$

From (2.40) the upper threshold is set by the smallest eigenvalue of the Green's matrix $\mathcal{G}_0$ in the $N-1$ dimensional subspace orthogonal to $\mathbf{e}$. Since $D_{\text{split}} = \mathcal{O}(1)$ and $D_{\text{comp}} \sim \mathcal{O}(\nu^{-1})$, the range in (2.41) of linear stability is asymptotically large.

2.2.2 *Symmetric Spot Patterns: Hopf Bifurcations*

Next, we formulate the problem for oscillatory instabilities in the spot amplitudes, arising from a Hopf bifurcation in the GCEP (2.30) as τ is increased past some threshold. We again consider symmetric patterns for which (2.32) holds, so that $S_j = S_c \equiv |\Omega|/(2\pi\sqrt{D}N)$ and $\tilde{B}_j = \tilde{B}(S_c, \lambda)$ for $j = 1, \ldots, N$. For symmetric spot patterns we readily obtain from the GCEP (2.30) that the discrete eigenvalues of the linearization (2.17) are the roots of $\mathcal{C}_j(\lambda) = 0$, defined by

$$\mathcal{C}_j(\lambda) \equiv \omega_{\lambda,j} + \frac{1}{2\pi\nu} \left[1 + \nu\tilde{B}(S_c; \lambda) \right], \qquad j = 1, \ldots, N. \tag{2.42 a}$$

Here, $\omega_{\lambda,j}$, for $j = 1, \ldots, N$, are the matrix eigenvalues of the eigenvalue-dependent Green's matrix $\mathcal{G}_\lambda$,

$$\mathcal{G}_\lambda \mathbf{e} = \omega_{\lambda,1} \mathbf{e}, \quad \omega_{\lambda,1} \equiv R_\lambda(\mathbf{x}_1) + \sum_{j \neq 1}^{N} G_\lambda(\mathbf{x}_1; \mathbf{x}_j); \qquad \mathcal{G}_\lambda \mathbf{q}_j = \omega_{\lambda,j} \mathbf{q}_j, \quad \text{where} \quad \mathbf{q}_j^T \mathbf{e} = 0, \quad j = 2, \ldots, N. \qquad (2.42\,b)$$

A key remark is that since $\mathcal{G}_\lambda$ has the same eigenspace as $\mathcal{G}_0$ given in (2.36), oscillations in the amplitudes of the spots can either be synchronous ($\mathbf{c} = \mathbf{e}$) or asynchronous ($\mathbf{c} = \mathbf{q}_j$ for $j = 2, \ldots, N$). However, due to matrix eigenvalue degeneracy for $\mathcal{G}_\lambda$ there is typically less than $N - 1$ distinct asynchronous modes whenever (2.32) holds. To calculate the threshold τ_{H} at which a pair of eigenvalues $\pm i\lambda_I$ with $\lambda_I > 0$ first crosses the imaginary axis as τ is increased, we can fix D on the range (2.41) for which the spot pattern is linearly stable to self-replication and competition instabilities, and solve the system

$$\mathrm{Re}(\mathcal{C}_j(i\lambda_I)) = 0, \qquad \mathrm{Im}(\mathcal{C}_j(i\lambda_I)) = 0, \qquad j = 1, \ldots, N, \qquad (2.43)$$

for $\lambda_{IHj} > 0$ and τ_{Hj} using Netwon's method. The threshold for the synchronous mode corresponds to τ_{H1} while the thresholds for the asynchronous modes correspond to τ_{Hj}, for $j = 2, \ldots, N$. Therefore, it follows that if D satisfies (2.41), the symmetric spot pattern is linearly stable to $\mathcal{O}(1)$ time-scale oscillatory instabilities of the spot amplitudes when

$$\tau < \tau_{\mathrm{H}} \equiv \min_{1 \leq j \leq N} \tau_{Hj}. \qquad (2.44)$$

The simplest implementation of this theory is for a ring-pattern of N spots that is concentric within the unit disk (see Fig. 3). For this configuration, the symmetric Green's matrix $\mathcal{G}_\lambda$ is also cyclic, and so we can readily calculate its matrix spectrum analytically in terms of the first row of $\mathcal{G}_\lambda$ (see §6 of [**32**]), which we label as

$$a_{\lambda,1} = R_\lambda(\mathbf{x}_1), \qquad a_{\lambda,j} = G_\lambda(\mathbf{x}_1; \mathbf{x}_j), \quad j = 2, \ldots, N. \qquad (2.45\,a)$$

The eigenvalue $\omega_{\lambda,1}$ of $\mathcal{G}_\lambda$ for the synchronous mode, while the other eigenvalues $\omega_{\lambda,j}$, for $j = 2, \ldots, N$, for the asynchronous modes are

$$\omega_{\lambda,1} = \sum_{n=1}^{N} a_{\lambda,n}; \qquad \omega_{\lambda,j} = \sum_{n=0}^{N-1} \cos\left(\frac{2\pi(j-1)n}{N}\right) a_{\lambda,n+1}, \qquad j = 2, \ldots, N. \qquad (2.45\,b)$$

Since $\mathcal{G}_\lambda$ is symmetric, we observe that mode degeneracy occurs owing to the fact that $\omega_{\lambda,j} = \omega_{\lambda,N+2-j}$ for $j = 2, \ldots, \lceil N/2 \rceil$, where the ceiling function $\lceil x \rceil$ is defined as the smallest integer not less than x. When N is even, we notice that there is an eigenvalue of multiplicity one given by $\omega_{\lambda,\frac{N}{2}+1} = \sum_{n=0}^{N-1} (-1)^n a_{\lambda,n+1}$. The corresponding eigenvectors for $j = 2, \ldots, \lceil N/2 \rceil$ are written explicitly in §6 of [**32**]. By using separation of variables, the first row of the Green's matrix can be calculated explicitly for the unit disk in terms of an infinite series (see §6 of [**32**]).

Numerical realizations of this theory are shown in [**93**].

Three **open problems** in this area are the following:
- A key open problem is to develop a weakly nonlinear theory to show that the peanut-splitting linear instability is a subcritical instability as conjectured from the full PDE simulations in [**89**] and [**93**], where spot-splitting behavior was observed. Develop a similar weakly nonlinear analysis for competition instabilities associated with zero-eigenvalue crossing to show that these are also subcritical bifurcations (see [**89**] and [**93**]).
- In a disk or rectangular domain, where the Green's function is known explicitly, develop a hybrid asymptotic-numerical method to couple the slow spot dynamics (2.8) and the GCEP (2.30) so as to predict the occurrence of dynamically triggered spot amplitude instabilities for an arbitrary configuration of spots, rather than a simple ring-pattern of spots. Develop an efficient method to predict when the GCEP (2.30) has an eigenvalue in $\mathrm{Re}(\lambda) > 0$ for an arbitrary configuration of spots.
- Extend the hybrid approach above to allow for arbitrary 2-D domains where the Green's functions for the slow dynamics and the GCEP must be computed simultaneously using fast multipole theory (cf. [**48**], [**49**]).

3 NLEP Theory for Spot Patterns in 2-D

In this section we analyze the linear stability of N-spot quasi-equilibria for the distinguished limit $D = D_0/\nu \gg 1$, for which the GCEP (2.30) reduces to leading order in ν to a nonlocal eigenvalue problem (NLEP). By analyzing the spectrum of this NLEP we will determine both competition and Hopf stability thresholds on a finite domain, and will study the linear stability of a periodic pattern of spots where the spots are centered at the lattice points of a Bravais lattice in $\mathbb{R}^2$.

For the periodic problem we will identify the specific lattice that has an optimal stability property. Some open problems related to NLEP theory will also be discussed.

3.1 Refined Competition Stability Thresholds

For the distinguished limit $D = D_0/\nu \gg 1$, we first derive an NLEP from the GCEP (2.30) under the assumption that the spot pattern is symmetric in the sense that (2.32) holds. With $D = \mathcal{O}(\nu^{-1})$ it follows that the common spot source strength solution in (2.9) satisfies $S_c = \mathcal{O}(\nu^{1/2}) \ll 1$. To derive our NLEP we need to re-express Lemma 4, characterizing the asymptotics of the core problem, as an expansion in $\nu \ll 1$ rather than $S \ll 1$. This result is given in Lemma 5 of Appendix A

To begin the derivation of the NLEP, in (2.24) and (2.25) we introduce $B_j \equiv \tilde{B}_j c_j$ and expand

$$\Phi_j \sim \nu\left(\Phi_{j0} + \nu\Phi_{j1} + \cdots\right), \quad N_j \sim N_{j0} + \nu N_{j1} + \cdots, \quad B_j = B_{j0} + \nu B_{j1} + \cdots, \quad c_j = \nu\left(c_{j0} + \nu c_{j1} + \cdots\right). \quad (3.1)$$

Upon substituting (3.1) into (2.25), and by using (A.2 a) for the core solution v_j and u_j, we obtain that

$$L_0\Phi_{j0} + \frac{w^2}{f\chi_0^2}N_{j0} = \lambda\Phi_{j0}, \qquad \Phi_{j0} \to 0 \quad \text{as} \quad \rho \to \infty,$$
$$\Delta_\rho N_{j0} = 0, \qquad N_{j0} \sim B_{j0} \quad \text{as} \quad \rho \to \infty, \tag{3.2}$$

where $L_0\Phi_{j0} \equiv \Delta_\rho\Phi_{j0} - \Phi_{j0} + 2w\Phi_{j0}$. We conclude that $N_{j0} = B_{j0}$. At next order, we obtain that N_{j1} satisfies

$$\Delta_\rho N_{j1} = -\left(1 - \frac{2w}{f}\right)\Phi_{j0} + \frac{w^2}{f^2\chi_0^2}N_{j0}, \qquad N_{j1} \sim c_{j0}\log\rho + B_{j1} \quad \text{as} \quad \rho \to \infty. \tag{3.3}$$

By using the divergence theorem on (3.3), we obtain that

$$c_{j0} = \frac{b}{f^2\chi_0^2}B_{j0} + \int_0^\infty \rho\left(\frac{2w}{f} - 1\right)\Phi_{j0}\,d\rho. \tag{3.4}$$

Next, we integrate the equation for Φ_{j0} in (3.2) to isolate $\int_0^\infty \rho\Phi_{j0}\,d\rho$ as

$$\int_0^\infty \rho\Phi_{j0}\,d\rho = \frac{1}{\lambda+1}\left[2\int_0^\infty \rho w\Phi_{j0}\,d\rho + \frac{b}{f\chi_0^2}B_{j0}\right]. \tag{3.5}$$

We then eliminate $\int_0^\infty \rho\Phi_{j0}\,d\rho$ in (3.4) for c_{j0}. Then, by substituting $c_j = \nu c_{j0} + \cdots$ and $B_j = B_{j0} + \cdots$ into the GCEP (2.30), we obtain in vector form that

$$(\mathcal{I} + 2\pi\nu\mathcal{G}_\lambda)\mathbf{c}_0 + \mathbf{B}_0 = 0, \tag{3.6}$$

where $\mathbf{c}_0 \equiv (c_{10}, \ldots, c_{N0})^T$ and $\mathbf{B}_0 \equiv (B_{10}, \ldots, B_{N0})^T$, and where for self-consistency we must ensure that $\nu\mathcal{G}_\lambda = \mathcal{O}(1)$ (as shown below). By substituting (3.5) and (3.4) into (3.6), we obtain a matrix expression for $\mathbf{B}_0$, which can be written as

$$\left[\frac{b}{f\chi_0^2}(\lambda + 1 - f)\mathcal{I} + f(\lambda + 1)\left(\mathcal{I} + 2\pi\nu\mathcal{G}_\lambda\right)^{-1}\right]\mathbf{B}_0 = -2(\lambda + 1 - f)\int_0^\infty \rho w\mathbf{\Phi}_0\,d\rho, \tag{3.7}$$

where $\mathbf{\Phi}_0 \equiv (\Phi_{10}, \ldots, \Phi_{N0})^T$. We then use (A.2 b) for χ_0, together with $S_0 = |\Omega|/(2\pi N\sqrt{D_0})$, to write

$$\frac{f^2\chi_0^2}{b} = D_0\theta, \qquad \theta \equiv \frac{4\pi^2 N^2(1-f)^2 b}{f^2|\Omega|^2}. \tag{3.8}$$

Upon substituting (3.7) into (3.2) for Φ_{j0}, and using (3.8), we obtain the vector NLEP

$$L_0\mathbf{\Phi}_0 - \mathcal{K}w^2\frac{\int_0^\infty \rho w\mathbf{\Phi}_0\,d\rho}{\int_0^\infty \rho w^2\,d\rho} = \lambda\mathbf{\Phi}_0, \qquad \mathbf{\Phi}_0 \to 0 \quad \text{as} \quad \rho \to \infty, \tag{3.9 a}$$

where the matrix $\mathcal{K}$ is given by

$$\mathcal{K} \equiv 2(\lambda + 1 - f)\left[(\lambda + 1 - f)\mathcal{I} + D_0\theta(\lambda + 1)\left(\mathcal{I} + 2\pi\nu\mathcal{G}_\lambda\right)^{-1}\right]^{-1}. \tag{3.9 b}$$

To diagonalize the vector NLEP, we introduce the matrix spectrum of the λ-dependent Green's matrix $\mathcal{G}_\lambda$ as

$$\mathcal{G}_\lambda \mathbf{v}_j = \kappa_j \mathbf{v}_j, \quad j = 1, \ldots, N. \tag{3.10}$$

In this way, in terms of κ_j, (3.9) yields the N scalar NLEPs given by

$$L_0 \Psi - \beta_j(\lambda) w^2 \frac{\int_0^\infty w\Psi\rho\,d\rho}{\int_0^\infty w^2\rho\,d\rho} = \lambda\Psi, \qquad \Psi \to 0 \quad \text{as} \quad \rho \to \infty, \tag{3.11 a}$$

where the N choices of the multiplier $\beta_j(\lambda)$ of the NLEP are

$$\beta_j = \frac{2(\lambda + 1 - f)}{(\lambda + 1)\left(1 + \frac{D_0\theta}{1+2\pi\nu\kappa_j}\right) - f}, \qquad j = 1, \ldots, N. \tag{3.11 b}$$

Here $D_0 = D\nu$, θ is defined in (3.8), and κ_j depends on λ through the Green's matrix $\mathcal{G}_\lambda$.

We will analyze (3.11) for two different parameter regimes that ensure that $\nu\kappa_j = \mathcal{O}(1)$ for at least some $j \in \{1, \ldots, N\}$. The first regime is the conventional NLEP regime where $D = D_0/\nu$ and $\tau = \mathcal{O}(1)$. This regime is studied in this section. The second, and new, regime is for $D = D_0/\nu$ but where τ has the anomalous scaling $\tau = \mathcal{O}(\epsilon^{-\tau_c}/\nu)$ for some $\tau_c > 0$. This second regime is motivated and analyzed in §3.2 below.

For the conventional regime where $D = D_0/\nu$ and $\tau = \mathcal{O}(1)$, we readily calculate from (2.28) that for $\nu \ll 1$

$$G_\lambda = \frac{D_0}{\nu\tau\lambda|\Omega|} + G_0 + \mathcal{O}(\nu), \qquad R_\lambda = \frac{D_0}{\nu\tau\lambda|\Omega|} + R_0 + \mathcal{O}(\nu), \tag{3.12}$$

where G_0 is the Neumann Green's function with regular part R_0 from (2.5). Thus, for $\nu \ll 1$, the Green's matrix is

$$\mathcal{G}_\lambda = \frac{D_0 N}{\nu\tau\lambda|\Omega|}\mathcal{E} + \mathcal{G}_0 + \mathcal{O}(\nu), \qquad \mathcal{E} \equiv \frac{1}{N}\mathbf{e}\mathbf{e}^T, \tag{3.13}$$

where $\mathbf{e} \equiv (1, \ldots, 1)^T$. Now since $\mathcal{E}\mathbf{e} = \mathbf{e}$ and $\mathcal{E}\mathbf{q}_j = 0$ for $j = 2, \ldots, N$, where $\mathbf{q}_j^T\mathbf{e} = 0$, the eigenvalues κ_j of $\mathcal{G}_\lambda$ are $\kappa_1 \sim D_0 N/[\nu\tau\lambda|\Omega|]$ and $\kappa_j = \mathcal{O}(1)$ for $j = 2, \ldots, N$. This yields that

$$2\pi\nu\kappa_1 \sim \frac{\mu}{\tau\lambda}; \qquad 2\pi\nu\kappa_j = \mathcal{O}(\nu), \quad \text{for} \quad j = 2, \ldots, N, \quad \text{where} \quad \mu \equiv \frac{2\pi N D_0}{|\Omega|}. \tag{3.14}$$

We refer to the eigenpair κ_1 and $\mathbf{v}_1 = \mathbf{e}$ as the synchronous mode, while the other $N-1$ eigenpairs κ_j and $\mathbf{v}_j = \mathbf{q}_j$, with $\mathbf{q}_j^T\mathbf{e} = 0$ for $j = 2, \ldots, N$, are referred to as the asynchronous, or competition, modes. We remark that the competition modes correspond to asynchronous perturbations in the spot amplitudes, as they preserve the sum of the spot amplitudes owing to the fact that $\mathbf{q}_j^T\mathbf{e} = 0$, for $j = 2, \ldots, N$.

Upon substituting (3.14) into (3.11), we obtain two distinct multipliers of the NLEP (3.11 a) corresponding to either asynchronous or synchronous perturbations in the spot amplitudes. They are given, respectively, by

$$\beta_a \equiv \frac{2(\lambda + 1 - f)}{(\lambda + 1)(1 + D_0\theta) - f}, \quad \beta_s \equiv \frac{2(\lambda + 1 - f)}{(\lambda + 1)h(\tau\lambda) - f}, \quad \text{where} \quad h(\tau\lambda) \equiv 1 + \frac{D_0\theta\tau\lambda}{\tau\lambda + \mu}, \quad \mu \equiv \frac{2\pi D_0 N}{|\Omega|}. \tag{3.15}$$

In [108] and [109] several key rigorous results have been established for the spectrum of NLEPs of the form (3.11 a) for the case where β_j is a bilinear function of λ, i.e. $\beta_j = (\tilde{c} + \tilde{d}\lambda)/(\tilde{e} + \tilde{f}\lambda)$. More recently in §2 of [94], a rigorous winding number approach has been developed to determine the number M of unstable eigenvalues of (3.11 a), satisfying $\text{Re}(\lambda) > 0$, for different ranges of the parameters in the NLEP with a bilinear multiplier. Since β_a in (3.15) is bilinear, these results can readily be used to analyze the linear stability properties of the asynchronous modes. One such specific result of [94] that pertains to these asynchronous modes is as follows:

Lemma 1 *Consider the NLEP (3.11 a) with a bilinear multiplier $\beta_j = (\tilde{c} + \tilde{d}\lambda)/(\tilde{e} + \tilde{f}\lambda)$. where $\tilde{c} > 0$, $\tilde{d} > 0$, $\tilde{e} > 0$, and $\tilde{f} > 0$ are constants. Then, if $\tilde{e}/\tilde{c} < 1$ and $\tilde{e}/\tilde{c} > \tilde{f}/\tilde{d}$, we have $M = 0$ and so any discrete eigenvalue of (3.11) satisfies $\text{Re}(\lambda) < 0$. In contrast, if $\tilde{e}/\tilde{c} > 1$ and $\tilde{f}/\tilde{d} > 1$, then $M = 1$ and so the NLEP has an unstable real positive eigenvalue.*

The proof of this result is given in Lemma 1 and Lemma 2 of [94], and is not repeated here. These results are readily used to obtain the following main linear stability result for the asynchronous modes.

Proposition 2 *Let $N \geq 2$ and consider the NLEP (3.11 a) for the asynchronous modes where $\beta = \beta_a$, as defined in*

(3.15). Then, $Re(\lambda) < 0$ if and only if $D_0 < D_{0c}$. When $D > D_{0c}$, the NLEP (3.11) has a unique positive real eigenvalue. This critical value D_{0c}, referred to as the competition stability threshold, is $D_{0c} = (1-f)/\theta$, and is given explicitly by

$$D_{0c} \equiv \frac{|\Omega|^2 f^2}{4\pi^2 N^2 b(1-f)}, \quad where \quad b \equiv \int_0^\infty \rho w^2 \, d\rho. \tag{3.16}$$

Proof: The proof follows by using Lemma 1 with $\tilde{e} = 1 + D_0\theta - f$, $\tilde{c} = 2(1-f)$, $\tilde{f} = 1 + D_0\theta$, and $\tilde{d} = 2$. We calculate that $\tilde{e}/\tilde{c} > 1$ iff $D_0\theta > 1 - f$ and $\tilde{f}/\tilde{d} > 1$ iff $D_0\theta > 1$. Since $0 < f < 1$, we conclude that $\tilde{e}/\tilde{c} > 1$ and $\tilde{f}/\tilde{d} > 1$ both hold when $D_0\theta > 1 - f$. The second result of Lemma 1 yields that $M = 1$ when $D_0\theta > 1 - f$. Next, we obtain that $\tilde{e}/\tilde{c} > \tilde{f}/\tilde{d}$ reduces to $f < (1 + D_0\theta)f$, which always holds. Therefore, from the first result of Lemma 1 we have $M = 0$ when $\tilde{e}/\tilde{c} < 1$, which yields $D_0\theta < (1-f)$. Finally, by using (3.8) for θ, the stability threshold $D_{0c} = (1-f)/\theta$ is given in (3.16). $\blacksquare$

An important observation is that the leading-order competition stability threshold $D \sim D_{0c}/\nu$ for $\nu \ll 1$ occurs as a result of a zero-eigenvalue crossing for an $N-1$ dimensional subspace of asynchronous perturbations in the spot amplitudes characterized by $\mathbf{q}_j^T \mathbf{e} = 0$ for $j = 2, \dots, N$. In this sense, this leading order stability threshold $D \sim D_{0c}/\nu$ is degenerate, and a higher-order asymptotic analysis is required to unfold this zero-eigenvalue crossing, and in such a way determine a more refined prediction of the competition instability threshold. In particular, by introducing the de-tuning parameter D_1 by $D = D_{0c}/\nu + D_1 + o(1)$, the detailed analysis given in [**17**], originating from [**16**], determines all of the eigenvalues λ within a small ball $|\lambda| = \mathcal{O}(\nu) \ll 1$ near the origin that are associated with asynchronous perturbations in the spot amplitudes. The main result of [**17**] (see also [**16**]), obtained from a rather lengthy higher-order asymptotic analysis involving the correction terms in the asymptotic expansion in (3.1), is as follows:

Proposition 3 *Let $\nu \ll 1$, $N \geq 2$, and suppose that the symmetry condition (2.32) on the spot configuration $\{\mathbf{x}_1, \dots, \mathbf{x}_N\}$ holds. Then, for $D = D_{0c}/\nu + D_1 + o(1)$, the spectrum of the NLEP corresponding to asynchronous perturbations in the spot amplitudes has discrete eigenvalues λ near the origin, with $|\lambda| = \mathcal{O}(\nu) \ll 1$, given by*

$$\lambda = 2\nu(1-f)\left[-\pi\kappa_{0j} + \frac{D_1}{2D_{0c}} + \frac{1}{2b^2(1-f)}\int_0^\infty \rho\tilde{v}_{1p}\,d\rho\right] + \mathcal{O}(\nu^2), \tag{3.17 a}$$

where $\tilde{v}_{1p}$ is defined in (A.1 d). Here κ_{0j} for $j = 2, \dots, N$ are the eigenvalues of the Neumann Green's matrix $\mathcal{G}_0$ in the $N-1$ dimensional subspace orthogonal to $\mathbf{e}$, i.e.

$$\mathcal{G}_0\mathbf{q}_j = \kappa_{0j}\mathbf{q}_j, \quad j = 2, \dots, N, \qquad \mathbf{q}_j^T\mathbf{e} = 0. \tag{3.17 b}$$

By setting $\lambda = 0$ in (3.17 a), Proposition 3 shows that $\lambda = 0$ at the (possibly) $N-1$ distinct values of D, given by

$$D \sim D_{j\epsilon} \equiv \frac{D_{0c}}{\nu}\left[1 + \nu\left(2\pi\kappa_{0j} - \frac{1}{b^2(1-f)}\int_0^\infty \rho\tilde{v}_{1p}\right)\right], \quad j = 2, \dots, N. \tag{3.18}$$

This result agrees precisely with that derived in (2.40) by identifying a zero-eigenvalue crossing from the nonlinear algebraic system (2.7). However, the result in Proposition 3 is more refined in that it characterizes all the eigenvalues near the origin when $D \sim D_{0c}/\nu + \mathcal{O}(1)$. Finally, the competition instability threshold, defined by $D_{\text{comp}} = \min_j D_{j\epsilon}$, is

$$D_{\text{comp}} \sim \frac{D_{0c}}{\nu}\left[1 + \nu\left(2\pi\kappa_{\min} - \frac{1}{b^2(1-f)}\int_0^\infty \rho\tilde{v}_{1p}\right)\right], \qquad \kappa_{\min} \equiv \min_{j\in\{2,\dots,N\}}\kappa_{0j}. \tag{3.19}$$

For the asynchronous modes, we have $Re(\lambda) < 0$ when $D < D_{\text{comp}}$.

The interpretation of these zero-eigenvalue crossings for the asynchronous modes is that they correspond to bifurcation values of D where asymmetric solution branches of quasi-equilibria, characterized by spots of different source strengths, bifurcate from the common source strength solution of (2.7). To leading order in ν when $D = D_0/\nu$, the emergence of such asymmetric solution branches is predicted to occur at the common bifurcation point $D = D_{0c}/\nu$, where this leading-order threshold is in fact independent of whether the symmetry condition (2.32) holds or not. However, the higher-order analysis of [**17**], resolving the degeneracy of the leading-order threshold and leading to (3.18), relies crucially on the assumption (2.32) that $\mathbf{e}$ is an eigenvector of $\mathcal{G}_0$. In fact, if the spot configuration is such that $\mathbf{e}$ is not an eigenvector of $\mathcal{G}_0$, then we conjecture that the inclusion of higher order terms in ν leads to an imperfection sensitivity in the bifurcation structure of

solutions to the nonlinear algebraic system (2.7). This imperfection sensitivity structure was first identified in [**89**] in the context of three localized spots on the sphere (see Fig. 5–6 in [**89**]).

We suggest four specific **open problems**:

- For a given domain shape Ω, numerically identify both quasi-equilibrium and steady-state spot configurations for which the symmetric condition (2.32) holds. Recall that steady-state spot patterns are equilibria of the DAE system (2.8).
- For any $N \geq 2$, analyze the local imperfection sensitivity of solution branches to (2.7) for $D = D_{0c}/\nu + O(1)$ when the symmetry condition (2.32) fails to hold. Analyze the linear stability of these branches from NLEP theory.
- For the case where (2.32) holds, develop a weakly nonlinear theory for competition instabilities to show that they correspond to subcritical bifurcations. Full numerical computations (cf. [**93**]) have shown that this linear instability mechanism triggers a nonlinear process through which spots are annihilated in finite time.
- Extend the methodology of [**17**] for calculating refined thresholds for competition instabilities to other RD systems with localized spot solutions, such as the Gray-Scott, Schnakenberg, and Gierer-Meinhardt RD systems.

3.2 Hopf Bifurcation Threshold

In this sub-section we analyze the spectrum of the NLEP (3.11 a) for the synchronous mode where the multiplier β_s is given in (3.15). We first observe that for $\tau \ll 1$, we have $\beta_s = 2 + \mathcal{O}(\tau)$, so that by Theorem 3.7 of [**108**] we have $\mathrm{Re}(\lambda) < 0$. Therefore, the synchronous mode is linearly stable for all D_0 when $\tau \ll 1$. Secondly, we observe from (3.15) that $\beta_s = 2$ when $\lambda = 0$, which yields the null-solution $\Psi = 0$. Therefore, $\lambda = 0$ can never be an eigenvalue of the NLEP (3.11) for the synchronous mode for any parameter values. As such, it is natural to seek Hopf bifurcation threshold values for τ where a complex conjugate pair of eigenvalues enter $\mathrm{Re}(\lambda) > 0$ through the imaginary axis as τ is increased. We remark that for the synchronous mode, the multiplier β_s is a biquadratic function of λ, for which only a few rigorous results on the NLEP spectrum are available (see Principal Result 4.5 of [**81**]). Since these results do not provide sharp bounds for the parameter space where a Hopf bifurcation occurs (see Principal Result 4.7 of [**81**]), we will proceed below by seeking a new parameterization of the Hopf threshold.

First, we readily observe that the discrete eigenvalues of (3.11 a) with multiplier β_s are the roots λ of $g(\lambda) = 0$, where

$$g(\lambda) \equiv \frac{(\lambda + 1)h(\tau\lambda) - f}{2(\lambda + 1 - f)} - \mathcal{F}(\lambda), \qquad \mathcal{F}(\lambda) \equiv \frac{\int_0^\infty w \left[(L_0 - \lambda)^{-1} w^2 \right] \rho \, d\rho}{\int_0^\infty w^2 \rho \, d\rho}, \tag{3.20}$$

where $h(\tau\lambda)$ is given in (3.15). We now look for a purely complex root $\lambda = i\lambda_I$ to $g(i\lambda_I) = 0$ by decomposing $\mathcal{F}(i\lambda_I)$ into real and imaginary parts as $\mathcal{F}(i\lambda_I) = \mathcal{F}_R(\lambda_I) + i\mathcal{F}_I(\lambda_I)$, where

$$\mathcal{F}_R(\lambda_I) \equiv \frac{\int_0^\infty \rho w L_0 \left[L_0^2 + \lambda_I^2 \right]^{-1} w^2 \, d\rho}{\int_0^\infty \rho w^2 \, d\rho}, \qquad \mathcal{F}_I(\lambda_I) \equiv \lambda_I \frac{\int_0^\infty \rho w \left[L_0^2 + \lambda_I^2 \right]^{-1} w^2 \, d\rho}{\int_0^\infty \rho w^2 \, d\rho}. \tag{3.21}$$

By setting $g(i\lambda_I) = 0$ and separating (3.20) into real and imaginary parts, and solving for τ and D_0, we obtain after some lengthy but straightforward algebraic manipulations an implicitly-defined parameterization, with parameter λ_I, of any Hopf bifurcation curve $\tau = \tau_H(D_0)$. This parameterization has the form

$$D_0\theta = \frac{z_R^2 + z_I^2}{z_I}, \qquad \frac{\tau}{\mu} = \frac{z_I}{\lambda_I z_R}, \tag{3.22 a}$$

where $\mu = 2\pi N D_0/|\Omega|$. Here z_I and z_R are defined by

$$z_R = \frac{k_I - \lambda_I k_R - \lambda_I f}{1 + \lambda_I^2}, \qquad z_I = \frac{k_R + \lambda_I k_I - \lambda_I^2 - (1 - f)}{1 + \lambda_I^2}, \tag{3.22 b}$$

in terms of k_R and k_I given by

$$k_R = 2(1 - f)\mathcal{F}_R(\lambda_I) - 2\lambda_I \mathcal{F}_I(\lambda_I), \qquad k_I = 2\lambda_I \mathcal{F}_R(\lambda_I) + 2(1 - f)\mathcal{F}_I(\lambda_I). \tag{3.22 c}$$

By varying λ_I on $0 < \lambda_I < \infty$, and numerically computing $\mathcal{F}_R$ and $\mathcal{F}_I$ from (3.21), we obtain a Hopf bifurcation curve in the τ/μ versus D_0/D_{0c} parameter plane, where $D_{0c} \equiv (1 - f)/\theta$. This is shown in Fig. 6(a) for $f = 0.5$. The corresponding eigenvalue, denoted by λ_{IH} is plotted versus D_0/D_{0c} in Fig. 6(b). By specifying N and $|\Omega|$, and using $\mu = 2\pi N D_0/|\Omega|$,

the curve in Fig. 6(a) determines τ_H. From Fig. 6(a), we observe that there is a unique Hopf bifurcation threshold τ_H for the synchronous mode only on the range $D_0 > D_{0c}$. However, it is only on this range of D_0 that a competition instability associated with the asynchronous modes always occurs for any $\tau > 0$. Our numerical results shown in Fig. 6 also suggest that $\tau_H \to +\infty$ and $\lambda_{IH} \to 0^+$ as $D_0 \to D_{0c}^+$.

To determine the scaling of the Hopf bifurcation threshold as $D \to D_{0c}^+$ from above, we first need to recall the following properties of $\mathcal{F}_R$ and $\mathcal{F}_I$ as $\lambda_I \to 0$ as rigorously established in [**101**]:

$$\mathcal{F}_R(\lambda_I) \sim 1 - \kappa_c \lambda_I^2 + \cdots, \quad \text{as} \quad \lambda_I \to 0^+; \qquad \mathcal{F}_R'(\lambda_I) < 0 \quad \text{for} \quad \lambda_I > 0; \qquad \mathcal{F}_R(\infty) = 0, \tag{3.23 a}$$

$$\mathcal{F}_I(\lambda_I) \sim \lambda_I/2, \quad \text{as} \quad \lambda_I \to 0^+; \qquad \mathcal{F}_I(\lambda_I) > 0 \quad \text{for} \quad \lambda_I > 0; \qquad \mathcal{F}_I(\infty) = 0, \tag{3.23 b}$$

where $\kappa_c \equiv \int_0^\infty \rho \left(w + \rho w'/2 \right)^2 d\rho / \int_0^\infty \rho w^2 d\rho \approx 0.436$. This numerical result for κ_c was obtained by numerically computing the ground-state solution w from (A.1 c) and using a numerical quadrature. By substituting (3.23) into (3.22 a), and defining $\mu_0 \equiv 2\pi N D_{0c}/|\Omega|$, we readily derive the limiting asymptotics

$$\lambda_{IH} \sim \sqrt{\frac{D_0}{D_{0c}} - 1} \left(\frac{1}{(1-f)^2} - 2\kappa_c \right)^{-1/2}, \qquad \tau_H \sim \frac{\mu_0(1-f)}{\left(\frac{D_0}{D_{0c}} - 1 \right)} \left(\frac{1}{(1-f)^2} - 2\kappa_c \right), \quad \text{as} \quad D_0 \to D_{0c}^+. \tag{3.24}$$

Since $0 < f < 1$ and $2\kappa_c < 1$, we remark that the expression above for λ_{IH} is well-defined.

Since our parameterization of the Hopf threshold has shown that there is no Hopf bifurcation threshold value of τ for the range $D_0 < D_{0c}$, we conclude that the synchronous mode is linearly stable when $D_0 < D_{0c}$ for any $\tau > 0$. Since the asynchronous modes are also linearly stable when $D_0 < D_{0c}$ from Proposition 2, it follows that for any $\tau > 0$ with $\tau = \mathcal{O}(1)$ an N-spot quasi-equilibrium pattern is linearly stable on the parameter regime $D = D_0/\nu \gg 1$, whenever $D_0 < D_{0c}$, where D_{0c} is given in (3.16). This implies that on $D_0 < D_{0c}$ and when $\tau = \mathcal{O}(1)$, an N-spot quasi-equilibrium pattern will exhibit slow spot dynamics over the long $t = \mathcal{O}(\epsilon^{-2})$ time-scale towards some steady-state spot configuration. Recall that this slow spot dynamics was characterized by Proposition 1.
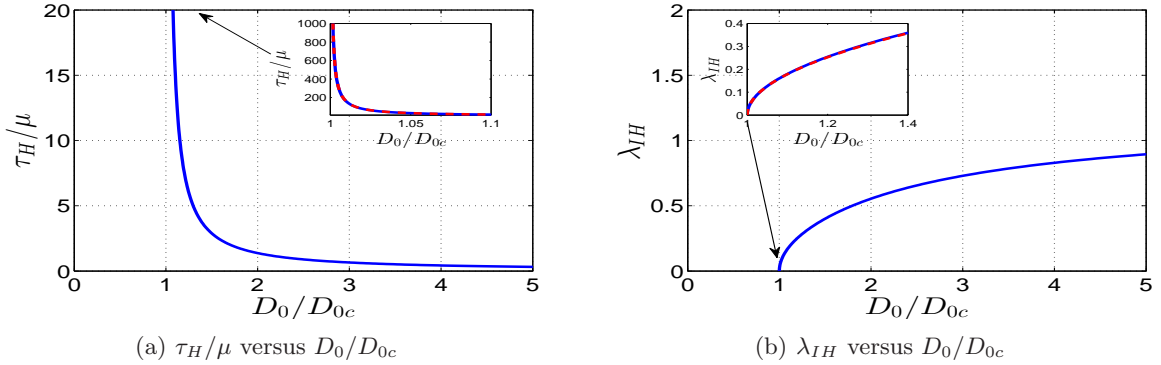

(a) τ_H/μ versus D_0/D_{0c} (b) λ_{IH} versus D_0/D_{0c}

FIGURE 6. Plot of the Hopf bifurcation threshold τ_H/μ (left panel) and imaginary eigenvalue λ_{IH} (right panel) versus D_0/D_{0c} when $f = 0.5$ for the synchronous mode of instability for the Brusselator, as obtained from (3.22). There is no Hopf threshold for $D_0/D_{0c} < 1$, and $\tau_H \to +\infty$ while $\lambda_{IH} \to 0^+$ as $D_0/D_{0c} \to 1^+$. The inserts validate the asymptotic results of (3.24) (dashed curves) for τ_H/μ and λ_{IH} as $D_0/D_{0c} \to 1^+$.

Although, for $\tau = \mathcal{O}(1)$, there is no synchronous oscillatory instability of the spot amplitudes for an N-spot quasi-equilibrium pattern on the parameter range $D_0 < D_{0c}$ where the asynchronous mode is linearly stable, the result in (3.24) that $\tau_H \to +\infty$ as $D_0 \to D_{0c}^+$ suggests that we revisit the NLEP analysis allowing for $\tau \gg 1$. By examining a modified NLEP problem we will show that, in fact, there is a Hopf bifurcation when $D < D_{0c}$ for which $\tau_H \gg 1$ as $\epsilon \to 0$.

With this motivation, we now consider the new limiting regime where $\tau \gg 1$, in such a way that $|\tau \lambda \nu/D_0| \gg 1$. To analyze this regime, we first reformulate the NLEP (3.11) by observing that its discrete spectra are the union of the roots λ of $g_j(\lambda) = 0$, for $j = 1, \ldots, N$, where

$$g_j(\lambda) \equiv \frac{1}{2} + \frac{(\lambda+1)}{2(\lambda+1-f)} \frac{D_0(1-f)}{D_{0c}(1+2\pi\nu\kappa_j)} - \mathcal{F}(\lambda), \qquad \mathcal{F}(\lambda) \equiv \frac{\int_0^\infty w \left[(L_0 - \lambda)^{-1} w^2 \right] \rho \, d\rho}{\int_0^\infty w^2 \rho \, d\rho}. \tag{3.25}$$

Here κ_j for $j = 1, \ldots, N$, which depend on λ, are the eigenvalues of the Green's matrix $\mathcal{G}_\lambda$ in (3.10).

In the limit $|\tau\lambda\nu/D_0| \gg 1$, the Green's function $G_\lambda(\mathbf{x};\mathbf{x}_0)$ of (2.28) decays rapidly away from $\mathbf{x}_0$ so that, except within a thin boundary layer near $\partial\Omega$, it is well-approximated by the free-space Green's function given by

$$G_\lambda(\mathbf{x};\mathbf{x}_0) \sim \frac{1}{2\pi} K_0\left(\theta_\lambda |\mathbf{x} - \mathbf{x}_0|\right) , \qquad \theta_\lambda \equiv \sqrt{\tau\lambda\nu/D_0} . \tag{3.26}$$

Here the principal branch of the square root is specified to ensure that $G_\lambda(\mathbf{x};\mathbf{x}_0)$ decays exponentially away from $\mathbf{x}_0$. By using the local behavior of the modified Bessel function $K_0(z) \sim -\log z + \log 2 - \gamma_e + \mathcal{O}(z^2 \log z)$, where $\gamma_e \approx 0.57721\ldots$ is Euler's constant, we calculate that the regular part of G_λ at $\mathbf{x}_0$, defined in (2.28), is simply

$$R_\lambda \equiv \frac{1}{2\pi}\left(-\frac{1}{2}\log(\nu\tau\lambda) + \log\left(2\sqrt{D_0}\right) - \gamma_e\right) . \tag{3.27}$$

When $|\theta_\lambda| \gg 1$, the off-diagonal entries of the Green's matrix $\mathcal{G}_\lambda$ are exponentially small and can be neglected. Therefore, for $|\theta_\lambda| \gg 1$, we have $\mathcal{G}_\lambda \sim R_\lambda \mathcal{I}$, so that (3.10) yields the common matrix eigenvalue $\kappa_j \sim R_\lambda$ for $j = 1, \ldots, N$. This shows that in the regime $|\theta_\lambda| \gg 1$, any temporal oscillations of the spot amplitudes cannot be classified as being either synchronous or asynchronous. More specifically, since $\mathcal{G}_\lambda$ is, asymptotically, a multiple of the identity, the perturbations of the spot amplitudes, characterized by the eigenvectors $\mathbf{v}_j$ for $j = 1, \ldots, N$ of $\mathcal{G}_\lambda$, now span all of $\mathbb{R}^N$.

A key observation is that we can enforce $\nu\kappa_j = \mathcal{O}(1)$ in (3.25) when $\theta_\lambda \gg 1$ by introducing a positive exponent $\tau_c > 0$ together with an anomalous re-scaling of τ in terms of ϵ, of the form

$$\tau \equiv \epsilon^{-\tau_c}/\nu . \tag{3.28}$$

To ensure that the consistency condition (2.19) holds, we must require that τ_c is not too large, so that $\epsilon^{2-\tau_c}\lambda/D_0 \ll 1$. By using the scaling (3.28) in (3.27), we get in terms of Euler's constant γ_e that

$$2\pi\nu\kappa_j = -\frac{\tau_c}{2} + \nu\mathcal{K}_0 , \qquad \mathcal{K}_0 \equiv -\frac{1}{2}\log\lambda + \log\left(2\sqrt{D_0}\right) - \gamma_e . \tag{3.29}$$

By substituting (3.29) into (3.25) we obtain that the $g_j(\lambda)$, for $j = 1, \ldots, N$, reduce to the common "modified" NLEP

$$g_c(\lambda) \equiv \frac{1}{2} + \frac{(\lambda+1)}{2D_{0c}(\lambda+1-f)}\frac{D_0(1-f)}{\left(1-\frac{\tau_c}{2}+\nu\mathcal{K}_0\right)} - \mathcal{F}(\lambda) , \qquad \mathcal{F}(\lambda) \equiv \frac{\int_0^\infty w\left[(L_0-\lambda)^{-1} w^2\right]\rho\,d\rho}{\int_0^\infty w^2\rho\,d\rho} . \tag{3.30}$$

In this parameter regime, where $|\theta_\lambda| \gg 1$, the discrete eigenvalues of the NLEP (3.11) are the roots λ of $g_c(\lambda) = 0$.

We now determine a Hopf bifurcation threshold value of τ_c by seeking a pure imaginary pair of roots to (3.30) with $\lambda = i\lambda_I$ and $\lambda_I \ll 1$. By setting $g_c(i\lambda_I) = 0$, and separating the resulting expression into real and imaginary parts, we can obtain asymptotic expansions for τ_c and λ_I upon using the local behavior $\mathcal{F}(i\lambda_I) \sim 1 + i\lambda_I/2 - \kappa_c\lambda_I^2 + \cdots$ for $\lambda_I \ll 1$ from (3.23). After some algebraic manipulations, we obtain the following main result:

Proposition 4 *Consider an N-spot quasi-equilibrium pattern for the Brusselator (1.2) when $D = D_0/\nu$ and $D_0 < D_{0c}$, where D_{0c} is the competition instability threshold defined in (3.16). Then, for $\nu \ll 1$ the NLEP (3.11) has a Hopf bifurcation, corresponding to temporal oscillations in the spot amplitudes, when $\tau = \tau_H$ and $\lambda = \pm i\lambda_I$, where*

$$\tau_H \sim \frac{1}{\nu}\epsilon^{-\tau_c} , \quad \tau_c = 2\left(1 - \frac{D_0}{D_{0c}}\right) - \nu\log\nu + \nu\left(2\log\left(2\sqrt{D_0}\right) - 2\gamma_e - \log\lambda_{I0}\right) + \mathcal{O}(\nu^2) ,$$

$$\lambda \sim i\nu\lambda_{I0} + \mathcal{O}(\nu^3) , \qquad \lambda_{I0} \equiv \frac{\pi D_{0c}}{4D_0}(1-f) . \tag{3.31}$$

We now make some remarks on this main result. We first observe that since $D_0 < D_{0c}$, we have for $\nu \ll 1$ that $0 < \tau_c < 2$, and so with $\lambda = \mathcal{O}(\nu)$ it follows that the consistency condition (2.19) always holds. Secondly, we observe that in the regime $D_0 < D_{0c}$ where the anomalous scaling (3.28) applies, the Hopf bifurcation threshold depends only on the number of spots and is independent of their spatial locations. This feature was also shown to hold in the limit $\nu \ll 1$ for the conventional NLEP analysis in the regime $D_0 > D_{0c}$ and $\tau = \mathcal{O}(1)$, where (3.22) holds. Finally, we remark that our analysis is not uniformly valid in the limit $D_0 \to D_{0c}^+$ where $\tau_c \to 0^+$. It is only in the thin transition regime, for which $D_0/D_{0c} - 1 \ll 1$, where the spatial configuration of spots is important for determining the Hopf bifurcation threshold. To study this transition regime, it is convenient to set $g_j(i\lambda_I) = 0$ in (3.25) and solve for κ_j. This yields that the Hopf

bifurcation threshold is $\tau_H = \min_j \tau_{Hj}$, where τ_{Hj} and λ_{Ij} are the roots of the complex-valued system

$$\kappa_j + \frac{1}{2\pi\nu}\left[1 - \frac{D_0(1-f)}{2D_{0c}}\frac{(\lambda+1)}{(\lambda+1-f)\left(\mathcal{F}(i\lambda_I)-1/2\right)}\right] = 0\,, \qquad j = 1,\ldots,N\,. \tag{3.32}$$

Here κ_j for $j = 1,\ldots,N$ are the eigenvalues of the Green's matrix $\mathcal{G}_\lambda$, which depends on the configuration of spots. Numerical results for the Hopf bifurcation from this formulation are shown in [**93**].

3.3 Periodic Spot Patterns

In this sub-section we highlight some results for the linear stability of steady-state periodic spot patterns for the Brusselator (1.2) when the spots are centered in the limit $\epsilon \to 0$ at the lattice points of a general oblique Bravais lattice Λ with fixed area $|\Omega|$ of the primitive cell of the lattice. To leading order in $\nu = -1/\log\epsilon$, the linearization of the steady-state periodic spot pattern has a zero eigenvalue when $D = D_{0c}/\nu$, where

$$D_{0c} \equiv \frac{f^2|\Omega|^2}{4\pi^2 b(1-f)}\,, \qquad b \equiv \int_0^\infty \rho w^2\,d\rho\,, \tag{3.33}$$

and where $w(\rho)$ is the ground-state satisfying (A.1 c) . This leading-order threshold depends only on the area $|\Omega|$ of the primitive cell, and is independent of the specific lattice Λ. Analogous to that analyzed in §3.1 for spot patterns on a finite domain, this zero eigenvalue corresponds to a competition instability of the spot amplitudes.

Before giving the main linear stability result, and discussing our criterion to identify the optimal lattice, we outline a few basic facts regarding Bravais lattices and their duals and we introduce some terminology. Let $\boldsymbol{l}_1$ and $\boldsymbol{l}_2$ denote two linearly independent vectors in $\mathbb{R}^2$, with angle θ between them, where for convenience $\boldsymbol{l}_1$ is aligned with the positive x_1-axis. The Bravais lattice Λ is defined in terms of these generators $\boldsymbol{l}_1$ and $\boldsymbol{l}_2$ by

$$\Lambda = \left\{m\boldsymbol{l}_1 + n\boldsymbol{l}_2 \,\middle|\, m,\, n \in \mathbb{Z}\right\}, \tag{3.34}$$

where $\mathbb{Z}$ denotes the set of integers. The *primitive* cell is the parallelogram obtained by $\boldsymbol{l}_1$ and $\boldsymbol{l}_2$ of area $|\boldsymbol{l}_1 \times \boldsymbol{l}_2|$. The *Wigner-Seitz* (WS) or Voronoi cell centered at a given lattice point of Λ consists of all points in the plane that are closer to this point than to any other lattice point. The WS cell is a convex polygon with the same area of the primitive cell, and the union of the WS cells tile all of $\mathbb{R}^2$, i.e. $\mathbb{R}^2 = \bigcup_{z\in\Lambda}(z + \Omega)$, where Ω is the fundamental WS cell centered at the origin $\mathbf{x} = \mathbf{0}$. In Fig. 7 we give a schematic plot of the union of the WS cells for a specific Bravais lattice.
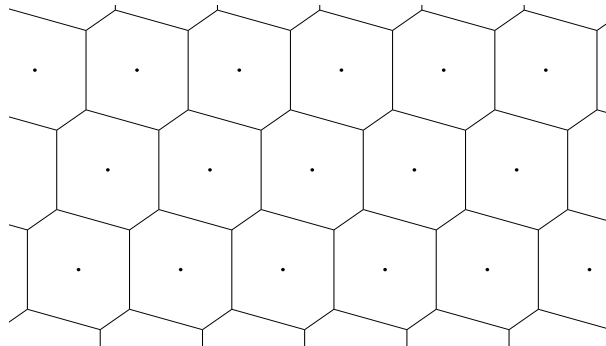

FIGURE 7. WS cells for an oblique Bravais lattice with generators $\boldsymbol{l}_1 = (1,0)$, $\boldsymbol{l}_2 = (\cot\theta, 1)$, and $\theta = 74°$, so that $|\Omega| = 1$. These cells tile $\mathbb{R}^2$. The boundary of the WS cells generically (except for the square) consist of three pairs of parallel lines of equal length.

Following [**8**], we define the reciprocal or dual lattice $\Lambda^\star$ in terms of the two independent vectors $\boldsymbol{d}_1$ and $\boldsymbol{d}_2$, which are obtained from the lattice Λ by requiring that

$$\boldsymbol{d}_i \cdot \boldsymbol{l}_j = \delta_{ij}\,, \tag{3.35}$$

where δ_{ij} is the Kronecker symbol. The reciprocal lattice $\Lambda^\star$ is defined by

$$\Lambda^\star = \left\{m\boldsymbol{d}_1 + n\boldsymbol{d}_2 \,\middle|\, m,\, n \in \mathbb{Z}\right\}. \tag{3.36}$$

The first Brillouin zone, labeled by Ω_B, is defined as the WS cell centered at the origin in the reciprocal space.

In our linear stability analysis below for periodic spot patterns for the Brusselator (1.2), we require some properties of the regular part $R_{b0}(\boldsymbol{k})$ of the Bloch Green's function $G_{b0}(\mathbf{x})$ for the Laplacian, which for $\boldsymbol{k}/(2\pi) \in \Omega_B \backslash \{\boldsymbol{0}\}$ satisfies

$$\Delta G_{b0} = -\delta(\mathbf{x}); \qquad G_{b0}(\mathbf{x} + \boldsymbol{l}) = e^{-i\boldsymbol{k}\cdot\boldsymbol{l}} G_{b0}(\mathbf{x}), \qquad \boldsymbol{l} \in \Lambda. \tag{3.37 a}$$

In terms of G_{b0}, the regular part $R_{b0}(\boldsymbol{k})$ of this Bloch Green's function is defined by

$$R_{b0}(\boldsymbol{k}) \equiv \lim_{\mathbf{x}\to 0} \left(G_{b0}(\mathbf{x}) + \frac{1}{2\pi}\log|\mathbf{x}| \right). \tag{3.37 b}$$

The following results, as established in Lemmas 2.1 and 2.2 of [37], provide two key properties of $R_{b0}(\boldsymbol{k})$.

Lemma 2 *The regular part $R_{b0}(\boldsymbol{k})$ of the Bloch Green's function $G_{b0}(\mathbf{x})$ satisfying (3.37 a) is real-valued for $|\boldsymbol{k}| \neq 0$.*

Lemma 3 *For $|\boldsymbol{k}| \to 0$, the regular part $R_{b0}(\boldsymbol{k})$ has the singular asymptotic behavior*

$$R_{b0}(\boldsymbol{k}) \sim \frac{1}{\boldsymbol{k}^T \mathcal{Q} \boldsymbol{k}} = \mathcal{O}(|\mathcal{Q}^{1/2}\boldsymbol{k}|^{-2}) \gg 1, \quad as \quad |\boldsymbol{k}| \to 0, \tag{3.38}$$

where $\mathcal{Q}$ is a positive-definite matrix defined in terms of the lattice generators.

In [17] (see also [16]) the spectrum of the linearization of a periodic steady-state pattern for the Brusselator (1.2) was analyzed when D is near the critical threshold D_{0c}/ν. Upon introducing the de-tuning parameter D_1 by

$$D = \frac{D_{0c}}{\nu} + D_1 + o(1),$$

we use the method of matched asymptotic expansions to calculate the steady-state solution in the fundamental WS cell. This solution is then extended periodically to the entire lattice. Upon linearizing (1.2) around this periodic solution, and letting $\epsilon \to 0$, it follows that the eigenfunction Ψ for the perturbation in the long-range solution component u satisfies an elliptic PDE with coefficients that are spatially periodic on the lattice. Therefore, by the Floquet-Bloch theorem this eigenfunction must satisfy the quasi-periodic boundary conditions $\Psi(\mathbf{x} + \boldsymbol{l}) = e^{-i\boldsymbol{k}\cdot\boldsymbol{l}}\Psi(\mathbf{x})$ for $\boldsymbol{l} \in \Lambda$, $\mathbf{x} \in \mathbb{R}^2$ and $\boldsymbol{k}/(2\pi) \in \Omega_B \backslash \{\boldsymbol{0}\}$. From a detailed characterization of the fundamental WS cell (see §2 in [37]), this quasi-periodicity condition can be used to formulate a boundary operator $\mathcal{P}_k$ on the boundary $\partial\Omega$ of the WS cell (see equation (2.35) of [37]). Then, from imposing a solvability condition on the correction terms to the leading-order NLEP problem, similar to that in the derivation of Proposition 3, we can explicitly determine the continuous band of spectrum lying within an $\mathcal{O}(\nu)$ ball of the origin in the spectral plane when $D = D_{0c}/\nu + D_1$. This band of spectrum is real-valued and depends on the regular part $R_{b0}(\boldsymbol{k})$ of the Bloch Green's function for the Laplacian as well as the de-tuning parameter D_1.

In this way, from our combination of singular perturbation analysis, Floquet-Bloch theory, and NLEP theory, the following main result characterizing this band of spectra was derived in Proposition 5.1 of [17] (see also [16]):
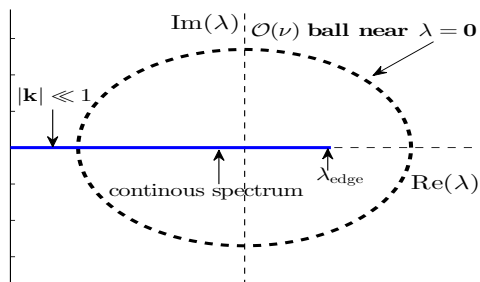

FIGURE 8. The continuous band of spectra near the origin when $D = D_{0c}/\nu + D_1$ (see (3.39)).

Proposition 5 *In the limit $\epsilon \to 0$, consider a steady-state periodic pattern of spots for the Brusselator (1.2) where the spots are centered at the lattice points of a Bravais lattice Λ where the fundamental WS cell Ω has area $|\Omega|$. Then, for $D = D_{0c}/\nu + D_1$, where D_{0c} is given in (3.33), the portion of the continuous spectrum of the linearization that satisfies*

$|\lambda| \leq \mathcal{O}(\nu) \ll 1$, *is given by*

$$\lambda = 2(1-f)\nu \left[-\pi R_{b0} + \frac{D_1}{2D_{0c}} + \frac{1}{2b^2(1-f)} \int_0^\infty \rho \tilde{v}_{1p} \, d\rho \right] + \mathcal{O}(\nu^2), \tag{3.39}$$

where $\tilde{v}_{1p}$ is defined in (A.1 d). Here $R_{b0} = R_{b0}(\mathbf{k})$ is the regular part of the Bloch Green's function G_{b0}, satisfying (3.37 a), with $\mathbf{k}/(2\pi) \in \Omega_B \backslash \{\mathbf{0}\}$.

Since $R_{b0}(\mathbf{k})$ is real-valued from Lemma 2, this result shows that the band of spectrum satisfying $|\lambda| = \mathcal{O}(\nu) \ll 1$ when $D = D_{0c}/\nu + \mathcal{O}(1)$ is also real-valued. Thus, to determine the stability threshold for a given lattice Λ, we need only locate the right-most edge of the band as $\mathbf{k}/(2\pi)$ is varied in the first Brillouin zone of the reciprocal lattice, and ensure that this leading edge satisfies $\lambda < 0$. Although (3.39) is not uniformly valid as $\mathbf{k} \to 0$, owing to the fact that $R_{b0} = \mathcal{O}(|\mathcal{Q}^{1/2}\mathbf{k}|^{-2}) \to +\infty$ as $|\mathbf{k}| \to 0$ from Lemma 3, we observe that $\lambda < 0$ for $\mathcal{O}(\nu^{1/2}) \ll |\mathbf{k}| \ll 1$. Therefore, long-wavelength perturbations do not determine the stability threshold. For a schematic plot of the spectrum near the origin see Fig. 8.

We conclude from (3.39) that a periodic pattern of spots on a fixed lattice Λ is linearly stable on $\mathcal{O}(1)$ time-scales when

$$D_1 < D_1^\star \equiv D_{0c} \left[2\pi R_{b0}^\star - \frac{1}{b^2(1-f)} \int_0^\infty \rho \tilde{v}_{1p} \, d\rho \right], \qquad R_{b0}^\star \equiv \min_{\mathbf{k}/(2\pi) \in \Omega_B} R_{b0}(\mathbf{k}). \tag{3.40}$$

Then, for a fixed area $|\Omega|$ of the WS cell, we define the *optimal* lattice Λ as the one that maximizes $D_1^\star$, thereby maximizing the range of D for which the periodic spot pattern is linearly stable. This leads to the following result:

Proposition 6 *The optimal arrangement of a periodic pattern of spots for the Brusselator (1.2) is the one for which $R_{b0}^\star$ is maximized over the class of Bravais lattices (3.34) with fixed area $|\Omega|$ of the primitive cell. A two-term asymptotic expansion for this optimal stability threshold for D is*

$$D_{optim} \sim \frac{D_{0c}}{\nu} \left[1 + \nu \left(2\pi \max_\Lambda R_{b0}^\star - \frac{1}{b^2(1-f)} \int_0^\infty \rho \tilde{v}_{1p} \, d\rho \right) \right], \qquad R_{b0}^\star \equiv \min_{\mathbf{k}/(2\pi) \in \Omega_B} R_{b0}(\mathbf{k}), \tag{3.41}$$

where D_{0c} is given in (3.33). Here $R_{b0}(\mathbf{k})$ satisfies (3.37 a), $\tilde{v}_{1p}$ is defined in (A.1 d), and $b \equiv \int_0^\infty w^2 \rho \, d\rho$ where $w(\rho) > 0$ is the ground-state solution of (A.1 c).

In order to numerically identify the optimal lattice, an explicit and rapidly converging infinite series representation for $R_{b0}(\mathbf{k})$ is required. This was done in §6 of [**37**], based on an Ewald-type summation procedure resulting from the Poisson summation formula, as motivated by [**8**]. From §6 of [**37**], we have

$$R_{b0}(\mathbf{k}) = \sum_{\mathbf{d} \in \Lambda^*} \exp\left(-\frac{|2\pi\mathbf{d} - \mathbf{k}|^2}{4\eta^2} \right) \frac{1}{|2\pi\mathbf{d} - \mathbf{k}|^2} + \sum_{\substack{\mathbf{l} \in \Lambda \\ \mathbf{l} \neq \mathbf{0}}} e^{i\mathbf{k}\cdot\mathbf{l}} F_{\text{sing}}(\mathbf{l}) - \frac{\gamma_e}{4\pi} - \frac{\log \eta}{2\pi}, \tag{3.42}$$

where $F_{\text{sing}}(\mathbf{l}) = E_1(|\mathbf{l}|^2\eta^2)/(4\pi)$, $E_1(z) = \int_z^\infty t^{-1}e^{-t} \, dt$ is the exponential integral (cf. §5.1.1 of [**1**]), and γ_e is Euler's constant. Here $\eta > 0$ is an Ewald cut-off parameter, used to ensure rapid convergence of the two infinite sums in (3.42) over the lattice and its dual. This rapidly converging infinite series representation was used in [**37**] to readily calculate the minimum value $R_{b0}^\star$ of $R_{b0}(\mathbf{k})$ over the first Brillouin zone.

Then, by using the explicit representation (3.42) of $R_{b0}(\mathbf{k})$ in [**37**] (see Fig. 5 and Fig. 7 in [**37**]), a numerical sweep in $\mathbf{k}/(2\pi)$ over the first Brillouin zone together with a sweep over the class of Bravais lattices with $|\Omega| = 1$, has identified that $R_{b0}^\star$ is maximized for a regular hexagonal lattice. With this numerical procedure, we identify that it is the hexagonal lattice that has an optimum stability threshold, in the sense that for such a lattice the periodic spot pattern is linearly stable for the largest range of D.

This approach to identify optimal lattice arrangements of spots was developed in [**37**] for the Gierer-Meinhardt, Schnakenberg, and Gray-Scott models. Results similar to Propositions 5 and 6, but with other model-dependent objective functions to optimize involving both the regular parts of the Bloch Green's function and the periodic Green's function, were derived in [**37**] for the Gray-Scott, Schnakenberg, and Gierer-Meinhardt RD models. For each of these RD models, by performing this optimization procedure numerically it was established that the regular hexagonal lattice has the optimal stability threshold. The extension of this method to the Brusselator (see [**16**] and [**17**]) is more involved as the underlying NLEP has two nonlocal terms, one of which must be eliminated in a self-consistent way.

Three specific **open problems** in this area are the following:

- Establish analytically, rather than numerically, that over the class of Bravais lattices with fixed area $|\Omega| = 1$ of the primitive cell, $R_{b0}^\star$ is maximized for a regular hexagon.
- Extend the NLEP stability analysis for periodic patterns to consider a honeycomb-type periodic arrangement of localized spots. Does such a lattice offer a larger stability threshold for D?
- For a periodic pattern of spots on a Bravais lattice, analyze the small eigenvalues of $\mathcal{O}(\epsilon^2)$ in the spectrum of the linearization and identify the corresponding optimal lattice. For this analysis we require an explicit representation for a new type of Bloch-Green's function having a dipole singularity.

4 Two Specific Applications of Strong Localized Perturbation Theory

In this section we discuss two related problems in 2-D where strong localized perturbation theory has been applied to resolve the effect of small traps or patches for a linear scalar PDE.

4.1 Eigenvalue Problem in a 2-D Domain with Traps

We now show a clear analogy between the GCEP (2.30) for spot patterns of the Brusselator (1.2) and the problem in [**45**] (see also [**99**] and [**22**]) of calculating the lowest eigenvalue of the Laplacian in a bounded planar 2-D domain Ω with a reflecting outer boundary that is perturbed by the presence of N small holes, or traps, of a common radius ϵ in the interior of Ω. The eigenvalue problem for the case of N such localized traps is formulated as

$$\Delta u + \lambda u = 0, \quad \mathbf{x} \in \Omega \backslash \Omega_p; \qquad \int_{\Omega \backslash \Omega_p} u^2 \, d\mathbf{x} = 1, \tag{4.1 a}$$

$$\partial_n u = 0, \quad \mathbf{x} \in \partial\Omega; \qquad u = 0, \quad \mathbf{x} \in \partial\Omega_p \equiv \cup_{i=1}^N \partial\Omega_{\epsilon_i}. \tag{4.1 b}$$

Here $\Omega_p = \cup_{i=1}^N \Omega_{\epsilon_i}$ is a collection of N small interior holes or traps Ω_{ϵ_i}, for $i = 1, \ldots, N$, of an assumed common shape, with radius ϵ, centered at $\mathbf{x}_i$ for $i = 1, \ldots, N$, with $|\mathbf{x}_i - \mathbf{x}_j| = \mathcal{O}(1)$ for $i \neq j$ as $\epsilon \to 0$.

The objective in [**45**] was to determine an asymptotic expansion of the lowest eigenvalue λ_0 of (4.1), which must tend to zero as $\epsilon \to 0$. This lowest eigenvalue determines the average mean first capture time $\bar{v}$ for a Brownian particle, with diffusivity D, to become absorbed at one of the N traps (cf. [**82**], [**73**]). In particular, for $\epsilon \to 0$, we have (cf. [**73**])

$$\bar{v} \sim \frac{1}{D\lambda_0}. \tag{4.2}$$

The asymptotic methodology of [**45**] to determine an approximation λ_0^* to λ_0 that accounts for all logarithmic terms in the asymptotic expansion, as initiated in [**99**], is closely related to the approach used in §2.1 to derive the GCEP (2.30) governing the linear stability of N-spot quasi-equilibria for the Brusselator (1.2). We only briefly highlight this methodology and some results from it here.

In the inner region near the j-th trap Ω_{ϵ_j}, the canonical local problem is to solve

$$\Delta_{\mathbf{y}} v_c = 0, \quad \mathbf{y} \notin \Omega_0; \qquad v_c = 0, \quad \mathbf{y} \in \partial\Omega_0, \tag{4.3 a}$$

$$v_c \sim \log |\mathbf{y}| - \log d + o(1), \quad \text{as} \quad |\mathbf{y}| \to \infty, \tag{4.3 b}$$

where $\mathbf{y} \equiv \epsilon^{-1}(\mathbf{x} - \mathbf{x}_j)$ and $\Omega_0 \equiv \epsilon^{-1}\Omega_{\epsilon_j}$. In (4.3 b), the constant d depends on the shape of Ω_0 and is called the logarithmic capacitance of Ω_0 (cf. [**76**]). Since it is known analytically only for a few simple shapes (cf. [**76**], [**99**], [**51**]), d must in general be computed numerically (cf. [**24**]). In terms of some unknown constant S_j, the inner solution for (4.1) near the j-th trap is $u \sim S_j v_c(\mathbf{y})$, where $\nu \equiv -1/\log(\epsilon d)$. By asymptotically matching the far-field behavior of this inner solution we can readily obtain a singularity condition for the outer solution to (4.1).

As shown in [**45**] (see also [**99**] and [**100**]), we have that $\lambda_0(\epsilon) = \lambda_0^*(\nu) + \mathcal{O}(\sigma)$, where $\sigma \ll \nu^m$ for any $m > 0$. Here $\lambda_0^*(\nu)$ is the lowest eigenvalue of the outer problem with singularity conditions

$$\Delta u^* + \lambda_0^* u^* = 0, \quad \mathbf{x} \in \Omega \backslash \{\mathbf{x}_1, \ldots, \mathbf{x}_N\}; \qquad \int_\Omega (u^*)^2 \, d\mathbf{x} = 1; \qquad \partial_n u^* = 0, \quad \mathbf{x} \in \partial\Omega, \tag{4.4 a}$$

$$u^* \sim S_j \log |\mathbf{x} - \mathbf{x}_j| + S_j/\nu, \quad \text{as} \quad \mathbf{x} \to \mathbf{x}_j, \quad \text{for} \quad j = 1, \ldots, N, \tag{4.4 b}$$

where S_j, for $j = 1, \ldots, N$, and λ_0^* is to be found. In comparison with the derivation of the GCEP (2.30) for the stability of spot patterns, (4.3) and (4.4) replace (2.25) and (2.26), respectively.

To represent the solution to (4.4) we introduce the Helmholtz Green's function, $G_h(\mathbf{x}; \mathbf{x}_0)$, and its regular part, $R_h(\mathbf{x}_0)$, satisfying

$$\Delta G_h + \lambda_0^* G_h = -\delta(\mathbf{x} - \mathbf{x}_0)\,, \quad \mathbf{x} \in \Omega\,; \qquad \partial_n G_h = 0\,, \quad \mathbf{x} \in \partial\Omega\,, \qquad (4.5\,a)$$

$$G_h(\mathbf{x}; \mathbf{x}_0) \sim -\frac{1}{2\pi} \log|\mathbf{x} - \mathbf{x}_0| + R_h(\mathbf{x}_0) + o(1)\,, \quad \text{as} \quad \mathbf{x} \to \mathbf{x}_0\,. \qquad (4.5\,b)$$

In terms of this Helmholtz Green's function, we have $u^* = -2\pi \sum_{i=1}^N S_i G_h(\mathbf{x}; \mathbf{x}_i)$, and from the singularity conditions in (4.4 b) we obtain the homogeneous matrix system

$$(\mathcal{I} + 2\pi\nu\mathcal{G}_h)\,\mathbf{S} = \mathbf{0}\,, \qquad (4.6)$$

where $\mathbf{S} \equiv (S_1, \ldots, S_N)^T$. Here λ_0^* is a root of $\det(\mathcal{I} + 2\pi\nu\mathcal{G}_h) = 0$, where $\mathcal{G}_h$ is the Helmholtz Green's function defined by

$$(\mathcal{G}_h)_{ij} \equiv \begin{cases} R_h(\mathbf{x}_j) & i = j \\ G_h(\mathbf{x}_i; \mathbf{x}_j) & i \neq j \end{cases}. \qquad (4.7)$$

To obtain a two-term expansion for the lowest eigenvalue $\lambda_0^* \ll 1$, we use the small λ_0^* asymptotics of (4.5) to obtain

$$\mathcal{G}_h \sim -\frac{N}{|\Omega|\lambda_0^*}\mathcal{E} + \mathcal{G}_0 + \mathcal{O}(\lambda_0^*)\,, \qquad \text{where} \qquad \mathcal{E} \equiv \frac{1}{N}\mathbf{e}\mathbf{e}^T\,, \quad \mathbf{e} \equiv (1, \ldots, 1)^T\,, \qquad (4.8)$$

and $\mathcal{G}_0$ is the Neumann Green's matrix of (2.7 b). Upon substituting (4.8) into (4.6), and introducing σ^* by

$$\lambda_0^* \equiv \frac{2\pi N\nu}{|\Omega|}\sigma^*\,, \qquad (4.9)$$

we obtain the matrix eigenvalue problem

$$\left[\mathcal{I} + 2\pi\nu\mathcal{G}_0 + \mathcal{O}(\nu^2)\right]^{-1}\mathcal{E}\mathbf{S} = \sigma^*\mathbf{S}\,. \qquad (4.10)$$

By calculating the approximate inverse for $\nu \ll 1$ in (4.10), we obtain that

$$\mathcal{E}\mathbf{S} - 2\pi\nu\mathcal{G}_0\mathcal{E}\mathbf{S} + \mathcal{O}(\nu^2) = \sigma^*\mathbf{S}\,. \qquad (4.11)$$

Since $\mathcal{E}\mathbf{e} = \mathbf{e}$, we readily obtain that $\sigma^* = 1 + \nu\sigma_1^* + \cdots$ and $\mathbf{S} = \mathbf{e} + \nu\mathbf{S}_1 + \cdots$, where

$$(\mathcal{E} - \mathcal{I})\,\mathbf{S}_1 = \mathbf{f} \equiv \sigma_1^*\mathbf{e} + 2\pi\mathcal{G}_0\mathcal{E}\mathbf{e}\,. \qquad (4.12)$$

From the Fredholm alternative, we require that $\mathbf{e}^T\mathbf{f} = 0$. Upon using $\mathcal{E}\mathbf{e} = \mathbf{e}$ and $\mathbf{e}^T\mathbf{e} = N$, this gives $\sigma_1^* = -2\pi N^{-1}\mathbf{e}^T\mathcal{G}_0\mathbf{e}$, which yields a two-term expansion for σ^* and λ_0^*. The result, given in equation (2.24) of [**45**], is summarized as follows:

Proposition 7 *Let λ_0 be the smallest eigenvalue of (4.1) when Ω has N small traps of radius $\mathcal{O}(\epsilon) \ll 1$ of a common shape centered at $\mathbf{x}_1, \ldots, \mathbf{x}_N$ with $|\mathbf{x}_i - \mathbf{x}_j| = \mathcal{O}(1)$ as $\epsilon \to 0$. Then, for $\epsilon \to 0$, a two-term expansion for λ_0 is*

$$\lambda_0 \sim \lambda_0^* = \frac{2\pi N\nu}{|\Omega|} - \frac{4\pi^2\nu^2}{|\Omega|}p(\mathbf{x}_1, \ldots, \mathbf{x}_N) + \mathcal{O}(\nu^3)\,, \qquad \text{where} \qquad p(\mathbf{x}_1, \ldots, \mathbf{x}_N) \equiv \mathbf{e}^T\mathcal{G}_0\mathbf{e}\,. \qquad (4.13)$$

Here $\mathcal{G}_0$ is the Neumann Green's matrix in (2.7 b), and $\nu \equiv -1/\log(\epsilon d)$, where d is the common logarithmic capacitance of the traps, as defined by (4.3).

For a fixed N, an interesting optimization problem is to determine the spatial configuration of traps that minimize $p(\mathbf{x}_1, \ldots, \mathbf{x}_N)$. Such a configuration of traps minimizes the average mean first capture time $\bar{v}$ of a Brownian particle with diffusivity D, given for $\epsilon \to 0$ by $\bar{v} \sim 1/(D\lambda_0^*)$. When Ω is the unit disk, for which $\mathcal{G}_0$ can be calculated explicitly, it was shown in [**45**] that this problem of minimizing $\bar{v}$ is equivalent to the discrete variational problem of minimizing the function $\mathcal{H}_{\text{ball}}(\mathbf{x}_1, \ldots, \mathbf{x}_N)$ defined by

$$\mathcal{H}_{\text{ball}}(\mathbf{x}_1, \ldots, \mathbf{x}_N) = -\sum_{j=1}^N \sum_{\substack{k=1 \\ k \neq j}}^N \log|\mathbf{x}_j - \mathbf{x}_k| - \sum_{j=1}^N \sum_{k=1}^N \log|1 - \mathbf{x}_j\bar{\mathbf{x}}_k| + N\sum_{j=1}^N |\mathbf{x}_j|^2\,, \qquad |\mathbf{x}_j| < 1\,, \qquad (4.14)$$

for $\mathbf{x}_j \neq \mathbf{x}_k$ when $j \neq k$, and where $\bar{\mathbf{x}}_k$ denotes the complex conjugate of $\mathbf{x}_k$.

The minimization of (4.14) is a challenging numerical problem for large N owing to the existence of a large number of local minima with nearly identical energies. If one instead considers a restricted optimization problem whereby N traps are equally-spaced on a ring of radius r_0 concentric within the unit disk, we can readily calculate that (cf. [**45**])

$$\lambda_0^* = 2N\nu - 4\pi\nu^2 p(r_0) + \mathcal{O}(\nu^3); \qquad p(r_0) \equiv \frac{1}{2\pi}\left[-N\log\left(Nr_0^{N-1}\right) - N\log\left(1 - r_0^{2N}\right) + r_0^2 N^2 - \frac{3N^2}{4}\right]. \qquad (4.15)$$

For such a ring-pattern of N traps, the optimal trap configuration that minimizes the average MFPT is the one that minimizes $p(r_0)$ on $0 < r_0 < 1$. Upon comparing (4.15) with (2.11) and (2.12), we observe that the optimal ring radius of traps is identical to the equilibrium ring radius for a ring-pattern of spots for the Brusselator (1.2).

We remark that a result analogous to (4.13) can be derived for the related singularly perturbed eigenvalue problem where N locally circular traps of a common radius ϵ are centered at $\mathbf{x}_j$ for $j = 1, \ldots, N$ on the surface of the unit sphere, for which $|\mathbf{x}_j| = 1$ (cf. [**22**]). Since the curvature of the sphere provides only a negligible $\mathcal{O}(\epsilon)$ correction to the solution in the inner region near each trap, the two-term asymptotics for the lowest eigenvalue is obtained by using (2.13) for the Neumann Green's function on the sphere in (4.13), together with $d = 1$ and $|\Omega| = 4\pi$. In this way, the following result was derived in equation (4.17) of [**22**]:

Proposition 8 *Let λ_0 be the smallest eigenvalue of the Laplacian on the surface Ω of the unit sphere, when Ω has N small locally circular traps of a common radius ϵ centered at $\mathbf{x}_1, \ldots, \mathbf{x}_N$ with $|\mathbf{x}_i - \mathbf{x}_j| = \mathcal{O}(1)$ as $\epsilon \to 0$. Then, for $\epsilon \to 0$ a two-term expansion for λ_0 is*

$$\lambda_0 \sim \lambda_0^* = \frac{\nu N}{2} + \nu^2\left[-\frac{N^2}{4}\left(2\log 2 - 1\right) - p(\mathbf{x}_1, \ldots, \mathbf{x}_N)\right] + \mathcal{O}(\nu^3), \qquad (4.16\,a)$$

where $\nu \equiv -1/\log\epsilon$ and $p(\mathbf{x}_1, \ldots, \mathbf{x}_N)$ is the discrete logarithmic energy on the sphere, defined by

$$p(\mathbf{x}_1, \ldots, \mathbf{x}_N) \equiv -\sum_{i=1}^{N}\sum_{j>i}^{N}\log|\mathbf{x}_j - \mathbf{x}_i|. \qquad (4.16\,b)$$

This result shows that the optimal configuration $\{\mathbf{x}_1, \ldots, \mathbf{x}_N\}$ of the centers of the traps that minimizes the expected mean first capture time for a Brownian particle on the surface of the unit sphere is at the so-called elliptic Fekete points that minimize the discrete logarithmic energy $p(\mathbf{x}_1, \ldots, \mathbf{x}_N)$. This well-known discrete variational problem has a long history in approximation theory (cf. [**50**], [**75**]). As discussed at the end of §2, this optimization problem is closely related to the problem of identifying stable equilibria for N-spot patterns for the Brusselator (1.2) on the unit sphere.

Our discussion here has only focused on the 2-D problem. We remark that the extension of (4.1) to the 3-D context leads to different scaling laws for the lowest eigenvalue (cf. [**70**], [**99**], [**21**]).

A few specific **open problems** for the 2-D case are the following:

- In the unit disk, determine the optimal spatial configuration of $N \gg 1$ circular traps, valid in the dilute fraction limit $N\pi\epsilon^2/|\Omega| \ll 1$, that globally minimizes the discrete energy $\mathcal{H}_{\text{ball}}$ in (4.14). Determine rigorously, following a similar framework as in [**7**], a scaling law valid for $N \gg 1$ for the optimal energy $\mathcal{H}_{\text{ball}}$. In particular, does the optimal arrangement of the centers of the traps have a hexagonal lattice structure in the interior of the unit disk, together with a boundary layer near the rim of the disk?
- By computing the Neumann Green's matrix $\mathcal{G}_0$ numerically using fast-multipole methods (cf. [**48**]), use the two-term asymptotics (4.13) to investigate optimal trap configurations in other planar domains or on closed manifolds.
- For the unit sphere, study the relationship between elliptic Fekete point distributions and stable equilibria of the DAE system (2.14) governing slow spot dynamics in the Brusselator (1.2).

4.2 The Persistence Threshold Problem in a Patchy 2-D Landscape

In [**55**] strong localized perturbation theory was used to analyze the persistence threshold for the diffusive logistic model in a 2-D planar domain with spatially localized food resources, referred to here as patches. We now highlight a few results of [**55**] and suggest some open problems.

The diffusive logistic model describing the evolution of a population with density $u(\mathbf{x}, t)$ with constant diffusivity

$D = 1/\lambda > 0$ throughout some habitat represented by a bounded domain $\Omega \subset \mathbb{R}^2$, is formulated as [**86**]

$$u_t = \Delta u + \lambda u \left[m_\epsilon(\mathbf{x}) - u \right], \quad x \in \Omega \in \mathbb{R}^2; \qquad \partial_n u = 0, \quad \mathbf{x} \in \partial\Omega; \qquad u(\mathbf{x}, 0) = u_0(\mathbf{x}) \geq 0, \qquad \mathbf{x} \in \Omega. \qquad (4.17)$$

With the Neumann boundary condition on $\partial\Omega$ we assume that there is no population flux either into, or out of, the domain. The "habitat" function $m_\epsilon(\mathbf{x})$, specified in detail below, represents the growth rate for the species and models the available food resources. In favorable parts of the habitat we have $m_\epsilon(\mathbf{x}) > 0$, while in unfavorable parts $m_\epsilon(\mathbf{x}) < 0$, with $\int_\Omega m_\epsilon(\mathbf{x}) \, dx$ representing the total amount of resources available in the spatially heterogeneous environment.

To study the stability of the extinct solution $u = 0$, we set $u = \phi(\mathbf{x}) e^{-\sigma t}$ in (4.17) and linearize to get

$$\Delta\phi + \lambda m_\epsilon(\mathbf{x})\phi = -\sigma\phi, \quad \mathbf{x} \in \Omega; \qquad \partial_n \phi = 0, \quad \mathbf{x} \in \partial\Omega. \qquad (4.18)$$

The threshold value of λ for species persistence is determined by finding the first zero-eigenvalue crossing in σ for (4.18). This persistence threshold is characterized by the first eigenpair (λ_1, ϕ_1) of the indefinite weight eigenvalue problem

$$\Delta\phi + \lambda m_\epsilon(\mathbf{x})\phi = 0, \quad \mathbf{x} \in \Omega; \qquad \partial_n \phi = 0, \quad \mathbf{x} \in \partial\Omega. \qquad (4.19)$$

We refer to $\lambda_1 > 0$ as the positive principal eigenvalue of (4.19) if the corresponding eigenfunction ϕ_1 satisfies $\phi_1 > 0$ in Ω. It is well-known that there is a unique positive principal eigenvalue λ_1 iff $\int_\Omega m_\epsilon \, d\mathbf{x} < 0$ and the set $\Omega^+ \equiv \{\mathbf{x} \in \Omega \; ; \; m_\epsilon(\mathbf{x}) > 0\}$ has positive measure (cf. [**10**], [**35**], [**84**]).

The positive principal eigenvalue λ_1 is the persistence threshold for the specifies, in that if $\lambda < \lambda_1$, then for (4.17) it follows that $u(\mathbf{x}, t) \to 0$ uniformly in $\bar{\Omega}$ for all non-negative initial data, so that the population tends to extinction. In contrast, if $\lambda > \lambda_1$, then $u(\mathbf{x}, t) \to u^*(x)$ uniformly in $\bar{\Omega}$ as $t \to \infty$, where u^* is the unique positive steady-state solution of (4.17), and so the species will persist (cf. [**12**], [**13**] and the monograph [**15**]).

A key problem, originally posed in [**12**] and [**14**], is to determine among all habit functions $m_\epsilon(\mathbf{x})$ for which a persistence threshold exists, which such $m_\epsilon(\mathbf{x})$ yields the smallest λ_1 for a fixed amount of total resources $\int_\Omega m_\epsilon \, d\mathbf{x}$. For (4.18) in $\mathbb{R}^2$ it was proved in Theorem 1.1 of [**57**] that the optimal $m_\epsilon(\mathbf{x})$ is piecewise continuous. For the 1-D analogue of (4.18) it was proved in Theorem 1.2 of [**57**] that the optimal $m_\epsilon(x)$ consists of a single favorable habitat attached to one of the two endpoints of the interval. Related results in a cylindrical domain are given in [**39**].

In [**55**] a restricted optimization problem for (4.18) was analyzed in which $m_\epsilon(x)$ was taken to be piecewise constant and localized within N small circular patches of radii $\mathcal{O}(\epsilon)$, each of which is centered either inside Ω or on $\partial\Omega$. A spatially uniform background habit $-m_b$ was prescribed. The domain boundary $\partial\Omega$ was assumed to be piecewise differentiable, with a finite numbers of corners, each with a non-zero contact angle. Our piecewise continuous form for $m_\epsilon(x)$, specified in detail below, is motivated by the optimality result of Theorem 1.1 of [**57**], and the more local result of [**80**], which establishes that a sufficiently small optimum favorable habitat must be a circular disk. In the formulation of [**55**], $\Omega^I \equiv \{\mathbf{x}_1, \ldots, \mathbf{x}_N\} \cap \Omega$ is the set of the centers of the interior patches and $\Omega^B \equiv \{\mathbf{x}_1, \ldots, \mathbf{x}_N\} \cap \partial\Omega$ is the set of the centers of the boundary patches, where we assume that $|\mathbf{x}_i - \mathbf{x}_j| = \mathcal{O}(1)$ for $i \neq j$ and $\text{dist}(\mathbf{x}_j, \partial\Omega) \gg \mathcal{O}(\epsilon)$ for $\mathbf{x}_j \in \Omega^I$. For each patch, we associate an angle $\pi\alpha_j$ denoting the angular fraction of a small circular patch that is contained within Ω. In particular, $\alpha_j = 2$ when $\mathbf{x}_j = \Omega^I$, $\alpha_j = 1$ when $\mathbf{x}_j \in \Omega^B$ and $\mathbf{x}_j$ is a point where $\partial\Omega$ is smooth, and $\alpha_j = 1/2$ when $\mathbf{x}_j \in \partial\Omega$ is at a corner point of $\partial\Omega$ where the two (one-sided) tangent lines to the boundary intersect at a $\pi/2$ contact angle (see Fig. 9). With this notation, the piecewise constant habitat function $m = m_\epsilon(\mathbf{x})$ in (4.19) is specified in terms of constants m_b and m_j for $j = 1, \ldots, N$ by

$$m = m_\epsilon(x) \equiv \begin{cases} m_j/\epsilon^2, & x \in \Omega_{\epsilon_j}, \quad j = 1, \ldots, N, \\ -m_b, & x \in \Omega \setminus \bigcup_{j=1}^n \Omega_{\epsilon_j}, \end{cases} \qquad (4.20)$$

where $\Omega_{\epsilon_j} \equiv \{\mathbf{x} \, | \, |\mathbf{x} - \mathbf{x}_j| \leq \epsilon\rho_j \cap \Omega\}$. To specify that the j-th patch is a favorable or unfavorable habitat we set $m_j > 0$ or $m_j < 0$, respectively. In terms of $m_\epsilon(\mathbf{x})$, the criterion of [**10**], [**35**], and [**84**] for the existence of a persistence threshold is that $m_J > 0$ for some $J \in \{1, \ldots, N\}$, and that $\int_\Omega m_\epsilon(\mathbf{x}) \, d\mathbf{x} < 0$. For $\epsilon \ll 1$, this second condition is satisfied when

$$\int_\Omega m_\varepsilon \, dx = -m_b |\Omega| + \frac{\pi}{2} \sum_{j=1}^N \alpha_j m_j \rho_j^2 + \mathcal{O}(\epsilon^2) < 0, \qquad (4.21)$$

where $|\Omega|$ is the area of Ω. A schematic plot of a domain Ω having both interior and boundary patches is shown in Fig. 9.

In [**55**] strong localized perturbation theory was used to derive a two-term asymptotic expansion for the persistence threshold λ_1 in powers of $\nu = -1/\log\epsilon$ for $\epsilon \ll 1$. This result involves both the Neumann Green's function G_0, defined in
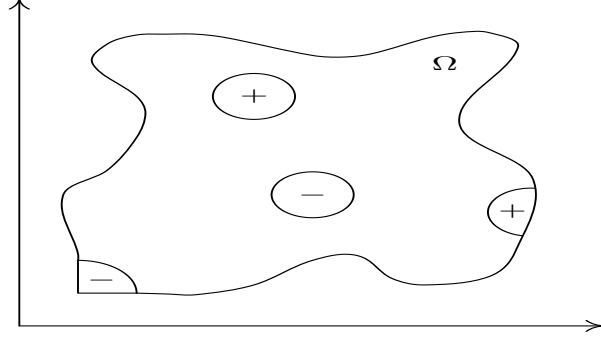
FIGURE 9. Schematic plot of a 2-D domain Ω with localized strongly favorable $(+)$ or unfavorable $(-)$ habitats, or patches, as given by (4.20). The interior patches are small circular disks. On the domain boundary, the patches are the portions of circular disks that lie within the domain. The unfavorable boundary habitat in the lower left corner of this figure is at a $\pi/2$ corner of $\partial\Omega$.

(2.5), and the surface Neumann Green's function $G_{0s}(\mathbf{x}; \mathbf{x}_0)$, defined for $\mathbf{x}_0 \in \partial\Omega$, by

$$\Delta G_{0s} = \frac{1}{|\Omega|}, \quad \mathbf{x} \in \Omega; \qquad \partial_n G_{0s} = 0, \qquad \mathbf{x} \in \partial\Omega \backslash \{\mathbf{x}_0\}; \qquad \int_\Omega G_{0s}\, d\mathbf{x} = 0, \tag{4.22 a}$$

$$G_{0s}(\mathbf{x}; \mathbf{x}_0) \sim -\frac{1}{\alpha_0 \pi} \log |\mathbf{x} - \mathbf{x}_0| + R_{0s}(\mathbf{x}_0), \quad \text{as } \mathbf{x} \to \mathbf{x}_0 \in \partial\Omega. \tag{4.22 b}$$

Here $R_{0s}(\mathbf{x}_0)$ is the regular part of the surface Neumann Green's function at $\mathbf{x} = \mathbf{x}_0$. The second-term in the asymptotic expansion of λ_1 given below in (4.24) is written in terms of a modified Green's function $G_m(\mathbf{x}; \mathbf{x}_j)$ depending on whether $\mathbf{x}_j$ is in the interior or on the boundary of Ω. We define G_{0m} by

$$G_{0m}(\mathbf{x}; \mathbf{x}_j) \equiv \begin{cases} G_0(\mathbf{x}; \mathbf{x}_j), & \mathbf{x}_j \in \Omega, \\ G_{0s}(\mathbf{x}; \mathbf{x}_j), & \mathbf{x}_j \in \partial\Omega, \end{cases} \tag{4.23 a}$$

where $G_0(\mathbf{x}; \mathbf{x}_j)$ is the Neumann Green's function of (2.5). The local singular behavior of $G_{0m}(\mathbf{x}; \mathbf{x}_j)$, given by

$$G_{0m}(\mathbf{x}; \mathbf{x}_j) \sim -\frac{1}{\alpha_j \pi} \log |\mathbf{x} - \mathbf{x}_j| + R_{0m}(\mathbf{x}_j), \quad \text{as } \mathbf{x} \to \mathbf{x}_j, \qquad R_{0m}(\mathbf{x}_j) \equiv \begin{cases} R_0(\mathbf{x}_j), & \mathbf{x}_j \in \Omega, \\ R_{0s}(\mathbf{x}_j), & \mathbf{x}_j \in \partial\Omega, \end{cases} \tag{4.23 b}$$

gives the regular part $R_{0m}(\mathbf{x}_j)$ of G_{0m}. The two-term asymptotics for λ_1 (see Principal Result 3.1 of [**55**]) is as follows:

Proposition 9 *Consider the habit function $m_\epsilon(\mathbf{x})$ of (4.20), and assume that $m_J > 0$ for some $J \in \{1, \ldots, N\}$ and that (4.21) holds. In the limit $\epsilon \to 0$ of small patch radius, the positive principal eigenvalue λ_1 of (4.19) has the asymptotics*

$$\lambda_1 = \mu_0 \nu + \mu_1 \nu^2 + \mathcal{O}(\nu^3); \qquad \mu_1 \equiv -\mu_0 \nu^2 \left(\frac{\kappa^t \left(\pi \mathcal{G}_{0m} - \mathcal{P}\right) \kappa}{\kappa^t \kappa} + \frac{1}{4} \right), \tag{4.24}$$

where $\nu \equiv -1/\log \epsilon$. Here $\mu_0 > 0$ is the first positive root of $\mathcal{B}(\mu_0) = 0$, where $\mathcal{B}(\mu_0)$ is defined by

$$\mathcal{B}(\mu_0) \equiv -m_b |\Omega| + \pi \sum_{j=1}^N \frac{\alpha_j m_j \rho_j^2}{2 - m_j \rho_j^2 \mu_0}. \tag{4.25}$$

In (4.24), $\kappa = (\kappa_1, \ldots, \kappa_N)^t$, where κ_j is defined by $\kappa_j \equiv \sqrt{\alpha_j} m_j \rho_j^2 / \left(2 - m_j \rho_j^2 \mu_0\right)$, while $\mathcal{G}_{0m}$ and $\mathcal{P}$ are the $N \times N$ matrices with matrix entries defined by

$$(\mathcal{G}_{0m})_{ij} = \sqrt{\alpha_i \alpha_j} G_{0mij}, \quad i \neq j; \qquad (\mathcal{G}_{0m})_{jj} = \alpha_j R_{0mjj}; \qquad (\mathcal{P})_{ij} = 0, \quad i \neq j; \qquad (\mathcal{P})_{jj} = \log \rho_j. \tag{4.26}$$

Since $\int_\Omega m_\epsilon\, d\mathbf{x} < 0$ from (4.21), we have $\mathcal{B}(0) < 0$ together with $\mathcal{B}(\mu_0) \to +\infty$ as $\mu_0 \to 2/(m_J \rho_J^2)$ from below, where

$$m_J \rho_J^2 \equiv \max_{m_j > 0} \{ m_j \rho_j^2 \,|\, j = 1, \ldots, N \}. \tag{4.27}$$

Then, since $\mathcal{B}'(\mu_0) > 0$ on $0 < \mu_0 < 2/(m_J \rho_J^2)$, we must have a unique root $\mu_0 = \mu_0^\star$ on $0 < \mu_0 < 2/(m_J \rho_J^2)$ to $\mathcal{B}(\mu_0) = 0$. This root provides the leading-order term in the asymptotic expansion of the positive principal eigenvalue of (4.19).

In [**55**] the effect of fragmentation and the location of favorable habitats on the coefficients μ_0 and μ_1 in the asymptotic expansion of the persistence threshold λ_1 was analyzed under the assumption that $\int_\Omega m_\epsilon \, d\mathbf{x}$ in (4.21) is fixed, so that there is a prescribed amount of resources. More specifically, the goal in [**55**] was to determine the patch configuration that minimizes μ_0, or in certain degenerate situations, minimizes the coefficient μ_1 in (4.24), under the constraint that

$$-m_b|\Omega| + \frac{\pi}{2} \sum_{j=1}^{N} \alpha_j m_j \rho_j^2 + \mathcal{O}(\epsilon^2) = \int_\Omega m_\epsilon \, d\mathbf{x} = -K \,, \tag{4.28}$$

for some fixed constant $K > 0$. For the case of exactly one favorable habitat, the following result was obtained in [**55**]:

Proposition 10 *For a favorable habitat of area $\pi\epsilon^2$, λ_1 is always smaller for a boundary patch than for an interior patch. For a domain boundary with corners, λ_1 is minimized when the boundary patch is centered at the corner with the smallest corner contact angle $\pi\alpha_1$, as opposed to a patch on the smooth part of the boundary, only if $\alpha_1 < 1$. For a domain with smooth boundary, for which $\alpha_1 = 1$ for any $\mathbf{x}_1 \in \partial\Omega$, λ_1 in (4.24) is minimized when the center $\mathbf{x}_1$ of the boundary patch is located at the global maximum of the regular part $R_{0s}(\mathbf{x}_1)$ of the surface Neumann Green's function of (4.22) on $\partial\Omega$.*

This result shows that the movement of a single favorable habitat to the boundary of the domain is advantageous for the persistence of the species.

A related question is to study the effect of the fragmentation of resources on the leading-order term μ_0 for the persistence threshold in (4.24). More specifically, suppose that the i-th patch, of radius $\epsilon\rho_i$ and growth rate $m_i > 0$ is split into two distinct patches, one with radius $\epsilon\rho_j$ and growth rate $m_j > 0$, and the other with radius $\epsilon\rho_k$ and growth rate $m_k > 0$, while maintaining $m_i \rho_i^2 = m_j \rho_j^2 + m_k \rho_k^2$ so that the constraint (4.28) holds. We assume that $\alpha_i = \alpha_j = \alpha_k$, so that we are either splitting an interior patch into two interior patches, or a boundary patch into two boundary patches, with each boundary patch centered at either a smooth point of $\partial\Omega$ or at a corner point of $\partial\Omega$ with the same contact angle. As shown in [**55**], the effect of such a fragmentation leads to the following qualitative result:

Proposition 11 *The fragmentation of one favorable interior habitat into two separate favorable interior habitats is not advantageous for species persistence. Similarly, the fragmentation of a favorable boundary habitat into two favorable boundary habitats with each either centered at either a smooth point of $\partial\Omega$, or at a corner point of $\partial\Omega$ with the same contact angle, is not advantageous. Finally, the fragmentation of an unfavorable habitat into two separate unfavorable habitats increases the persistence threshold λ_1, and thereby is not favorable to species persistence.*

By combining these two results in Propositions 10 and 11 it follows that, given some fixed amount of favorable resources to distribute, the optimal strategy is to clump them all together at a point on the boundary of the domain, and more specifically at the corner point of the boundary (if any are present) with the smallest contact angle less than π degrees. This will ensure that the value of μ_0, and consequently the leading-order term for λ_1, is as small as possible.

A further qualitative result in [**55**] addresses whether it is advantageous to fragment a single interior favorable habitat into a smaller interior favorable habit together with a favorable boundary habitat. The effect on λ_1 of this action involves a trade-off in the sense that the fragmentation of a favorable interior habitat into two favorable interior habitats will increase the persistence threshold λ_1, but the relocation of a favorable interior habitat to the boundary decreases λ_1. To study the effect of this action, we let i index the original interior habitat, and let j and k index the new smaller interior habitat and new boundary habitat, respectively. We then minimize μ_0 maintaining the constraint

$$m_i \rho_i^2 = m_j \rho_j^2 + \frac{\alpha_k}{2} m_k \rho_k^2 \,, \tag{4.29}$$

with $\alpha_i = \alpha_j = 2$, and $\alpha_k < 2$, so that (4.28) holds. In [**55**] the following qualitative result was obtained:

Proposition 12 *The fragmentation of one favorable interior habitat into a new smaller interior favorable habitat together with a favorable boundary habitat is advantageous for species persistence when the boundary habitat is sufficiently strong in the sense that*

$$m_k \rho_k^2 > \frac{4}{2 - \alpha_k} m_j \rho_j^2 > 0 \,. \tag{4.30}$$

Fragmenting the favorable interior habitat is not advantageous when the new boundary habitat is too weak in the sense

that

$$0 < m_k \rho_k^2 < m_j \rho_j^2 \,. \tag{4.31}$$

Finally, the clumping of a favorable boundary habitat and an unfavorable interior habitat into one single interior habitat is not advantageous for species persistence when the resulting interior habitat is still unfavorable.

These three qualitative results in Propositions 10 – 12 obtained from optimizing the leading-order coefficient μ_0 in the asymptotic expansion of the persistence threshold are illustrated numerically in [**55**]. In certain degenerate situations, the optimization of the persistence threshold involves μ_1, which involves the spatial locations of the patches.

Three **open problems** in this direction are the following:

- Provide a rigorous derivation of the asymptotic expansion of the persistence threshold λ in (4.24) of Proposition 9 by using a variational framework and gamma convergence theory similar to that used in [**19**] to analyze bubble solutions for the Cahn-Hillard equation of phase transition theory.
- Analyze the persistence threshold in our 2-D patchy landscape with a partially open domain boundary modeled by a Robin boundary condition. Some results in this direction are given in [**52**].
- Extend the analysis above for the persistence threshold of a single species to that for multiple interacting species, such as competing species or predator-prey interactions. With predator-prey interactions we expect that a partial fragmentation of the prey habitat can be beneficial to species persistence.

5 Perspective and New Frontiers

In this article we have surveyed the development of a singular perturbation methodology for analyzing the existence, linear stability, and dynamics of 2-D localized spot patterns for nonlinear RD systems in the large diffusivity ratio limit. Although this strong localized perturbation theory has has been illustrated only for the Brusselator RD model (1.2), the framework of the methodology readily applies to other RD systems in the singular limit. Several new results for the linear stability of spot patterns for the Brusselator have been presented in §3. In §4 we have also re-visited two linear PDE eigenvalues problems with localized solution behavior, and have shown how the analysis of one of these problems, originating in [**99**] and [**100**], has some clear common elements with the analysis of localized spot patterns. Some specific open problems in these areas have been discussed. In this concluding section, we adopt a broader perspective and briefly discuss three new research frontiers, with diverse applications, for the analysis of localized patterns.

5.1 Coupled Bulk-Cell Models

One new frontier is the formulation and analysis of PDE models involving the interaction of spatially localized compartments or "cells" that communicate with each other via a signaling molecule that diffuses in the extracellular space between the segregated dynamically active units. In biology, this type of chemical signaling is believed to occur between colonies of the social amoebae *Dictyostelium discoideum* in low nutrient environments where cAMP is released into the medium where it diffuses and acts on each separate colony (cf. [**34**], [**83**]) and in groups of starving yeast cells that communicate through the diffusible chemical Acetaldehyde [**25**]. In chemical physics, catalyst-loaded small particles immersed in a Belousov-Zhabotinsky (BZ) reaction-mixture exhibit collective chemical oscillations triggered by two bulk diffusing species, that are produced on each particle and diffuse in the bulk mixture (cf. [**83**], [**87**], [**88**]). In each of these specific applications, groups of cells or localized units can exhibit sustained temporally synchronous oscillations that are triggered by the intercellular communication. In contrast to oscillator problems where synchronized oscillations occur by the entrainment of phase and frequencies of individually oscillating elements, the onset of synchronized oscillations for these collections of cells is characterized by a bifurcation, whereby individual cells in a quiescent state become oscillatory and synchronized from the effect of the bulk diffusing species.

A coupled cell-bulk PDE model to study the interaction between N dynamically active localized cells and a single bulk diffusible signaling species in a bounded 2-D domain, inspired by the modeling framework of [**62**] and [**63**], was formulated in [**32**]. In non-dimensional form, the model of [**32**] involves the dimensionless bulk concentration field U, which satisfies

$$
\begin{aligned}
\tau U_t &= D\Delta U - U \,, && \mathbf{x} \in \Omega \backslash \cup_{j=1}^{N} \Omega_{\epsilon_j} \,; && \partial_n U = 0 \,, && \mathbf{x} \in \partial\Omega \,, \\
\epsilon D \partial_{n_j} U &= d_1 U - d_2 u_j^1 \,, && \mathbf{x} \in \partial\Omega_{\epsilon_j} \,, && j = 1, \ldots, N \,,
\end{aligned}
\tag{5.1 a}
$$

where the j-th cell Ω_{ϵ_j} is assumed to be a disk of radius $\epsilon \ll 1$ centered at some $\mathbf{x}_j \in \Omega$. For each $j = 1, \ldots, N$, (5.1 a) is
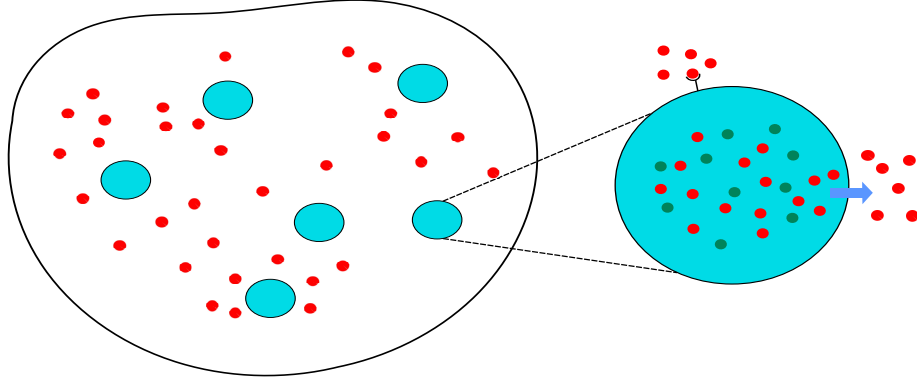
FIGURE 10. Schematic diagram showing the intracellular reactions and external bulk diffusion of the signal. The small shaded regions are the signaling compartments or cells (Figure from [**32**]).

coupled to the intracellular dynamics by

$$\frac{d\mathbf{u}_j}{dt} = \mathbf{F}_j(\mathbf{u}_j) + \frac{\mathbf{e}_1}{\epsilon\tau}\int_{\partial\Omega_{\epsilon_j}}\left(d_1 U - d_2 u_j^1\right)\,ds\,, \qquad j = 1,\ldots,N\,, \qquad \text{where} \quad \mathbf{e}_1 \equiv (1,0,\ldots,0)^T\,. \qquad (5.1\,b)$$

Here $\mathbf{u}_j = (u_j^1,\ldots,u_j^n)^T$ is the dimensionless mass of the n species inside the j-th cell, and $\mathbf{F}_j(\mathbf{u}_j)$ is the vector nonlinearity modeling the reaction dynamics within the j-th cell Ω_{ϵ_j}. In (5.1 a), ∂_{n_j} is the outer normal to boundary of the j-th cell, which points inside the bulk region. By specifying this form for $\mathbf{e}_1$ in (5.1 b), in our model the cells can release only a single specific signaling molecule into the bulk region. A schematic illustration is shown in Fig. 10. The key parameters in the model are the dimensionless bulk diffusivity D, the time-scale parameter τ, measuring the intracellular reaction rate to the rate of the bulk degradation process, and the dimensionless permeabilities d_1 and d_2, assumed to be the same for each cell.

In the small cell limit $\epsilon \to 0$, in [**32**] strong localized perturbation theory was used to formulate a nonlinear algebraic system for the steady-state solution and to derive a new class of globally coupled eigenvalue problem (GCEP), with a similar form to that for localized spot patterns, governing the linear stability of any steady-state solution. Similar to the analysis of spot patterns for the Brusselator, the linear stability problem involves an eigenvalue-dependent Green's matrix, which effectively couples the N cells. This linear stability framework of [**32**] was implemented for Sel'kov intracellular kinetics where it was shown that triggered synchronous oscillations due to a Hopf bifurcation can occur for a ring-shaped pattern of identical cells inside the unit disk. The analysis revealed a *diffusion-sensing* behavior, whereby oscillations could be triggered only when the cells were sufficiently clustered. For the large diffusivity limit $D \gg 1$, in [**32**] it was shown that (5.1) exhibits *quorum-sensing* behavior, whereby a Hopf bifurcation leading to synchronous oscillations only occurs when the number of cells N exceeds a threshold, with this threshold depending on the permeabilities d_1 and d_2.

There are many open-ended directions related to coupled bulk-cell models of the class (5.1), and its extensions, that warrant further study. We only mention three of these here (see [**32**] for a more detailed discussion). For (5.1), the use of fast numerical algorithms of potential theory (cf. [**48**]) to compute the eigenvalue-dependent Green's matrix would likely allow for the construction of chimera-type patterns whereby only distinct groups of cells in relatively close proximity undergo synchronous oscillations, with the other cells remaining in a quiescent state. Secondly, it would be interesting to extend the linear stability analysis to analyze large-scale oscillatory dynamics for (5.1). Furthermore, by extending (5.1) to allow for two bulk diffusing species, it should be possible to fully explore the idea originating in [**78**] that Turing patterns can occur when the two species have identical diffusivities, but are coupled together through small signaling cells.

5.2 3-D Spot Patterns and 3-D Mean First Capture Time Problems

A second new research frontier is to analyze the existence, stability, and dynamics of localized spot patterns for singularly perturbed RD systems in 3-D spatial domains. The first study of this type was presented in [**92**] for a limiting form of

the 3-D Schnakenberg model, which is given in dimensionless and re-scaled form by

$$v_t = \varepsilon^2 \Delta v - v + uv^2, \quad \mathbf{x} \in \Omega \in \mathbb{R}^3; \qquad \partial_n v = 0, \quad \mathbf{x} \in \partial\Omega, \tag{5.2 a}$$

$$\varepsilon^3 u_t = \frac{D}{\varepsilon} \Delta u + A - \frac{uv^2}{\varepsilon^3}, \quad \mathbf{x} \in \Omega; \qquad \partial_n u = 0, \quad \mathbf{x} \in \partial\Omega. \tag{5.2 b}$$

By constructing N-spot quasi-equilibria using strong localized perturbation theory in terms of a new type of local spot core problem, and then analyzing the linear stability of spot patterns to either competition or peanut-splitting instabilities, it was shown in [**92**] that an N-spot quasi-equilibrium pattern, with $N \geq 2$, is linearly stable on an $\mathcal{O}(1)$ time-scale iff

$$S_{\text{comp}} < S_c < \Sigma_2; \qquad S_c \equiv \frac{A|\Omega|}{4\pi N \sqrt{D}}, \qquad S_{\text{comp}} \approx 4.52 \qquad \Sigma_2 \approx 20.16, \tag{5.3}$$

where Σ_2 is the peanut-splitting threshold for a localized spot. In contrast to the case of 2-D spot patterns, for 3-D spot patterns of (5.2) there is an asymptotically common spot source strength with $S_j = S_c + \mathcal{O}(\epsilon)$. We remark that Σ_2 is independent of the parameters A and D since the inner problem near a spot is independent of A, and the diffusivity D can be eliminated through a re-scaling of u and v near the spot. The eigenvalue problem governing shape deformations of the spot profile is a purely local problem, with a decay condition at infinity, that involves only the common spot source strength S_c. The computations in §3.2 of [**92**] show that it is the peanut-splitting mode that goes unstable first as S_c crosses above $\Sigma_2 \approx 20.16$. We further remark that the competition instability threshold S_{comp} is another universal constant, independent of A and D. This follows from the fact that due to the assumed D/ϵ scaling for the inhibitor diffusivity in (5.2 b), the eigenfunction component for the inhibitor field is, to leading order, a universal constant (see §3.1 of [**92**] for details).

With regards to slow spot dynamics for (5.2) in 3-D, when (5.3) for S_c is satisfied, then to leading-order in ϵ the spot locations $\mathbf{x}_j$, for $j = 1 \ldots, N$, evolve slowly by the gradient flow (see equation (4.18) of [**92**])

$$\frac{d\mathbf{x}_j}{dt} \sim -\varepsilon^3 \gamma \nabla_{\mathbf{x}_j} \mathcal{H}(\mathbf{x}_1, \ldots, \mathbf{x}_N), \qquad j = 1, \ldots, N, \qquad \mathcal{H}(\mathbf{x}_1, \ldots, \mathbf{x}_N) \equiv \mathbf{e}^T \mathcal{G}_0 \mathbf{e}, \tag{5.4}$$

for some $\gamma = \gamma(S_c) > 0$ (see Lemma 4.1 of [**92**]). Here $\mathbf{e} \equiv (1, \ldots, 1)^T$, and $\mathcal{G}_0$ is the 3-D Neumann Green's matrix obtained by solving (2.5) for $\Omega \in \mathbb{R}^3$. Since $\gamma(S_c) > 0$, it readily can be shown from (5.4) that two spots that are sufficiently close together will repel.

The result (5.4) shows that linearly stable fixed points of the spot dynamics (5.4) coincide with local minima of the discrete energy $\mathcal{H}$. We remark that for the singularly perturbed eigenvalue problem (4.1) posed in a bounded 3-D domain with N small spherical traps $\Omega_{\epsilon,j}$ of radius ϵ centered at $\mathbf{x}_1, \ldots, \mathbf{x}_N$, it was shown in [**21**] that the global minimum of $\mathcal{H}$ also provides the optimal spatial configuration of localized traps that minimizes the expected mean first capture time of a Brownian particle in $\Omega \backslash \cup_{j=1}^N \Omega_{\epsilon_j}$. The discrete variational problem of seeking both local minima and a global minimum of $\mathcal{H}$ when $\mathbf{x}_j \in \Omega$, for $j = 1, \ldots, N$, is an extension of the well-known and classical Fekete point problems of [**50**] and [**75**]. For the unit sphere, where the Neumann Green's matrix is known analytically, global minima of $\mathcal{H}$ have been computed for $2 \leq N \leq 20$ (cf. [**21**], [**92**]). It is an open problem to investigate optimal configurations for larger values of N and to obtain a scaling law for the corresponding optimal discrete energy as $N \to \infty$. Since the number of local minima of $\mathcal{H}$ is expected to explode as N becomes large, the gradient dynamics (5.4) predicts that there will be many linearly stable equilibrium spot configurations. However, it is likely that the majority of these equilibria will have small basins of attraction for initial conditions. It would be worthwhile to explore these issues numerically, and to extend the analysis of [**92**] to other RD systems, such as the 3-D Brusselator model, so as to obtain a more comprehensive theory for spot patterns in a 3-D setting.

We remark that the assumed scaling of D/ϵ for the inhibitor diffusivity in (5.2 b) appears somewhat artificial, in that perhaps spot patterns in 3-D can still exist when the ϵ is removed, so that the inhibitor diffusivity is $D = \mathcal{O}(1)$. However, for this latter case, numerical evidence from full PDE simulations (not shown) suggests that, with this smaller inhibitor diffusivity, v concentrates on 2-D surfaces rather than at discrete points. It would be interesting to investigate this issue analytically.

Finally, we briefly discuss a new discrete variational problem that has recently been derived in [**56**] for the well-known biophysical problem of [**6**] of analyzing how diffusing ligands bind to cell surface receptors on a spherical surface of radius R_0. In this application, ligands are modeled as point Brownian particles with diffusivity D_0 that are trapped upon first contact with any one of N non-overlapping disk-shaped surface receptors of radius a_0, with $a_0 \ll R_0$. The steady-state

ligand concentration $u(\mathbf{x})$ satisfies

$$\Delta u = 0, \quad |\mathbf{x}| \geq R_0; \qquad u \sim 1 - C/|\mathbf{x}|, \quad \text{as} \quad |\mathbf{x}| \to \infty, \tag{5.5 a}$$

$$u = 0, \quad \mathbf{x} \in \partial\Omega_a, \qquad \partial_n u = 0, \quad \mathbf{x} \in \partial\Omega_r. \tag{5.5 b}$$

Here $\partial\Omega_a$ denotes the union of the N, non-overlapping, locally circular cell surface receptor traps of a common radius $a_0 \ll R_0$ centered at some $\mathbf{x}_j$, for $j = 1, \ldots, N$, with $|\mathbf{x}_j| = R_0$, while $\partial\Omega_r$ is the non-binding, or reflecting, portion of the the surface of the sphere. The key biophysical quantity for (5.5) is the flux J of ligands to the surface receptors, defined by $J \equiv \int_{\partial\Omega_a} D_0 u_r\big|_{r=R_0} ds$. From the divergence theorem, $J = 4\pi D_0 C$, where C is defined by (5.5). By using strong localized perturbation theory, the analysis in [56] showed that

$$\frac{1}{C} = \frac{\pi}{N\sigma R_0} \left[1 + \frac{\sigma}{\pi} \left(\log\left(2e^{-3/2}\sigma\right) + \frac{4}{N}\mathcal{H}_s(\mathbf{y}_1, \ldots, \mathbf{y}_N) \right) + \mathcal{O}\left(\sigma^2 \log\left(\frac{\sigma}{2}\right)\right) \right]. \tag{5.6 a}$$

Here $\sigma \equiv a_0/R_0$ and the discrete energy $\mathcal{H}_s(\mathbf{y}_1, \ldots, \mathbf{y}_N)$, with $\mathbf{y}_j = \mathbf{x}_j/R_0$, representing interactions between localized cell surface receptors, is defined in terms of a positive, convex, two-particle interaction energy $g(\mu)$ by

$$\mathcal{H}_s(\mathbf{y}_1, \ldots, \mathbf{y}_N) \equiv \sum_{j=1}^{N} \sum_{k=j+1}^{N} g(|\mathbf{y}_j - \mathbf{y}_k|), \qquad \text{where} \qquad g(\mu) \equiv \frac{1}{\mu} + \frac{1}{2} \log\left(\frac{\mu}{2+\mu}\right). \tag{5.6 b}$$

We remark that the derivation of (5.6) relies heavily on the availability of an explicit formula for a surface Green's function (cf. [56]). For a fixed N, a key question is to determine the trap configuration that globally minimizes $\mathcal{H}_s$, thereby maximizing both C and the flux of ligands. For large N, such optimal trap configurations should be uniformly distributed over the spherical surface, and the formal analysis in [56] predicts that the optimal energy $\mathcal{H}_{s,\text{opt}}$ for $N \to \infty$ has the form

$$\mathcal{H}_{s,\text{opt}} \sim \frac{N^2}{4} - d_1 N^{3/2} + \frac{1}{8} N \log N + d_2 N + d_3 N^{1/2} + \cdots, \tag{5.7}$$

where $d_1 \approx 0.55230$, $d_2 \approx 1/8$, and $d_3 \approx 1/4$. The substitution of (5.7) into (5.6 a) yields the new scaling law (cf. [56])

$$\frac{1}{C} \sim \frac{1}{R_0} \left[1 + \frac{\pi\sigma}{4f} + \frac{\pi\sigma}{4f} \left(-\frac{8d_1}{\pi} \sqrt{f} + \frac{\sigma}{\pi} \log\left(\beta\sqrt{f}\right) + \frac{2d_3\sigma^2}{\pi\sqrt{f}} \right) \right], \tag{5.8}$$

where $\beta \equiv 4e^{-3/2}e^{4d_2}$. This result is asymptotically valid provided that the trap surface area fraction $f \equiv N\pi\sigma^2/(4\pi)$ satisfies $f = \mathcal{O}(-\sigma^2 \log \sigma) \ll 1$. We remark that the first two terms in (5.8), yielding $C \approx R_0 N\sigma/(N\sigma + \pi)$, is the well-known Berg-Purcell formula [6] derived previously only formally, with the remaining terms in (5.8) providing new correction terms.

An open problem is to give a rigorous derivation of both (5.6) and the optimal energy expansion (5.7) for $N \gg 1$. An extension of the analysis of [56] to non-spherical cell surfaces would also be worthwhile.

5.3 Coupled Bulk-Surface Models

A third new research direction involves analyzing classes of RD models that result from the coupling of a passive 3-D bulk diffusion process to a 2-D surface reaction-diffusion process, due to chemical exchanges between the bulk and the surface. These coupled models arise in many applications, such as in receptor-binding models related to the initiation of biological cell-division (cf. [72], [54], [31]), the GTPase cycle in cell signaling [77], biological morphogenesis [58], and in the determination of the mean first capture time for a Brownian particle in a domain with either interior or boundary traps that diffuses in the bulk but that can intermittently bind with the surface (cf. [5]).

The general form of such coupled bulk-surface diffusion models is as follows: Let Ω be a bounded 3-D domain with smooth boundary $\partial\Omega \in \mathbb{R}^2$. When there are both nonlinear reactions and diffusion on the surface $\partial\Omega$, we have

$$u_t = D_u \Delta_s u + f(u, v) - c_u, \qquad v_t = D_v \Delta_s v + g(u, v) - c_v, \qquad \mathbf{x} \in \partial\Omega, \tag{5.9 a}$$

where Δ_s is the Laplace-Beltrami operator for $\partial\Omega$. This surface RD system is coupled to a passive bulk diffusion process

$$U_t = D_U \Delta U - \sigma_U U + M_U(\mathbf{x}), \qquad V_t = D_V \Delta V - \sigma_V V + M_V(\mathbf{x}), \qquad \mathbf{x} \in \Omega, \tag{5.9 b}$$

via a coupling

$$D_U \partial_n U = c_u, \qquad D_V \partial_n V = c_v, \quad \mathbf{x} \in \partial\Omega, \tag{5.9 c}$$

where ∂_n is the outward normal to $\partial\Omega$. The simplest type of exchange process between the bulk and the surface is to assume a linear coupling where $c_u \equiv k_1 u - k_2 U$ and $c_v \equiv k_3 v - k_4 V$ for some constants $k_i > 0$ for $i = 1, \ldots, 4$. In (5.9 a), $M_U(\mathbf{x})$ and $M_V(\mathbf{x})$ model the bulk production of signaling proteins that can diffuse to the surface and initiate reactions.

One key open direction is to analyze, in various asymptotic limits, how bulk diffusion influences the existence and stability of surface-bound patterns. In the singular limit where $D_v \ll 1$ and $D_u = \mathcal{O}(1)$, such a study would involve the analysis of new classes of nonlocal eigenvalue problems (NLEPs). In addition, in the limit $D_U \gg 1$ and $D_V \gg 1$ of large bulk diffusivities, new types of nonlocal PDE-ODE shadow problems arise. Finally, in the case when there is no surface diffusion $D_u = D_v = 0$, and when $M_U = M_V = 0$, an interesting open problem is to develop a weakly nonlinear theory to characterize either symmetry breaking or Hopf bifurcations from a background state. The novelty of this analysis for this latter problem is that the linearized problem has a Steklov structure where the eigenvalue parameter appears in both the differential operator and in the boundary condition. Although a linear stability analysis has been done in [**77**] and [**54**] for some specific models, and in [**58**] in a much more general context, the development of a weakly nonlinear analysis to characterize the local branching behavior of solutions near bifurcation points is an open problem.

Appendix A Asymptotics of the Core Problem

The following result for the asymptotics of the core problem (2.1) when $S \ll 1$, as derived in §4.1 of [**81**], is needed in §2.2.1 to determine an asymptotic approximation for the competition stability threshold associated with a zero-eigenvalue crossing:

Lemma 4 *In the limit $S \to 0$, a two-term expansion for the solution to the core problem (2.1) is*

$$v \sim S\left[\tilde{v}_0 + S^2 \tilde{v}_1 + \mathcal{O}(S^4)\right], \qquad u \sim \frac{1}{S}\left[\tilde{u}_0 + S^2 \tilde{u}_1 + \mathcal{O}(S^4)\right], \qquad \chi(S) \sim \frac{\tilde{\chi}_0}{S} + S\tilde{\chi}_1 + \mathcal{O}(S^3), \qquad \text{(A.1 a)}$$

where

$$\tilde{v}_0 = \frac{1}{f\tilde{\chi}_0}w, \qquad \tilde{v}_1 = -\frac{\tilde{\chi}_1}{f\tilde{\chi}_0^2}w - \frac{1}{\tilde{\chi}_0^3 f^3}\tilde{v}_{1p}, \qquad \tilde{u}_0 = \frac{b(1-f)}{f^2}, \qquad \tilde{u}_1 = \tilde{\chi}_1 + \frac{1}{\tilde{\chi}_0 f^2}\tilde{u}_{1p}. \qquad \text{(A.1 b)}$$

Here $b \equiv \int_0^\infty \rho w^2 \, d\rho$, and $w(\rho)$ is the unique ground-state solution satisfying

$$\Delta_\rho w - w + w^2 = 0, \quad 0 < \rho < \infty; \qquad w(0) > 0, \quad w'(0) = 0; \qquad w \to 0 \quad \text{as} \quad \rho \to \infty. \qquad \text{(A.1 c)}$$

In (A.1 b), $\tilde{v}_{1p}$ and $\tilde{u}_{1p}$ are defined uniquely by the linear BVPs

$$L_0 \tilde{v}_{1p} = w^2 \tilde{u}_{1p}, \qquad \Delta \tilde{u}_{1p} = w^2 - fw,$$
$$\tilde{v}_{1p} \to 0 \quad \text{as} \quad \rho \to \infty, \qquad \tilde{u}_{1p} \sim b(1-f)\log\rho + o(1) \quad \text{as} \quad \rho \to \infty, \qquad \text{(A.1 d)}$$

where the operator L_0 is defined by $L_0 \equiv \Delta_\rho - 1 + 2w$, with $\Delta_\rho \equiv \partial_{\rho\rho} + \rho^{-1}\partial_\rho$. Moreover, $\tilde{\chi}_0$ and $\tilde{\chi}_1$ are defined by

$$\tilde{\chi}_0 = \frac{b(1-f)}{f^2}, \qquad \tilde{\chi}_1 = -\frac{1}{b^2(1-f)}\int_0^\infty \rho \tilde{v}_{1p} \, d\rho. \qquad \text{(A.1 e)}$$

In §3.1, we need to re-express Lemma 4 as an expansion in $\nu \ll 1$ rather than $S \ll 1$. The result is as follows:

Lemma 5 *For $S \sim \nu^{1/2}(S_0 + \nu S_1 + \mathcal{O}(\nu^2))$, a two-term expansion for the solution to the core problem (2.1) is*

$$v \sim \nu^{1/2}\left(\tilde{v}_0 + \nu \tilde{v}_1 + \mathcal{O}(\nu^2)\right), \qquad u \sim \nu^{-1/2}\left(\tilde{u}_0 + \nu \tilde{u}_1 + \mathcal{O}(\nu^2)\right), \qquad \chi(S) \sim \nu^{-1/2}\left(\chi_0 + \nu \chi_1 + \mathcal{O}(\nu^2)\right), \qquad \text{(A.2 a)}$$

where $\tilde{v}_0$, $\tilde{u}_0$, $\tilde{v}_1$, and $\tilde{u}_1$ are defined as in (A.1 b), but where $\tilde{\chi}_0$ and $\tilde{\chi}_1$ in those expressions are replaced by χ_0 and χ_1, as given by

$$\chi_0 = \frac{b(1-f)}{f^2 S_0}, \qquad \chi_1 = -\frac{(1-f)b}{f^2}\left(\frac{S_1}{S_0^2}\right) - \frac{S_0}{b^2(1-f)}\int_0^\infty \rho \tilde{v}_{1p} \, d\rho. \qquad \text{(A.2 b)}$$

Acknowledgements

References

[1] M. Abramowitz, I. Stegun, *Handbook of mathematical functions*, 9th edition, New York, NY, Dover Publications.

[2] Y. A. Astrov, H. G. Purwins, *Spontaneous division of dissipative solitons in a planar gas-discharge system with high ohmic electrode*, Phys. Lett. A, **358**(5-6), (2006), pp. 404–408.

[3] D. Avitabile, V. Brena-Medina, M. J. Ward, *Spot dynamics in a plant root hair initiation model*, to appear, SIAM J. Appl. Math., (2017), (28 pages).

[4] I. Balazs, J. B. van den Berg, J. Courtois, J. Dudas, J.-P. Lessard, A. Vörös-Kiss, J. F. Williams, X. Y. Lin, *Computer-assisted proofs for radially symmetric solutions of PDEs*, submitted, (2017).

[5] O. Bénichou, R. Voituriez, *From first-passage times of random walks in confinement to geometry-controlled kinetics*, Physics Reports, **539**(4), (2014), pp. 225–284.

[6] H. C. Berg, E. M. Purcell, *Physics of chemoreception*, Biophys J., **20**(2), (1977), pp. 193–219.

[7] L. Bétermin, E. Sandier, *Renormalized energy and asymptotic expansion of optimal logarithmic energy on the sphere*, Constructive Approx. to appear, (2017).

[8] G. Beylkin, C. Kurcz, L. Monzón, *Fast algorithms for Helmholtz Green's functions*, Proc. R. Soc. A, **464**, (2008), pp. 3301-3326.

[9] S. Boatto, *Curvature perturbations and stability of a ring of vortices*, DCDS-B, **10**(2-3), (2008), pp. 349–375.

[10] K. J. Brown, S. S. Lin, *On the existence of positive eigenfunctions for an eigenvalue problem with indefinite weight function*, J. Math. Anal. Appl., **75**(1), (1980), pp. 112–120.

[11] T. K. Callahan, *Turing patterns with O(3) symmetry*, Physica D, **188**(1), (2004), pp. 65–91.

[12] R. S. Cantrell, C. Cosner, *Diffusive logistic equations with indefinite weights: Population models in disrupted environments*, Proc. Roy. Soc. Edinburgh, **112A**(3-4), (1989), pp. 293–318.

[13] R. S. Cantrell, C. Cosner, *Diffusive logistic equations with indefinite weights: Population models in disrupted environments II*, SIAM J. Math. Anal., **22**(4), (1991), pp. 1043–1064.

[14] R. S. Cantrell, C. Cosner, *The Effects of Spatial Heterogeneity in Population Dynamics*, J. Math. Biol., **29**(4), (1991), pp. 315–338.

[15] R. S. Cantrell, C. Cosner, *Spatial ecology via reaction-diffusion systems*, Wiley Series in Mathematical and Computational Biology, John Wiley & Sons, Ltd., Chichester, 2003, xvi+411 pp.

[16] Y. Chang, *The stability of spot patterns for the Brusselator reaction-diffusion system in two space dimensions: Periodic and finite domain settings*, M. Sc thesis, Univ. British Columbia, (2015).

[17] Y. Chang, J. Tzou, M. J. Ward, J. Wei, *Refined stability thresholds for localized spot patterns for the Brusselator model in $\mathbb{R}^2$*, submitted, Europ. J. Appl. Math., (26 pages), (2017).

[18] W. Chen, M. J. Ward, *The stability and dynamics of localized spot patterns in the two-dimensional Gray-Scott model*, SIAM J. Appl. Dyn. Sys., **10**(2), (2011), pp. 582–666.

[19] X. Chen, M. Kowalczyk, *Existence of equilibria for the Cahn-Hilliard equation via local minimizers of the perimeter*, Comm. Partial Diff. Eq., **21**(7-8), (1996), pp. 1207-1233.

[20] A. Cheviakov, M. J. Ward, R. Straube, *An asymptotic analysis of the mean first passage time for narrow escape problems: Part II: The sphere*, SIAM J. Multiscale Modeling and Simulation, **8**(3), (2010), pp. 836–870.

[21] A. Cheviakov, M. J. Ward, *Optimizing the fundamental eigenvalue of the Laplacian in a sphere with interior traps*, Mathematical and Computer Modeling, **53**(7-8), (2011), pp. 1394–1409.

[22] D. Coombs, R. Straube, M. J. Ward, *Diffusion on a sphere with localized traps: Mean first passage time, eigenvalue asymptotics, and Fekete points*, SIAM J. Appl. Math., **70**(1), (2009), pp. 302–332.

[23] P. W. Davis, P. Blanchedeau, E. Dullos and P. De Kepper, *Dividing blobs, chemical flowers, and patterned islands in a reaction-diffusion system*, J. Phys. Chem. A, **102**(43), (1998), pp. 8236–8244.

[24] W. Dijkstra, M. E. Hochstenbach, *Numerical approximation of the logarithmic capacity*, CASA Report 08-09, Technical U. Eindhoven, preprint, (2008).

[25] S. De Monte, F. d'Ovido, S. Dano, P. G. Sørensen, *Dynamical quorum sensing: population density encoded in cellular dynamics*, Proc. Nat. Acad. Sci., **104**(47), (2007), pp. 18377–18381.

[26] A. Doelman, R. A. Gardner, T. Kaper, *Large stable pulse solutions in reaction-diffusion equations*, Indiana U. Math. Journ., **50**(1), (2001), pp. 443-507.

[27] A. Doelman, R. A. Gardner, T. Kaper, *A stability index analysis of 1-d patterns of the Gray Scott model*, Memoirs of the AMS, **155**(737), (2002).

[28] A. Doelman, H. van der Ploeg, *Homoclinic stripe patterns*, SIAM J. Appl. Dyn. Systems, **1**(1), (2002), pp. 65-104.

[29] D. G. Dritschel, S. Boatto, *The motion of point vortices on closed surfaces*, Proc. Roy. Soc. A, **471**(2176), (2015), 20140890.

[30] S. Ei, M. Mimura, M. Nagayama, *Interacting spots in reaction-diffusion systems*, DCDS-A, **14**(1), (2006), pp. 31–62.

[31] W. Giese, M. Eigel, S. Westerheide, C. Engwer, E. Klipp, *Influence of cell shape, inhomogeneities, and diffusion barriers in cell polarization models*, Phys. Biol. **12**(6):066014 (2015).

[32] J. Gou, M. J. Ward, *An asymptotic analysis of a 2-d model of dynamically active compartments coupled by bulk diffusion*, J. Nonlinear Science, **26**(4), (2016), pp. 979–1029.

[33] C. C. Green, J. S. Marshall, *Green's function for the Laplace-Beltrami operator on a toroidal surface*, Proc. Roy. Soc. A, **469**:20120479, (2013).

[34] T. Gregor, K. Fujimoto, N. Masaki, S. Sawai, *The onset of collective behavior in social amoeba*, Science, **328**(5981), (2010), pp. 1021–1025.

[35] P. Hess, *Periodic-parabolic boundary value problems and positivity*, Pitman Research Notes in Mathematics, Vol. 247, Longman, Harlow, U.K. (1991).

[36] D. Holcman, Z. Schuss, *The narrow escape problem*, SIAM Review, **56**(2), (2014), pp. 213-257.

[37] D. Iron, J. Rumsey, M. J. Ward, J. Wei, *Logarithmic expansions and the stability of periodic patterns of localized spots for reaction-diffusion systems*, J. Nonlinear Science, **24**(5), (2014), pp. 857–912.

[38] A. Jamieson-Lane, P. Trinh, M. J. Ward, *Localized Spot Patterns on the Sphere for Reaction-Diffusion Systems: Theory and Open Problems*, book chapter in *Mathematical and Computational Approaches in Advancing Modern Science and Engineering*, J. Belair et al. editors, Springer 2016, pp. 641–651 (Conference Proceedings for AMMCS-CAIMS 2015).

[39] C. Y. Kao, Y. Lou, E. Yanagida, *Principal eigenvalue for an elliptic system with indefinite weight on cylindrical domains*, Math. Biosc. Eng. **5**(2), (2008), pp. 315–335.

[40] J. Kevorkian, J. Cole, *Multiple Scale and Singular Perturbation Methods*, Applied Mathematical Sciences Vol. 114, Springer-Verlag, (1996), 632pp.

[41] T. Koloklonikov, W. Sun, M. J. Ward, J. Wei, *The stability of a stripe for the Gierer-Meinhardt model and the effect of saturation*, SIAM J. Appl. Dyn. Sys., **5**(2), (2006), pp. 313-363.

[42] T. Kolokolnikov, M. J. Ward, *Reduced wave Green's functions and their effect on the dynamics of a spike for the Gierer-Meinhardt model*, Europ. J. Appl. Math., **14**(5), (2003), pp. 513–545.

[43] T. Koloklonikov, M. J. Ward, J. Wei, *Slow translational instabilities of spike patterns in the one-dimensional Gray-Scott model*, Interfaces and Free Bound., **8**(2), (2006), pp. 185–222.

[44] T. Kolokolnikov, M. J. Ward, J. Wei, *Spot self-replication and dynamics for the Schnakenberg model in a two-dimensional domain*, J. Nonlinear Sci., **19**(1), (2009), pp. 1–56.

[45] T. Kolokolnikov, M. Titcombe, M. J. Ward, *Optimizing the fundamental Neumann eigenvalue for the Laplacian in a domain with small traps*, Europ. J. Appl. Math., **16**(2), (2005), pp. 161–200.

[46] T. Kolokonikov, M. J. Ward, J. Wei, *The stability of hot-spot patterns for a reaction-diffusion system of urban crime*, DCDS-B, **19**(5), (2014), pp. 1373–1410.

[47] E. Knobloch, *Spatial localization in dissipative systems*, Annu. Rev. Cond. Mat. Phys., **6**, (2015), pp. 325–359.

[48] M. C. Kropinski, B. D. Quaife, *Fast integral equation methods for the modified Helmholtz equation*, J. Comp. Phys., **230**(2), (2011), pp. 425–434.

[49] M. C. Kropinski, N. Nigam, B. Quaife, *Integral equation methods for the Yukawa-Beltrami equation on the sphere*, Adv. Comput. Math., **42**(2), (2016), pp. 469–488.

[50] A. B. J. Kuijlaars, E. B. Saff, *Asymptotics for minimal discrete energy on the sphere*, Trans. Amer. Math. Soc., **350**(2), (1998), pp. 523–538.

[51] V. Kurella, J. Tzou, D. Coombs, M. J. Ward, *Asymptotic analysis of first passage time problems inspired by ecology*, Bulletin of Math Biology, **77**(1), (2015), pp. 83–125.

[52] J. Lamboley, A. Laurain, G. Nadim, Y. Privat, *Properties of optimizers of the principal eigenvalue with indefinite weight and Robin conditions*, Calc. Var. PDE, **55**:144, (2016)

[53] K. J. Lee, W. D. McCormick, J. E. Pearson, H. L. Swinney, *Experimental observation of self-replicating spots in a reaction-diffusion system*, Nature, **369**, (1994), pp. 215-218.

[54] H. Levine, W. J. Rappel, *Membrane-bound Turing patterns*, Phys. Rev. E., **72**, (2005), 061912.

[55] A. Lindsay, M. J. Ward, *An asymptotic analysis of the persistence threshold in highly patchy spatial environments*, DCDS-B, **14**(3), (2010), pp. 1139–1179.

[56] A. Lindsay, A. Bernoff, M. J. Ward, *First Passage Statistics for the Capture of a Brownian Particle by a Structured Spherical Target with Multiple Surface Traps*, SIAM J. Multiscale Modeling and Simulation, **15**(1), (2017), pp. 74–109.

[57] Y. Lou, E. Yanagida, *Minimization of the principal eigenvalue for an elliptic boundary value problem with indefinite weight and applications to population dynamics*, Japan J. Indust. Appl. Math., **23**(3), (2006), pp. 275–292.

[58] A. Madzvamuse, A. Chung, C. Venkataraman, *Stability analysis and simulations of coupled bulk-surface reaction-diffusion systems*, Proc. Roy. Soc. A, **471**, (2175), (2015).

[59] P. C. Matthews, *Transcritical bifurcation with $O(3)$ symmetry*, Nonlinearity, **16**(4), (2003), pp. 1449–1471.

[60] I. Moyles, M. J. Ward, *Existence, stability, and dynamics of ring and near-ring solutions to the Gierer-Meinhardt model in the semi-strong regime*, SIAM J. Appl. Dyn. Sys. **16**(1), (2017), pp. 597–639.

[61] I. Moyles, B. Wetton, *A numerical framework for singular limits of a class of reaction diffusion problems*, J. Comp. Phys., **300**, (2015), pp. 308–326.

[62] J. Müller, C. Kuttler, B. A. Hense, M. Rothballer, A. Hartmann, *Cell-cell communication by quorum sensing and dimension-reduction*, J. Math. Bio, **53**(4), (2006), pp. 672–702.

[63] J. Müller, H. Uecker, *Approximating the dynamics of communicating cells in a diffusive medium by ODEs*, J. Math. Bio, **67**(5), (2013), pp. 1023–1065.

[64] C. Muratov, V. V. Osipov, *Static spike autosolitons in the Gray-Scott model*, J. Phys. A: Math Gen. **33**, (2000), pp. 8893–8916.

[65] C. Muratov, V. V. Osipov, *Spike autosolitons and pattern formation scenarios in the two-dimensional Gray-Scott model*, Eur. Phys. J. B. **22**, (2001), pp. 213–221.

[66] C. Muratov, V. V. Osipov, *Stability of static spike autosolitons in the Gray-Scott model*, SIAM J. Appl. Math., **62**(5), (2002), pp. 1463–1487.

[67] Y. Nishiura, *Far-from equilibrium dynamics, translations of mathematical monographs*, Vol. **209**, (2002), AMS Publications, Providence, Rhode Island.

[68] Y. Nishiura, H. Fujii, *Stability of singularly perturbed solutions to systems of reaction-diffusion equations*, SIAM J. Math. Anal., **18**, (1987), pp. 1726-1770.

[69] Y. Nishiura, *Singular limit approach to stability and bifurcation for bistable reaction-diffusion systems*, Rocky Mountain J. Math., **21**(2), (1991), pp. 727-767.

[70] S. Ozawa, *Singular variation of domains and eigenvalues of the Laplacian*, Duke Math. J., **48**(4), (1981), pp. 767-778.

[71] J. E. Pearson, *Complex patterns in a simple system*, Science, **216**, (1993), pp. 189–192.

[72] Z. Petrásek, P. Schwille, *Simple membrane-based model of the Min oscillation*, New J. of Phys, **17**, (2015), 034023.

[73] S. Pillay, M. J. Ward, A. Pierce, T. Kolokolnikov, *An asymptotic analysis of the mean first passage time for narrow escape problems: Part I: Two-dimensional domains*, SIAM J. Multiscale Modeling and Simulation, **8**(3), (2010), pp. 803–835.

[74] I. Prigogine, R. Lefever, *Symmetry breaking instabilities in dissipative systems. II*, J. Chem. Physics, **48**, (1968), pp. 1695.

[75] E. A. Rakhmanov, E. B. Saff, Y. M. Zhou, *Minimal discrete energy on the sphere*, Math. Res. Lett., **1**(6), (1994), pp. 647–662.

[76] T. Ransford, *Potential theory in the complex plane*, Vol. 28 of London Mathematical Society Student Texts, Cambridge University Press, (1995), 232pp.

[77] A. Rätz, M. Röger, *Symmetry breaking in a bulk-surface reaction-diffusion model for signaling networks*, Nonlinearity, **27**(8), (2014), pp. 1805–1828.

[78] E. M. Rauch, M. Millonas, *The role of trans-membrane signal transduction in Turing-type cellular pattern formation*, J. Theor. Biol., **226**(4), (2004), pp. 401–407.

[79] S. Redner, *A guide to first-passage time processes*, Cambridge Univ. Press, (2001), Cambridge, U.K.

[80] L. Roques, F. Hamel, *Mathematical analysis of the optimal habitat configurations for species persistence*, Math. Biosci., **210**(1), (2007), pp. 34–59.

[81] I. Rozada, S. Ruuth, M. J. Ward, *The stability of localized spot patterns for the Brusselator on the sphere*, SIAM J. Appl. Dyn. Sys., **13**(1), (2014), pp. 564–627.

[82] Z. Schuss, A. Singer, D. Holcman, *The narrow escape problem for diffusion in cellular microdomains*, Proc. Nat. Acad. Sci., **104**(41), (2007), pp. 16098–16103.

[83] D. J. Schwab, A. Baetica, P. Mehta, *Dynamical quorum-sensing in oscillators coupled through an external medium*, Physica D, **241**(21), (2012), pp. 1782–1788.

[84] S. Senn, P. Hess, *On positive solutions of a linear elliptic boundary value problem with Neumann boundary conditions*, Math. Ann. **258**, (1982), pp. 459–470.

[85] L. Sewalt, A. Doelman, *Spatially periodic multi-pulse patterns in a generalized Klausmeier-Gray-Scott model*, to appear, SIAM J. Appl. Dyn. Sys., (2017)

[86] J. G. Skellam, *Random dispersal in theoretical populations*, Biometrika, **38**, (1951), pp. 196–218.

[87] A. F. Taylor, M. Tinsley, K. Showalter, *Insights into collective cell behavior from populations of coupled chemical oscillators*, Phys. Chemistry Chem. Phys., **17**(31), (2015), pp. 20047–20055.

[88] M. R. Tinsley, A. F. Taylor, Z. Huang, F. Wang, K. Showalter, *Dynamical quorum sensing and synchronization in collections of excitable and oscillatory catalytic particles*, Physica D, **239**(11), (2010), pp. 785–790.

[89] P. Trinh, M. J. Ward, *The dynamics of localized spot patterns for reaction-diffusion systems on the sphere*, Nonlinearity, **29**(3), (2016), pp. 766–806.

[90] J. C. Tzou, M. J. Ward, *The stability of localized spikes for the 1-D Brusselator reaction-diffusion model*, Europ. J. Appl. Math., **24**(4), (2013), pp. 515–564.

[91] J. C. Tzou, A. Bayliss, B. J. Matkowsky, V. A. Volpert, *Stationary and slowly moving localized pulses in a singularly perturbed Brusselator model*, Europ. J. Appl. Math., **22**(5), (2011), pp. 423-453.

[92] J. Tzou, S. Xie, T. Kolokolnikov, M. J. Ward, *The stability and slow dynamics of localized spot patterns for the 3-d Schnakenberg reaction-diffusion model*, SIAM J. Appl. Dyn. Sys. **16**(1), (2017), pp. 294–336.

[93] J. Tzou, M. J. Ward, *Effect of open systems on the existence, stability, and dynamics of spot patterns in the 2d Brusselator model*, submitted, Physica D, (2016), (35 pages).

[94] J. Tzou, M. J. Ward, J. Wei, *Anomalous scaling of Hopf bifurcation thresholds for the stability of localized spot patterns for reaction-diffusion systems in 2-D*, to appear, SIAM J. Appl. Dyn. Sys., (2017), (35 pages).

[95] A. Turing, *The chemical basis of morphogenesis*, Phil. Trans. Roy. Soc. B, **327**, (1952), pp. 37–72.

[96] V. K. Vanag, I. R. Epstein, *Localized patterns in reaction-diffusion systems*, Chaos **17**(3), 037110, (2007).

[97] H. Van der Ploeg, A. Doelman, *Stability of spatially periodic pulse patterns in a class of singularly perturbed reaction-diffusion equations*, Indiana Univ. Math. J., **54**(5), (2005), pp. 1219-1301.

[98] P. Van Heijster, B. Sandstede, *Bifurcation to travelling planar spots in a three-component Fitzhugh-Nagumo system*, Physica D, **275**, (2014), pp. 19–34.

[99] M. J. Ward, W. D. Henshaw, J. Keller, *Summing logarithmic expansions for singularly perturbed eigenvalue problems*, SIAM J. Appl. Math., **53**(3), (1993), pp. 799–828.

[100] M. J. Ward, J. B. Keller, *Strong localized perturbations of eigenvalue problems*, SIAM J. Appl. Math., **53**(3), (1993), pp. 770–798.

[101] M. J. Ward, J. Wei, *Hopf bifurcation of spike solutions for the shadow Gierer-Meinhardt model*, Europ. J. Appl. Math., **14**(6), (2003), pp. 677–711.

[102] M. J. Ward, J. Wei, *Hopf bifurcation and oscillatory instabilities of spike solutions for the one-dimensional Gierer-Meinhardt model*, J. Nonlinear Sci. **13**(2), (2003), pp. 209–264.

[103] J. Wei, M. Winter, *Spikes for the two-dimensional Gierer-Meinhardt system: the weak coupling case*, J. Nonlinear Sci., **11**(6), (2001), pp. 415–458.

[104] J. Wei, *Pattern formations in two-dimensional Gray-Scott model: existence of single-spot solutions and their stability*, Physica D, **148**(1-2), (2001), pp. 20–48.

[105] J. Wei, M. Winter, *Asymmetric spotty patterns for the Gray-Scott model in $\mathbb{R}^2$*, Studies in Appl. Math., **110**(1), (2003), pp. 63–102.

[106] J. Wei, M. Winter, *Existence and stability of multiple spot solutions for the Gray-Scott model in $\mathbb{R}^2$*, Physica D, **176**(3-4), (2003), pp. 147-180.

[107] J. Wei, M. Winter, *Stationary multiple spots for reaction-diffusion systems*, J. Math. Biol., **57**(1), (2008), pp. 53–89.

[108] J. Wei, *Existence and stability of spikes for the Gierer-Meinhardt system*, book chapter in: *Handbook of Differential Equations, Stationary Partial Differential Equations*, Vol. 5 (M. Chipot ed.), Elsevier, (2008), pp. 489–581.

[109] J. Wei, M. Winter, *Mathematical aspects of pattern formation in biological systems*, Applied Mathematical Science Series, Vol. 189, Springer, (2014).

[110] S. Xie, T. Kolokolnikov, *Moving and jumping spot in a two-dimensional reaction-diffusion model*, to appear, Nonlinearity, (2018).

[111] S. Zelik, A. Mielke, *Multi-pulse evolution and space-time chaos in dissipative systems*, Memoirs of the AMS, **198**(925), (2009).